port No. UMTA-MA-06-0025-75-15

CRASHWORTHINESS ANALYSIS OF THE UMTA STATE-OF-THE-ART CARS

Edward Widmayer
A. E. Tanner
Robert Klump

OCTOBER 1975
FINAL REPORT

Prepared for

U.S. DEPARTMENT OF TRANSPORTATION
URBAN MASS TRANSPORTATION ADMINISTRATION
Office of Research and Development
Washington DC 20590

Technical Report Documentation Page

1. Report No.	2. Government Accession No.	3. Recipient's Catalog No.
UMTA-MA-06-0025-75-15		

4. Title and Subtitle	5. Report Date
CRASHWORTHINESS ANALYSIS OF THE UMTA STATE-OF-THE-ART CARS,	October 1975
	6. Performing Organization Code
	8. ~~Performing Organization~~ Report No.
7. Author(s)	DOT-TSC-UMTA-75-19,
Edward Widmayer, A.E. Tanner, Robert Klump	
9. Performing Organization Name and Address	10. Work Unit No. (TRAIS)
Boeing Vertol Company*	UM604/R6745
Philadelphia PA 19142	11. Contract or Grant No.
	13. Type of Report and Period Covered
12. Sponsoring Agency Name and Address	Final Report
U.S. ~~Department of Transportation~~	April 1974 - April 1975
Urban Mass Transportation Administration.	
Office of Research and Development	14. Sponsoring Agency Code
Washington DC 20590	

15. Supplementary Notes
*Under contract to: U.S. Department of Transportation
Transportation Systems Center
Kendall Square
Cambridge MA 02142

16. Abstract An engineering assessment of the crashworthiness of the UMTA State-of-the-Art Car (SOAC) has been conducted for the Urban Mass Transit Administration under the technical direction of the Transportation Systems Center by the Boeing Vertol Company as part of a program to provide safer transportation to urban rail vehicles. Crash dynamics and crashworthiness methodology based on post-yield energy absorption characteristics and a "weighted acceleration" severity index has been applied. A review of the applicable static test data and crash damage has been conducted to provide a basis for the substantiation of the assumptions in the analysis. Sensitivity studies have been conducted to show the effect of car buff strength, passenger relative velocity, passenger spacing, and cushioning on casulaties as defined by the severity index. Major gains in injury reduction through improved internal cushioning are indicated. The prevention of car penetration by override is treated. The SOAC collision dynamics model is validated by comparison to the SOAC-gondola accident of August 11, 1973, and by comparison to a nonlinear finite element mathematical simulation of the SOAC in crash conditions. SOAC crashworthiness is assessed. Studies have been conducted leading to improved crashworthiness of the SOAC. Conclusions are presented and recommendations are made for further crashworthiness research.

17. Key Words	18. Distribution Statement
Crashworthiness SOAC Crashworthiness Structural Analysis Crash Investigation	DOCUMENT IS AVAILABLE TO THE PUBLIC THROUGH THE NATIONAL TECHNICAL INFORMATION SERVICE, SPRINGFIELD, VIRGINIA 22161

19. Security Classif. (of this report)	20. Security Classif. (of this page)	21. No. of Pages	22. Price
Unclassified	Unclassified	204	

Form DOT F 1700.7 (8-72) Reproduction of completed page authorized

PREFACE

In support of the Rail Programs Branch of the Office of Research and Development of the Urban Mass Transportation Administration (UMTA), Transportation Systems Center (TSC) has been assigned systems manager responsibility for the UMTA Rail Urban Supporting Technology Program. As part of this program, TSC is conducting analytical and experimental studies directed toward improved urban rail system safety. A specific goal in the area of safety is reduction of the number and severity of injuries that may result from collision of two trains.

On April 19, 1974 TSC contracted with Boeing Vertol Company to perform a 12-month study for an engineering evaluation of the UMTA State-of-the-Art Cars (SOAC). This report presents an overall description of the technical effort accomplished in the course of this study.

The authors take this opportunity to acknowledge the support of Mr. Frederick J. Rutyna, Assistant Program Manager for Rail Technology, and the technical contributions to the study made by the program's Technical Monitor, Dr. A. R. Raab of the Transportation Systems Center, U.S. Department of Transportation, Cambridge, Massachusetts.

TABLE OF CONTENTS

LIST OF ILLUSTRATIONS

LIST OF TABLES

State-of-the-Art Cars

1. INTRODUCTION

Under the technical direction of the Transportation Systems Center, Boeing Vertol Company has conducted an engineering assessment of the crashworthiness of the UMTA State-of-the-Art Car (SOAC) as part of the Urban Mass Transportation Administration's program to provide safer transportation for urban rail vehicles.

PRINCIPAL RESULTS

The general conclusions to be drawn from the study are:

- The SOAC "as built" meets the crashworthiness standards implied in the current practice of specifying buff strength.
- The penetration of occupant areas by overriding must be reduced.
- The reduction of first collision casualties may be achieved by increasing the buff strength requirement and by provision of adequate penetration resistance in the superstructure.
- The provision of adequate vertical posts in the car-end and truck retention would be an effective remedy to override penetration.
- The reduction of second collision casualties may be treated independently of the first collision (to the first order), and may be achieved by providing a "soft" car interior.

In addition, recommendations for further rail crashworthiness research are presented.

BACKGROUND

The survival and protection of vehicle occupants in accidents is receiving increased attention from the Department of

Transportation and from the transportation industry. As part of this effort in rail transportation, the Office of Research and Development of the Urban Mass Transportation Administration is conducting studies leading to the improvement of the crashworthiness of existing and new urban rail vehicles.

Acting as Systems Manager in this program the Transportation Systems Center has contracted with the Calspan Corporation and with Boeing Vertol to assess the crashworthiness of existing urban rail vehicles. Calspan has developed comparative methods of studying crash environment and correlating of passenger injury to these conditions. Calspan has also made comparative studies of five existing rail vehicles. Boeing Vertol is conducting an engineering assessment of the State-of-the-Art Car to complement the Calspan effort.

While rail travel is one of the safest methods of transportation, the opportunity exists to provide increased crashworthiness in future railcar designs. The technology developed by Calspan, together with the application of computer programs developed for aerospace and automotive vehicles to analyze structures in crash conditions, provides the necessary tools for this advancement. Improved crashworthiness may be achieved through a more complete understanding of the factors which contribute to passenger protection in a rail accident.

The engineering assessment of the crashworthiness of the SOAC became of special interest when the SOAC was involved in an unfortunate accident while undergoing testing at the High Speed Ground Test Center at Pueblo, Colorado on August 11, 1973. The accident conditions and the damage to the SOAC structure were investigated in detail by Boeing Vertol. The results of the investigation and related studies were made available to the NTSB in its investigation and report of the accident.[1] The accident data afforded a unique opportunity for a detailed analysis of the crashworthiness of the SOAC and for the validation of the crashworthiness technology.

The SOAC accident involved a rear-end collision in which a two-car SOAC train traveling at 35 mph (at impact) hit a standing train composed of a gondola (SOAC transition car) and a locomotive. The SOAC impacted the gondola, causing structural damage to both the SOAC and the gondola. The gondola detrucked, separated from the locomotive, and overrode the SOAC. The SOAC

---

1. National Transportation Safety Board, Washington, D.C., Collision of State-of-the-Art Transit Cars with a Standing Car, High Speed Ground Test Center, Pueblo CO, NTSB-RAR-74-2, August 1973, PB233254.

and gondola car body derailed, at which time the gondola car body separated from the SOAC. The damage to the SOAC train was confined to the forward-bolster-to-car-end area of the lead SOAC, except for a failure of intercar coupler shear pins and "dented" anticlimbers. The damage to the gondola was in the anticlimber modifications required for transition service and in the coupler and draft gear. A detailed sequence of events for the collision is presented in Appendix A.

The SOAC was built as a part of the Urban Rapid Rail Vehicle and Systems Program, and is the result of an integrated development program directed toward improving high-speed frequent-stop urban rail systems. The overall objective is to enhance the attractiveness of rail transportation to the urban traveler by providing service that is as comfortable, reliable, safe, and economical as possible. The objective of SOAC is to demonstrate the best state-of-the-art in rapid rail car design on two improved cars built using existing approved technology (circa 1970).

TECHNICAL APPROACH

This study contract has as its objective an engineering assessment of SOAC crashworthiness. The technical approach is to analyze the energy-absorbing capacity of the SOAC car body structure using conventional engineering stress techniques. In addition, the analysis has been extended to treat the structural dynamics during a collision by means of a finite element technique that treats the inelastic behavior of the structural components.

The accident damage to the primary structural elements such as the draft sill and end weldments was examined to substantiate the basis of the structural analyses and the failure modes of the structural components. In addition, this examination showed areas of potential improvement in SOAC crashworthiness.

The SOAC is sufficiently similar in construction to the R-44 car that the static test data for the R-44 was used to substantiate the SOAC design. This static test data was reviewed to substantiate the distribution of loads used in the stress analyses and to verify the predicted static buff load capability of the car.

Using the data generated in the above studies a force deflection curve was developed for the SOAC. The Calspan approach[2] was then applied to the SOAC to assess the crashworthiness of the SOAC for the end-on collision and

2. Department of Transportation, Urban Mass Transportation Administration, Washington DC, Cassidy, R.J. and Romeo, D.J., Assessment of Crashworthiness of Existing Urban Rail Vehicles, Report in preparation.

for the case of overclimbing. The similarity of the SOAC to the R-44 car allowed comparison of the SOAC results to those for the R-44 car as analyzed by Calspan. The SOAC results were in agreement with the Calspan results.

The sensitivity of passenger injury to the condition of a collision was studied. The basic parameters such as impact velocity, crush distance, passenger relative velocity to the car interior, and the hardness of the car interior were varied to show the effect on the severity of injury as measured by the abbreviated injury scale.

As a result of these studies, SOAC structural design modifications were identified for study to improve SOAC crashworthiness. The recommended modifications included improved collision posts, higher strength weld joints, and improved load distribution to major structural members. These studies also provided comparison of the energy absorption capability arising from the improvements, and representative data on the predicted crash loads to serve as engineering guidelines.

The body of this report is divided into three parts. The first part (Sections 2 through 4) contains the structural details of the SOAC design leading to the force deflection characteristics. The second part (Sections 5 through 8) contains the methodology for crash dynamics and crashworthiness, leading to an assessment of the crashworthiness of the "as-built" SOAC. The third part (Section 9) consists of studies for improvement of the SOAC crashworthiness.

The crashwothiness that might be achieved from these improvements has been assessed and recommendations and conclusions are presented.

2. STRUCTURAL DESIGN

The major SOAC elements are shown in Figure 2-1. The car underframe is a welded high tensile low allow steel frame similar to the New York City Transit Authority equipment contract R-44 design. The car sides have cutouts for four large doors and three picture windows. The car ends are molded fiberglass as approved for the R-44 cars and the cab end is contoured for styling. The cantilever collision post terminates 20 inches above the foor and does not obstruct vision through the large full front window panels. The B end has a door for passing through to the other car. The roof is of conventional design of carlins and purlins. It carries heavy air conditioning equipment at both ends and a pantograph at the B end.

CAR STRUCTURE

The underframe, shown in Figure 2-2, provides the primary longitudinal load path. The underframe is fabricated of high-strength, low-alloy steel with full-length side sill channels, formed crossbearers between bolsters, and rolled section cross-bearers near the car ends. Sides and roof are fabricated of stainless steel skins spot-welded to steel frames. Local reinforcement has been provided for support of the pantograph and for car jacking.

The anticlimber and the coupler mounting are integrated into an end weldment assembly which is built up around two 8-inch draft sill channels spaced 26 inches apart. The anticlimber (which is built up by welding two 3-inch channels together and is modified near the ends with welded flange extensions and gussets between flanges) extends 7.5 inches beyond the draft sill at each side. From the ends of the anticlimber, 6-inch intermediate draft-sill channels extended just over 2 feet aft to the end floor support beam, which consists of rolled angles welded together to form an 8-inch box beam between the side sill ends and the draft sills.

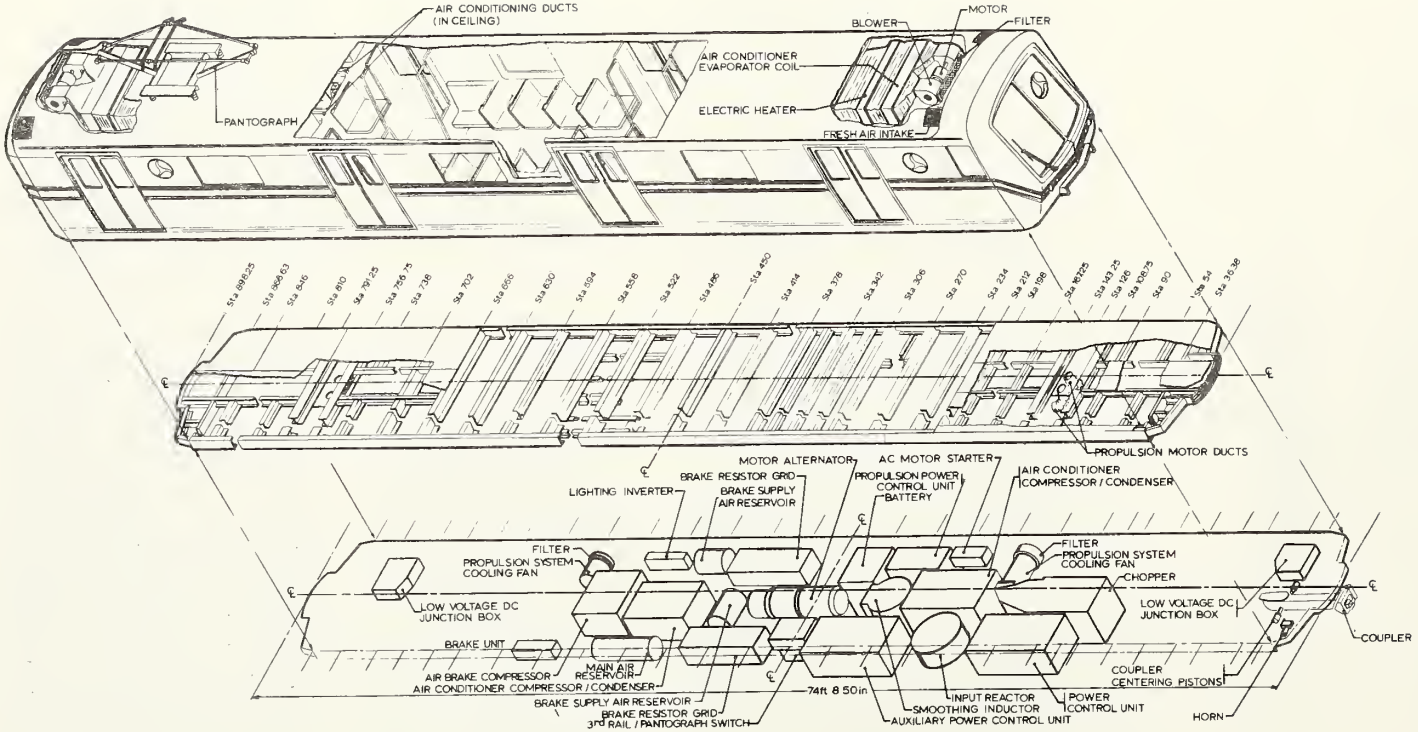

Figure 2–1. Major Elements of State-of-the-Art Car

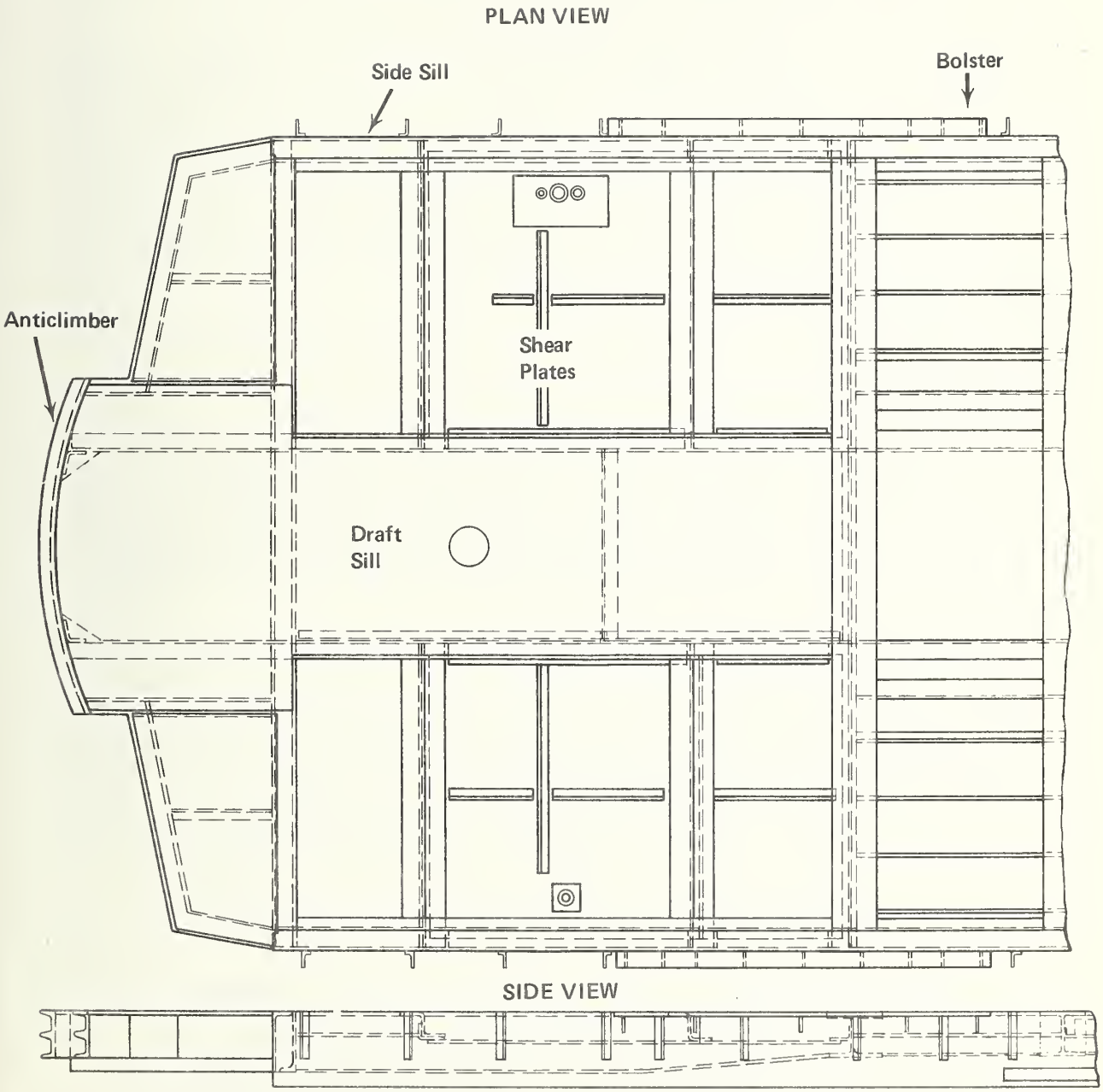

Figure 2–2. SOAC Underframe at Car End

Behind the anticlimber is a 0.375-inch center shear plate between the draft sills which extends to the end floor support beam, a 0.125-inch bottom shear plate extending to the coupler radial bar support channel, and a 0.125-inch top shear plate spanning the intermediate draft sills to the end floor support beam and the draft sills aft to the bolster. Secondary floor support structure, consisting of end and corner sills (6-inch formed channels) and 0.082-inch corner (top) plates complete the forward end of the end assembly.

Aft of the floor support beam, a 0.50-inch plate reinforced with 0.50-inch vertical transverse stiffeners is welded to the bottom flange of the draft sills to provide the mounting for the coupler anchor. Aft of the coupler anchor, the draft sill height tapers to 5.88-inches (by cutting the web, bending up the lower flange, and welding) and the sills are spanned by a 0.25-inch shear plate extending aft to the end of the weldment assembly.

The body bolster assembly provides one of the primary load paths from the anticlimber and coupler through the end weldment into the side sills. The bolster weldment consists of two 6-inch wide-flange I-beams spaced just under 3 feet apart, joined together (at approximately mid-web) by 0.31-inch base (shear) plates which extend 29 inches from each end. Numerous vertical and horizontal plate members plus four 6-inch rolled channels also join the I-beams and provide local stiffening for the lateral bumper brackets and the safety straps. The inboard channel members are spaced the same as the draft sill channels.

Above the car floor on the aft face of the fiberglass end fairing are two shear panel assemblies, located 17 inches on either side of the car centerline. Each assembly consists of a 0.188-inch thick plate, 26 inches high by 6 inches wide at the bottom and 12 inches at the top, with an integral aft flange and welded-on 2x2x0.188-inch angles on the other three edges. This assembly is welded to a 0.50x6-inch plate extending its full height and through the end weldment top plate. At the car body forward corner, the corner post structure consists of a 1.56x4x0.188-inch formed angle with the 4-inch leg parallel to the car centerline butt welded to the lateral (2-inch) leg of a 1.5x2x0.188-inch angle at the forward edge of the car side.

The detailed drawings of the SOAC structure are referenced in Paragraph 2.1.3 of the SOAC Specification (Reference 2-1[3]). The SOAC structure was modified from the R-44 car design. The structural arrangement of the R-44 underframe was applied to the SOAC. Some modifications to the R-44 draft sill and bolsters were required because of interference with the SOAC trucks. These modifications were shown, by analysis, to meet the buff requirements of the R-44.

3. Department of Transportation, Urban Mass Transportation Administration, Washington DC, Detail Specification for State-of-the-Art Car. IT-06-0026-73-2, May 1973, Revision A, October 1973.

The mass properties of the SOAC are summarized in Appendix B. The car-empty weight is 90,000 pounds with a maximum permitted load of 40,000 pounds (266 people at 150 pounds each).

In this study (See Crash Simulation, this section), the car-empty weight is treated as identifiable concentrated masses plus a distributed shell weight. The shell weight is distributed to the nodes by prorating the wetted area. The concentrated masses also are divided between the adjacent nodes. This procedure resulted in the assignment of all but 2,180 pounds, which was added in such a way as to give the proper gross weight and pitch inertia. This weight distribution gives an approximation of the distributed longitudinal inertial reaction of the crash forces during impact. The loading of the structural elements simulates that for a crash. Further, as nodes are arrested, the masses are subtracted from the energy-absorbing process.

Coupler

The mechanical coupler consists of the coupler head, drawbar and draft gear, anchorage, radial bar, and centering device. The coupler is capable of making automatic engagement with the opposing coupler and accommodates a misalignment of 3-3/8 inches to the left or right of the centerline or 3 inches above or below the standard height of the coupler. The coupler force deflection curve is given in Figure 2-3.

Two load path modes are accommodated by the coupler and attachments: buff and draft. Static loads of 400,000 pounds and 225,000 pounds, respectively, are the mode's maximum loads to be sustained by the coupler, drawbars and anchorage. An emergency release mechanism incorporated in the draft gear, consisting of four emergency release nut and stud assemblies, is designed to shear at 150,000 pounds. Only buff forces are transmitted through the emergency release bolts. Draft forces can still be withstood by the coupler after emergency release has occurred.

Prior to coupler emergency release, in the buff mode the draft gear cushion elements permit the draft gear yoke assembly to compress 1-1/4 inches under a load of 150,000 pounds shear and 1-5/8 inches under a load of 225,000 pounds. After the emergency release bolts shear, the coupler telescopes three inches under no-load to permit the anticlimber to engage.

For purpose of analysis for the coupler load deflection curve, an initial spring stiffness of 100,000 pounds per inch for 1.5 inches is assumed. At 150,000 pounds the four emergency release bolts shear causing the buff load to drop at the rate of 12.8×10^6 pounds per inch to near zero load at 1.513 inches movement. In the next 0.001 inch, a transition stiffness is

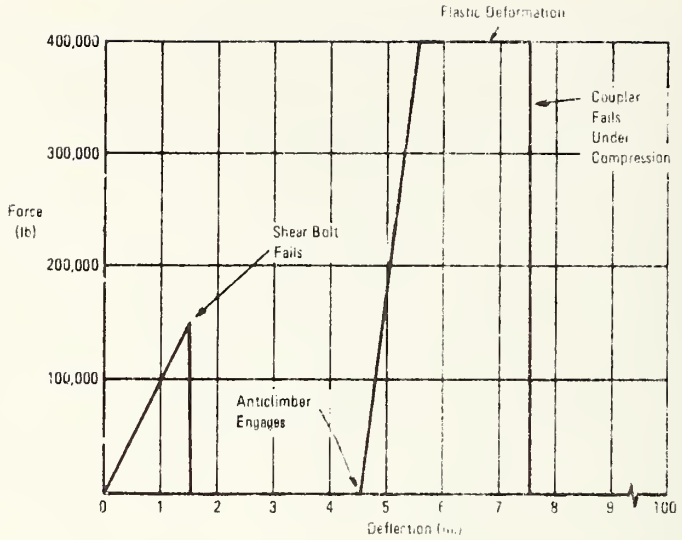

Figure 2–3. Coupler Force Deflection Characteristics

provided and no load is carried in the coupler for the next three inches of draft gear travel. Subsequently, both the draft gear impacts the drawbar and the anticlimber impacts the imposing mass.

If another car with anticlimber is impacted, full anticlimber engagement will occur within 2 inches after coupler release, while the anticlimber would impact a flat bumper within 1/4-inch after coupler release.

In the next one inch of coupler deformation a strain rate of 400,000 pounds per inch is assumed. Plastic compression deformation then occurs for the following two inches and, subsequent loss of load-carrying capability occurs immediately thereafter. The unloading rate is assumed to be 20,000,000 pounds per inch.

The total strain energy of structural deformation for the coupler assembly prior to failure is comprised of 112,000 inch-pounds elastic and 1,000,000 inch-pounds plastic energy.

Material Allowables

The basic material for the car body structure was Corten steel. This material has tension yield strength of 50,000 psi and an ultimate strength of 70,000 psi. Young's modulus is 29,600,000. These values were used throughout this study.

DESIGN CRITERIA

The design criteria for the SOAC are given in Reference 2-1. The design loads sections of that specification are given below.

Construction

The car body shall be constructed to meet the design and strength requirements as specified for the New York City Transit Authority Equipment Contract R-44 cars except as called for by this specification. The car structure shall be designed to maintain the passenger envelope within the limits and for the design loads as specified.

The car body and underframe shall be an integral structure and shall withstand the loads induced into the underframe by the trucks, coupler-draft gear and suspension units. Also, the car structure must be of sufficient stiffness to be commensurate with the requirements of Sections 2.7, Vibration, and 2.8, Noise, of this specification.

1. Vertical and Combined Loading

   The loads and forces used in calculating the fiber stresses in the various members of the car body shall be either of the following combinations. For any part of the structure the combination that results in the higher stress shall be used as a design goal.

   Combination A

   (1) A passenger load varying from 0 to 350 passengers at 140 pounds each, the maximum being 49,000 pounds per car.

   (2) An allowance for vertical impact of 26 percent of the total static load including the above maximum passenger load of 49,000 pounds.

   (3) A horizontal buff or pull applied at the center line of the coupler faces amounting to 60,000 pounds static load.

   (4) A force caused by the maximum acceleration or deceleration resulting from a 33 percent coefficient of adhesion.

   (5) A force caused by running on a sharp curve at a speed sufficient to throw the entire weight of the car, including trucks and motors, on the four wheels on the outside rail.

Combination B

(1) A passenger load varying from 0 to 350 passengers at 140 pounds each, the maximum being 49,000 pounds per car.

(2) Under this combination of conditions it may be assumed that the cars will not be running at high speeds and the allowance for vertical impact can be omitted.

(3) A horizontal buff at 250,000 pounds or a pull of 200,000 pounds static load applied at the center line of the coupler faces and/or of the inner frame.

(4) The forces caused by operation on curves will not apply in this combination.

2. Camber

Minimum positive camber between bolsters when assembled on jigs shall be 3/16 inch. Cambers shall be not less than zero (level) for a completed car loaded with maximum passenger weight.

3. Compression Loading

The car body shall withstand a static end load of 250,000 pounds applied on the center line of the anti-climber end sills, without exceeding 50 percent of the yield point of the structural material and shall not have a vertical deflection between body bolsters greater than 0.205 inch.

4. Crashworthiness Criteria (not specified)

5. Hoisting and Jacking

The car structure shall be capable of being raised by jacking at four jack pads located at the bolsters.

STRUCTURAL ANALYSIS

Fundamental to the problem of crashworthiness is the energy absorption capability of the structure. The major energy absorption is achieved through the plastic deformation and failure of the load carrying structure.

Good crashworthy design controls the energy absorbing modes of the structure. The location and type of failure are strongly influenced by the sequence of load application and the local restraints on the elements. The energy management problem involves maximizing the energy absorption without introducing undesirable failures in other locations within the structure.

The technical approach involves the determination of the loads required to fail the individual elements and the most probable mode of failure. The simple failure modes include elastic stability, tension-compression, the formation of plastic hinges in bending, and shear failures such as torsion. In the case of combined stresses, the estimation of the local strain conditions becomes more complex. Engineering stress methods have been used to evaluate the structure.

Two analytical approaches have been used to define the crash capability of the SOAC. In the first approach, major structural elements have been examined to determine the strength and the energy capacity of individual pieces of structure under static load conditions. The second approach uses a mathematical finite element beam model and the Army sponsored "KRASH"[4]. This is an extension of the first approach but includes the more complex interactions of inertia loadings and the adjacent structure. The two approaches are valuable since major differences in load distribution exist between the methods. The first approach, being less complex, offers ease of application and more rapid results but is less accurate. The second approach better represents the detailed crash behavior of the structure, but is more difficult to apply.

Prior to these analyses, detailed strength and stiffness properties of the SOAC were determined. The car was examined down to the detail of carlins, purlins and sheet gauges. Weld strengths were determined for major structural joints. These data formed the basis for analysis.

---

4. U.S. Army Air Mobility Research and Development Laboratory, Wittlin, G. and Gamon, M. A., Experimental Program for the Development of Improved Helicopter Structural Crashworthiness 72-72A, 72-72B, May 1973, AD764985.

Stiffness

The sectional properties of the structural elements were extracted from the drawing for the SOAC and, where applicable, from the R-44 drawings. These properties were converted to stiffness data for both an 80-node model (Figure 2-4) and an 28-node model (Figure 2-5). In this process the stiffness matrix for a fixed-fixed beam element was formed.

$$(F_i) = (K) \times (u_i)$$

where u_i is the deflection of one end of fixed-fixed beam relative to the other end. (See Appendix C)

$$K = \begin{bmatrix} \frac{EA}{L} & 0 & 0 & 0 & 0 & 0 \\ 0 & \frac{12EI_z}{L^3(1+\phi_y)} & 0 & 0 & 0 & -\frac{6EI_z}{L^2(1+\phi_y)} \\ 0 & 0 & \frac{12EI_y}{L^3(1+\phi_z)} & 0 & \frac{6EI_y}{L^2(1+\phi_z)} & 0 \\ 0 & 0 & 0 & \frac{GJ}{L} & 0 & 0 \\ 0 & 0 & \frac{6EI_y}{L^2(1+\phi_z)} & 0 & \frac{(4+\phi_z)EI_y}{L(1+\phi_z)} & 0 \\ 0 & -\frac{6EI_z}{L^2(1+\phi_y)} & 0 & 0 & 0 & \frac{(4+\phi_y)EI}{L(1+\phi_y)} \end{bmatrix}$$

$$\text{where} \quad \phi = \frac{12EI}{GA_SL^2}$$

$$A_S = \text{shear area}$$

Where the fixity departed from the above assumption (as in the case of the coupler draft anchor pin connection) suitable fixities were assigned. Torsional stiffness has not been included for elements where torsion is not an important factor.

The basic strength and stiffness characteristics of the SOAC structure indicate that the primary load paths through the car are from the anticlimber through the draft sill elements

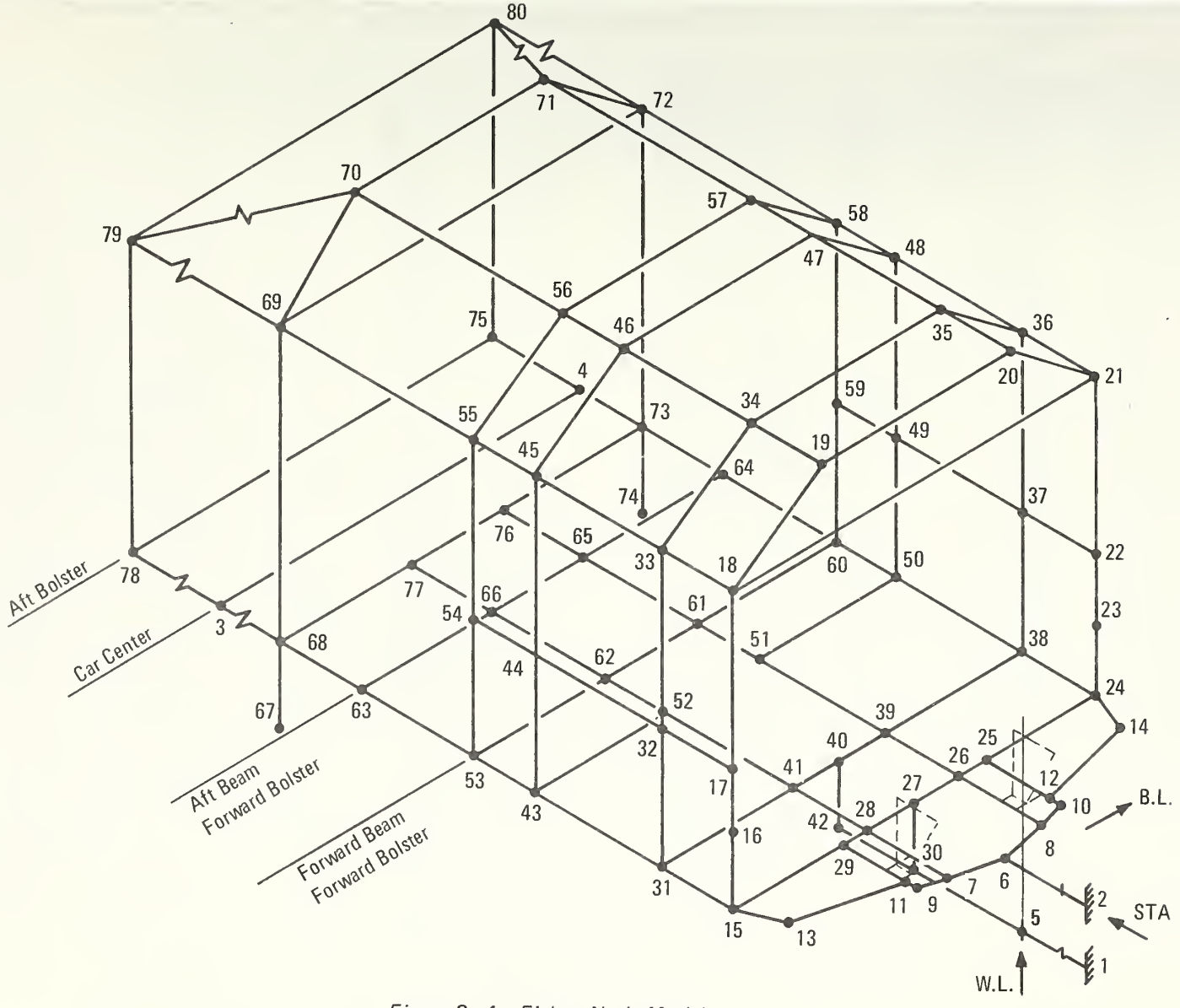

Figure 2–4. Eighty Node Model

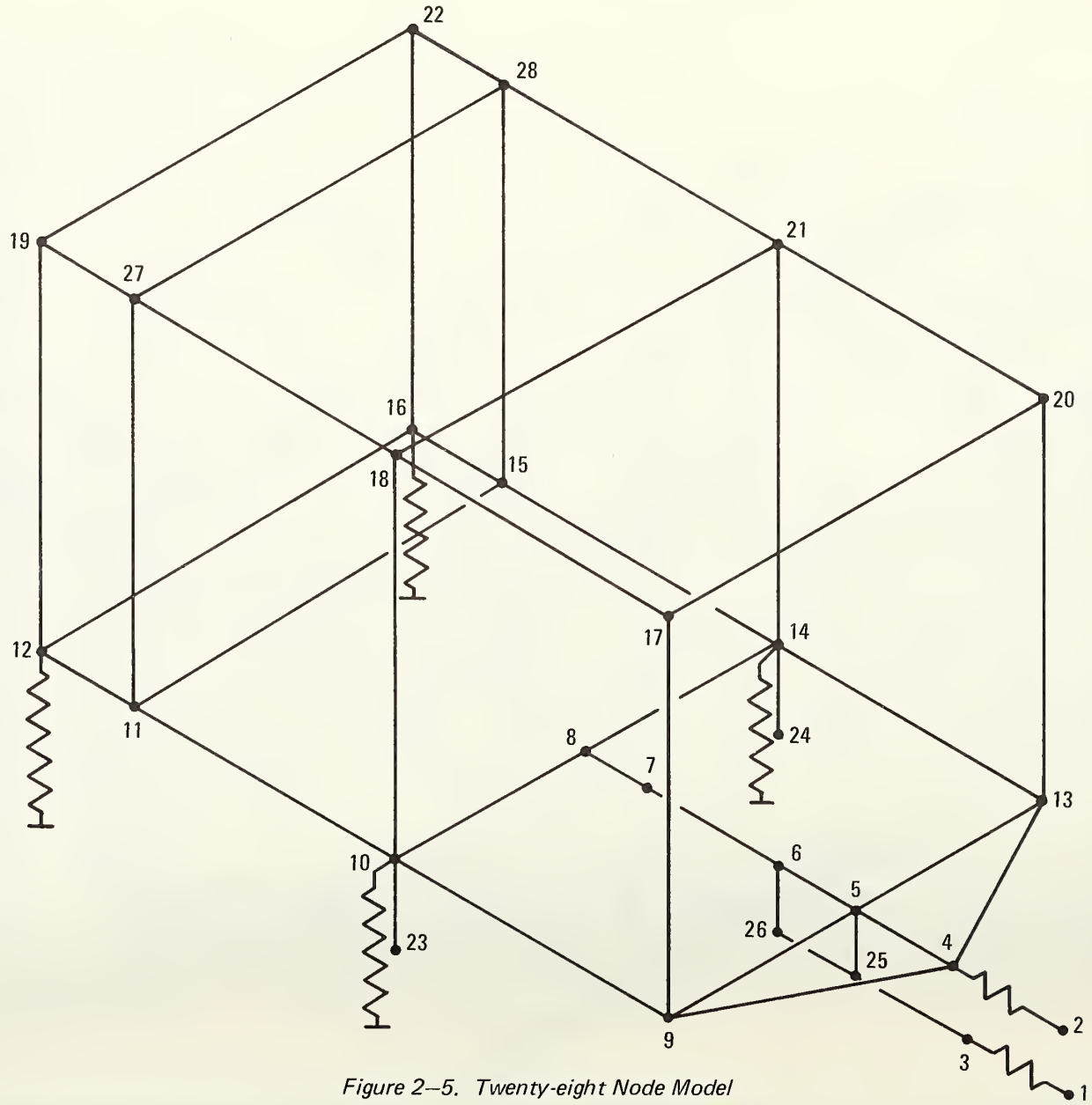

Figure 2–5. Twenty-eight Node Model

to the bolster and from the draft sill to the side sill through the shear plates. The bolster as a beam also carries the loads to the side sills. The car underframe is symmetric about the car center. The car sides, the coves, and the roof were determined to lack sufficient stiffness to be major contributors in analysis of component contribution in crash conditions. (See Table 2-1.)

The capacity of a structural element to absorb energy in a crash, while strongly dependent on the mode of deformation, does bear a relationship to the inherent strength of the element. These capacities are investigated below.

Analysis of Major Structural Components (Quasi-Static Loadings)

The results of analyses of major structural elements in carrying load and in absorbing crash energy to contribute to a force deflection curve are given in Table 2-1.

The elements analyzed are the collision posts, the draft sill, the shear panels, the bolster, the side sills, the side walls, the cove, the roof panel, the end posts, and the weld joint details. The element numbers that appear below refer to the elements as shown in the 80-node structural model shown in Figure 2-4.

The assumption and methods used in this approach generally are consistent with those used by Cassidy and Romeo.[2] Differences in failure sequence scenarios with resulting variations in force deflection curves (see Section 4) arise from the more specific role of structural analysis of this study. However, the differences are not expected to cause major differences in the crash dynamics of the SOAC as compared to the Cassidy-Romeo analysis[2] of the R-44 car.

In this approach, the general car body cross-sectional properties form the basis for car strength. These are then modified to account for load paths, stability, and other factors to approximate the structural force deflection curve.

Advantage was taken of the crash damage information (Section 3) in the conduct of these analyses. The selection of elements that participate in the dissipation of crash energy and the modes of failure were guided by the crash data.

CRASH SIMULATION (BEAM FINITE ELEMENT "KRASH" MODEL)

This approach to the study of structural crashworthiness involves an iterative cycle in which the model properties are improved to be consistent with the physics of the crash. One

TABLE 2-1. LOAD AND ENERGY CHARACTERISTICS

Element	Failure Mode	Limit Load	Strain Energy
Collision Post	Shear Bending	31,200 lbs. 614 lbs.	Small 1.7 in.-lbs.
Draft Sill	Beam Column Axial Compression	500,000 lbs. 500,000 lbs.	14×10^6 in.-lbs at $\theta = 45°$ 476,000 in./in.
Shear Panel	Plate Buckling Weld Rupture	286,300 lbs.	3552 (Elastic) in.-lbs.
Bolster	Fore and Aft Bending	172,478 lbs.	1,097,080 in.-lb./rad. included both sides
Side Sill	Column Buckling Strong Axis Weak Axis	 352,600 lbs. 352,600 lbs.	 460,000 in./lb. at θ 45° 60,000 in./lb. at $\theta = 45°$
Corner Post (End)	Bending (Plastic Hinge)	10,945 in-lbs.	47,000 in./lb. 4 in. Midspan Deflection 16,400 in.-lb/rad.
Side Wall	Sheet-Stiffner	48,000 lb.	80,000 in./lb. (4 in. Deflection)
Cove	Local Buckling	37,797 lb.	64,000* in.-lb. (4 in. Deflection) *Estimated
Roof (1/2 Section)	Local Buckling	1,612 lbs.	4,000 in.-lb. at Deflection = 4 in.

starts with a simple representation and proceeds to add complexities such as non-linear element behavior or rupture, or additional masses and/or beams to extend the validity of the solution as the crash progresses in time.

The use of programs such as KRASH to simulate the structural dynamics in the non linear behavioral range is still in an embryo stage. The degree of success achieved represents an expansion of the technology.

The initial simulation is a 28-mass model, with 51 beam elements supported on 4 vertical springs to provide ground reactions. The model is described below, followed by some analytical results.

Modeling Considerations

A review of the laws for modeling impacts is useful at this point. True modeling requires that both the energy and the forces be duplicated in the model as closely as possible and the constraints and boundary conditions should be matched.

For instance, for the impact of one train with another, with no rebound, the velocities are related by momentum conditions

Before Impact		After Impact
$V_1M_1 + V_2M_2$	=	$V_F\ (M_1+M_2)$

If one train is standing, i.e. $V_2=0$, then

$$V_F = V_1M_1/(M_1+M_2)$$

and the kinetic energy consumed is given by

$$D(KE) = 1/2\ M_1V_1^2 - 1/2\ (M_1+M_2)\ V_F^2$$

$$= 1/2\ M_1V_1^2 \left[\ 1 - \frac{M_1}{M_1 + M_2}\ \right]$$

The energy lost in a two train collision may be simulated by a barrier impact. This case, the relationship of the barrier impact velocity to the accident impact velocity into a standing train is given by

$$1/2\ M_1V_B^2 = 1/2\ M_1V_1^2 \left[1 - \frac{M_1}{M_1 + M_2}\right]$$

$$\text{or} \quad V_B = V_1 \left[1- \frac{M_1}{M_1+M_2}\right]^{\frac{1}{2}}$$

This implies that where crash energy management is the primary aim the above relationships are a necessary condition.

If the mechanism of energy consumption is to be studied, then additional relationships must be met. In this endeavor, the major energy consumption is in the failure nodes of the structure and in the sequence of occurence. Starting with the condition of stress being a function of strain and strain rate, a set of dimensionless parameters may be formed relating the material properties and the model properties for the prototype vehicle and the model. One such group is

$$\left(\frac{Xi}{L}, \varepsilon, \frac{\sigma}{E}, \frac{t}{L}\sqrt{\frac{E}{P}}, \dot{\varepsilon}t, \frac{Vt}{L}, \frac{\tau}{L}\sqrt{\frac{E}{P}}, \frac{\rho L g}{\sigma} \right)$$

where σ = stress
E = Young's modulus
ε = Strain
$\dot{\varepsilon}$ = Strain rate
τ = Strain rate constant
L = characteristic Length
Xi = Spatial coordinate
t = time
ρ = material density
g = acceleration due to gravity
v = velocity

If these quantities are matched between the prototype and the model, the model will respond like the prototype. The stresses will be matched, the failure sequence will be duplicated, and the energy consumption will be met. To achieve this, the velocity of impact must be met. Consequently, while barrier impacts may provide a simplification and may be instructive, they do not completely satisfy the scaling.

Model Description and Analytical Approach

The baseline model for the crashworthiness study is a lumped mass, beam element representation of the one SOAC, Figure 3-2. The model is designed to impact a barrier with the coupler and with the anticlimber.

The car is supported vertically by stiff external springs at the aft bolster and at the forward bolster. These springs are selected to be rigid relative to the carbody structure and have zero coefficient of friction with the ground plane. The barrier (nodes 1 and 2) is part of the model, and consists of two weights of $.9 \times 10^{15}$ lbs. each, which are supported by lift. Since the maximum permitted weight is 130,000 lbs., the barrier appears as an infinite mass relative to the car (a ratio of 10^{10}). For the coupler/anticlimber impact, the barrier is connected to the car by long (1000-inch) stiff links. The link to coupler is extremely stiff and elastic, while the link to the anticlimber has force deflection shaped to allow the force to be applied only after the coupler shear pins have failed and the coupler has retracted. When the anticlimber has advanced to the plane of the coupler face, the link (element 2-6) becomes extremely stiff.

The coupler axial force deflection curve (Figure 2-3) has been assigned to element 3-25).

The non-linear behavior of the structure may be depicted in the "KRASH" program by several devices. The shape of the force-deflection curve for each element for each degree of freedom may be specified. When the deflection of one node relative to an adjacent node in any of the six degrees of freedom would cause the connecting element to rupture, rupture can be specified and that element dropped from the ensuing computation.

To develop an understanding of the reaction of the structure an iterative approach to the development of the model has been taken. The initial crash cases were run at low impact velocities using an elastic car body to show the load distribution and to identify critical elements in the energy absorption process. The then critical failure mode of important elements such as the formation of plastic hinges, joint rupture at welds, welds, and crushing of elements was incorporated into the model. The crash velocity was also increased and the run re-analyzed.

The development of a mathematical representation that represents the structure throughout the impact is a difficult task. As the impact progresses and the structural elements distort and fail the validity of the equations tend to be exceeded. This requires additional refinements to extend the validity of the solution.

Crash Simulation Results

The simulated crash of the 28-mass model into a barrier has produced data that approximate the damage observed in the SOAC accident of August 11, 1973. These data include the rupture of welds and the formation of plastic hinges in the draft sill. Also of significance is that the model depicted the location of the failures to the forward end of the car (between the anticlimber and the bolster). No damage was indicated aft of the forward bolster.

The simulation model included rupture criteria for welds. These criteria are given in terms of the relative deflection of one end of a beam element to the other end. As such, they include the allowable stress, length and thickness of the weld and the manner of loading. The analyses are summarized in Table 2-2.

TABLE 2-2. SUMMARY OF WELD RUPTURE DISPLACEMENTS

° Values are for actual weld thickness (Factored 1/10" weld values).

° Drawing weld data used

° Member reference notation refers to the 80 mass model.

MEMBER	JOINT	$U_1 \times 10^2$ (in.)	U_2 (in.)	U_3 (in.)	$U_5 \times 10^3$ (rad.)	$U_6 \times 10^3$ (rad.)
15-16	15	3.4617	.27677	1.5188	5.622	2.2536
23-24	24	3.4617	.27677	1.5188	5.622	2.2536
31-32	31	3.4617	.27677	1.5188	5.622	2.2536
37-38	38	3.4617	.27677	1.5188	5.622	2.2536
43-44	43	3.4717	.27677	1.5188	5.622	2.2536
49-50	50	3.4617	.27677	1.5188	5.622	2.2536
53-54	53	3.4617	.27677	1.5188	5.622	2.2536
59-60	60	3.4617	.27677	1.5188	5.622	2.2536
15-29	15	2.9832	.3896	.0636	.1548	.288
24-25	24	2.9832	.3896	.0636	.1548	.288
31-41	31	8.112	2.9302	.52068	1.60	5.324
38-39	38	8.112	2.9302	.52068	1.60	5.324
31-41	41	8.112	2.9302	.52068	1.60	5.324
38-39	39	8.112	2.9302	.52068	1.60	5.324
17-18	18	2.4816	4.1458	4.3430	1.584	1.3078
21-22	21	2.4816	4.1458	4.3430	1.584	1.3078
25-26	26	.53922	.010535	.011225	.2360	.6666
28-29	28	.53922	.010535	.011225	.2360	.6666

TABLE 2-2. SUMMARY OF WELD RUPTURE DISPLACEMENTS

(Continued)

MEMBER	JOINT	U_1 (in.)	U_2 (in.)	U_3 (in.)	U_5 (rad.)	U_6 (rad.)
32-33	33	.77719	1.7204	.52853	.8006	1.2852
36-37	36	.77719	1.7204	.52853	.8006	1.2852
44-45	45	.77719	1.7204	.52853	.8006	1.2852
48-49	48	.77719	1.7204	.52853	.8006	1.2852
13-15	15	.81304	.066884	.030279	.44620	1.4759
14-24	24	.81304	.066884	.030279	.44620	1.4759

*In beam axes, the displacements are:

U_1 = axial

U_2 = lateral

U_3 = vertical

U_4 = torsion angle

U_5 = vertical bending slope

U_6 = lateral bending slope

NOTE: Weld strength was calculated using procedures given in Reference 5.

5. Blodgett, Omer W., Design of Welded Structures, The James F. Lincoln Arc Welding Foundation, Cleveland, Ohio, 1966.

These rupture criteria were included for the end sills, the corner posts, and the end weldment. Significantly. The model showed the end weldment (elements 4-9 and 4-13) to rupture at t = .0169 seconds after impact. The end sills (elements 5-9 and 5-13) ruptured at t = .0192 seconds and the corner posts (elements 9-17 and 13-20) ruptured at t = .0492 seconds As shown in Section 3, the SOAC coupler shear pins did fail and the coupler shank did rupture. Weld failures occurred at these locations in the car structure during the accident. Thus, while the time of rupture cannot be correlated, the location of weld ruptures correlated quite well.

From an energy absorption consideration the simulated draft sill behavior is significant. The simulation experienced the formation of plastic hinges (see Figure 2-6) at nodes 5, 6 and 7. In addition, significant axial plastic behavior in element 5-6 is observed. This plastic behavior accounts for about 90% of the strain energy in the simulation. Comparison with the crash damage to the draft sill indicates that the simulation presents an approximation to SOAC draft sill in the accident.

These results corroborate the analyses which are based upon physical evidence of the failure nodes and give an insight into the dynamic behavior of the structure in a crash. This insight will be used in the formulation of the crash scenarios for the force of deflection curves in Section 4.

On the basis of these initial achievements, additional studies were conducted to extend the applicability of the model and to provide further information on the structural behavior.

A 30-mode model was an extention from the 28-mass model by the addition of a simulated aft truck (shown by nodes 29 and 30 on Figure 2-7) A comparison of Figure 2-7 with Figure 2-5 shows that diagonal members were added to represent the shear transfer between the underframe and the roof and between the draft sill and the side sill.

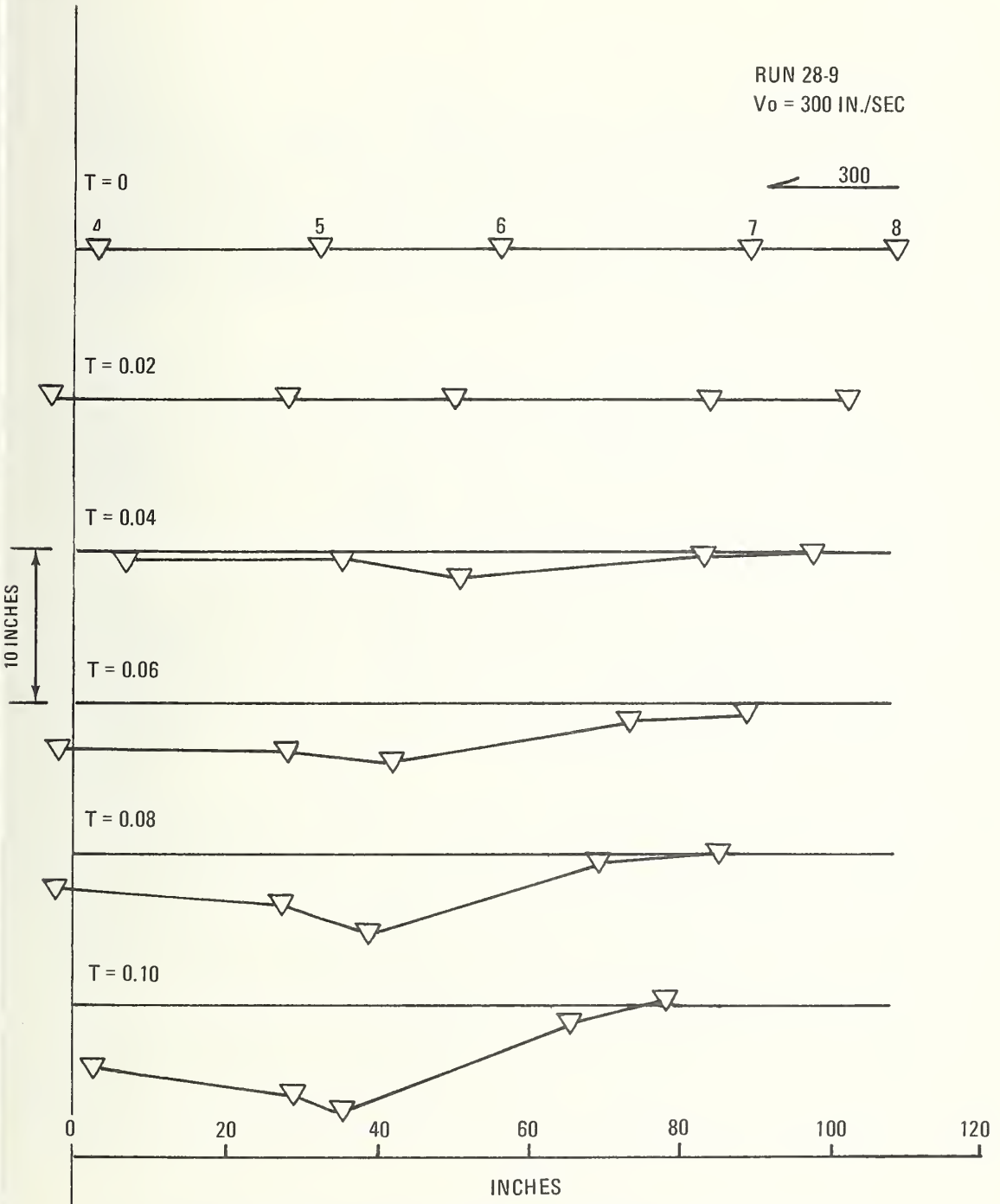

Figure 2–6. Draft Sill Deflection Coupler/Anticlimber Impact

In the first application is shown the results of a simulated static test. The "static" test case was treated to verify the load path assumptions of the analytical model. In this case (run 30-3), the model was modified by weights of 10^6 lbs. at nodes 12 and 19 for the 30 mass model. The model was then impacted into the barrier at 12 inches per second. The 12-inch per second impact velocity was a compromise between computer run time and the desire to reduce the inertial relief through the model.

In Figure 2-7 is shown the axial load distribution through the simulation at time = .0526 second. The car has experienced a compression of 0.6312 inch and is well within the elastic range. As can be seen, the principal load path is through the draft sill (nodes 4 through 8) and through the shear plates (elements 8-9 and 8-13) to the side sills. The bolster (8-10) transfers the draft sill load to the side sills by beam action.

The load distribution between the bolsters approximates that from static tests (Section 3). The static tests showed the side sills carried two-thirds of the load while the model shows approximately three-quarters of the load taken at a cut through the car between nodes 10 and 11. For a cut through the car between nodes 11 and 12 the side sills carry closer to one-half the load. In light of the simple modeling used, the model gives a good representation of the car.

The typical railcar design problems are clearly displayed by the model. The first is how to transmit load to the roof. Even if no cutouts for doors or windows were present, the car sides and the side posts are not efficient in transmitting axial load from the underframe to the roof. The second is how to take the loads from the draft sill to the side sills. The load may be transferred by bending of the end weldment (elements 4-9 and 5-9), by shear of the floor plates (element 8-9), or by bending of the bolster (element 8-10). Actually, the loads are transmitted by a combination of these actions. For this, the end weldment requires a truss or a shear web to form a beam of elements 4-9 and 5-9. The use of shear plates is limited by the compression buckling stress, which may be increased by increasing the thickness of the shear web or by a reduction in the unsupported dimensions of the panel.

The KRASH model is an approximation of the actual structure. The selection of elements was made to represent the dominant behavior of the car body without unduly expanding the computing effort by such means as including additional members in the

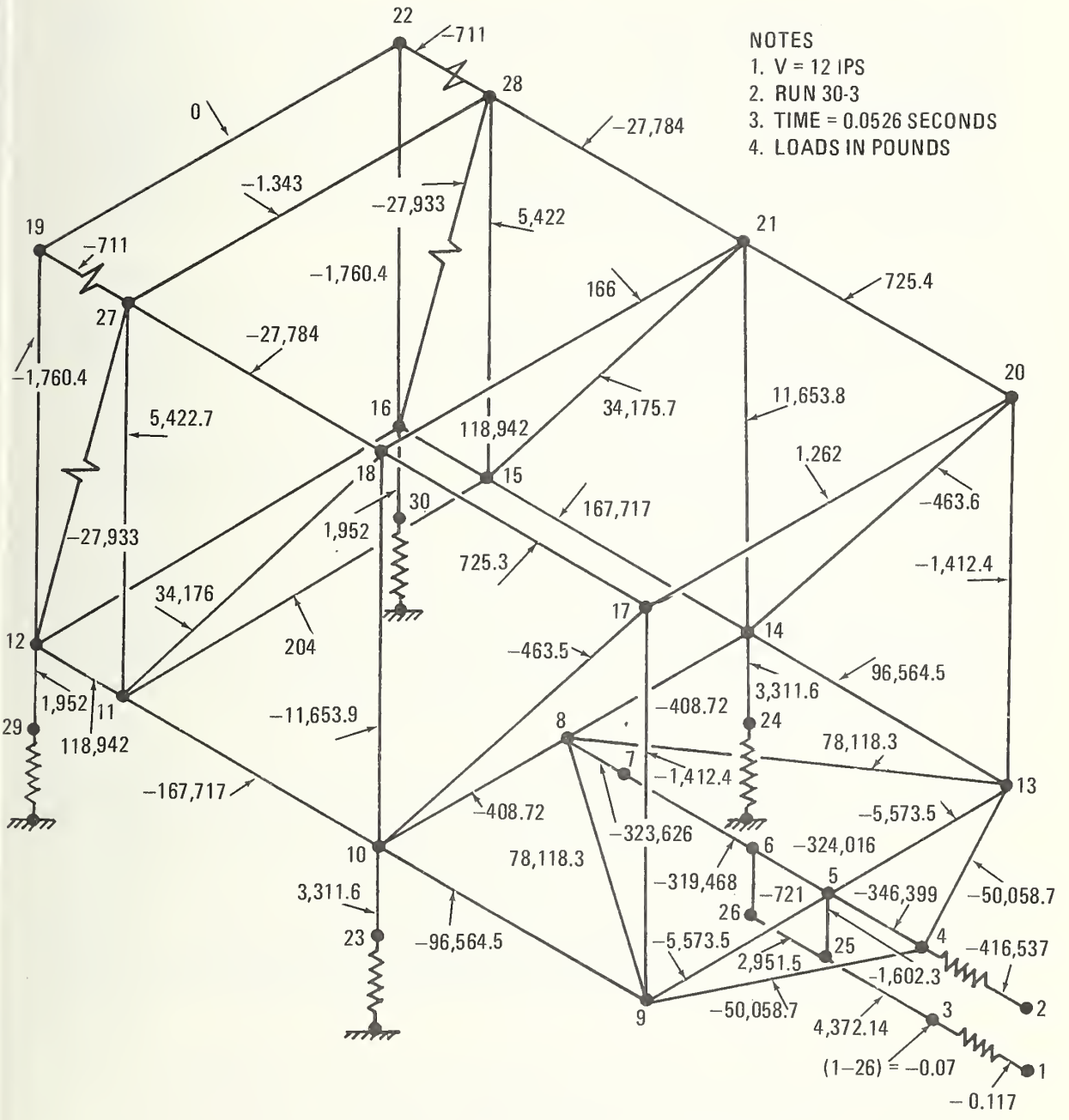

Figure 2−7. 30-Mass Model Static Test: Axial Loads in Members

underframe to represent the shear transfer across the frame. Elements such as 5-10 and 5-14 were considered. Also, for the transfer of shear through the car sides, elements such as 9-18 and 10-27 might have been used. The use of these elements would tend to modify the local load distributions. These elements would tend to act in compression. In compression, the shear elements have a relatively low buckling allowable stress and in the post-buckling region tend to unload rapidly with deflection. Consequently the gross model behavior does not suffer from the approximations.

Another application is the barrier impact in which the primary contact is made with the anticlimber. The initial velocity is 25 ft/sec (300 in/sec). The draft sill deformation as a function of time is shown in Figure 2-8. The solution is valid through t = .06 second, after which the barrier anticlimber element (2-4) goes into tension in the rebound action which is in violation of the crash conditions. The draft sill deforms in axial plastic yielding in element 5-6 and takes the characteristic buckled shape with plastic hinges at nodes 5, 6 and 7. The end sill and corner post welds ruptured early in the crash.

The axial load in element 4-5 is shown in Figure 2-9. The average load in the draft sill was 833,000 pounds for this condition. Comparison with Figure 5-4, the average load is 200,000 pounds greater than for the case where the initial impact is with the coupler followed by anticlimber contact. Further, the peak axial loads for the anticlimber contact reach 1.3×10^6 lbs. This is 2.6 times greater than the design static yield load.

Since the trucks comprise about 30% of the car empty weight, it was of interest to examine the behavior of the trucks during impact (Figure 2-10). The forward trucks reacted almost instantly to the impact by decelerating with a linear velocity change with time having a 100 cps vibration superimposed. The aft trucks experienced a delay of .01 second before starting to decelerate. If the "speed of sound" in steel is taken to be 15,000 ft/sec, the delay for a small disturbance would be .004 second. The aft trucks experience a constant deceleration giving a linear velocity change with time. The aft trucks showed a 40 cps vibration.

In the third case, Run 30-4, the coupler made contact with the barrier followed by the anticlimber contact. The draft sill deformation is given in Figure 2-11 and the loads in element 4-5 are given in Figure 2-9. In addition to the end sill (elements 5-9 and 5-13) and the corner posts (elements 9-17 and 13-20), rupture was experienced in the coupler (3-25) and in the coupler carrier (element 5-25).

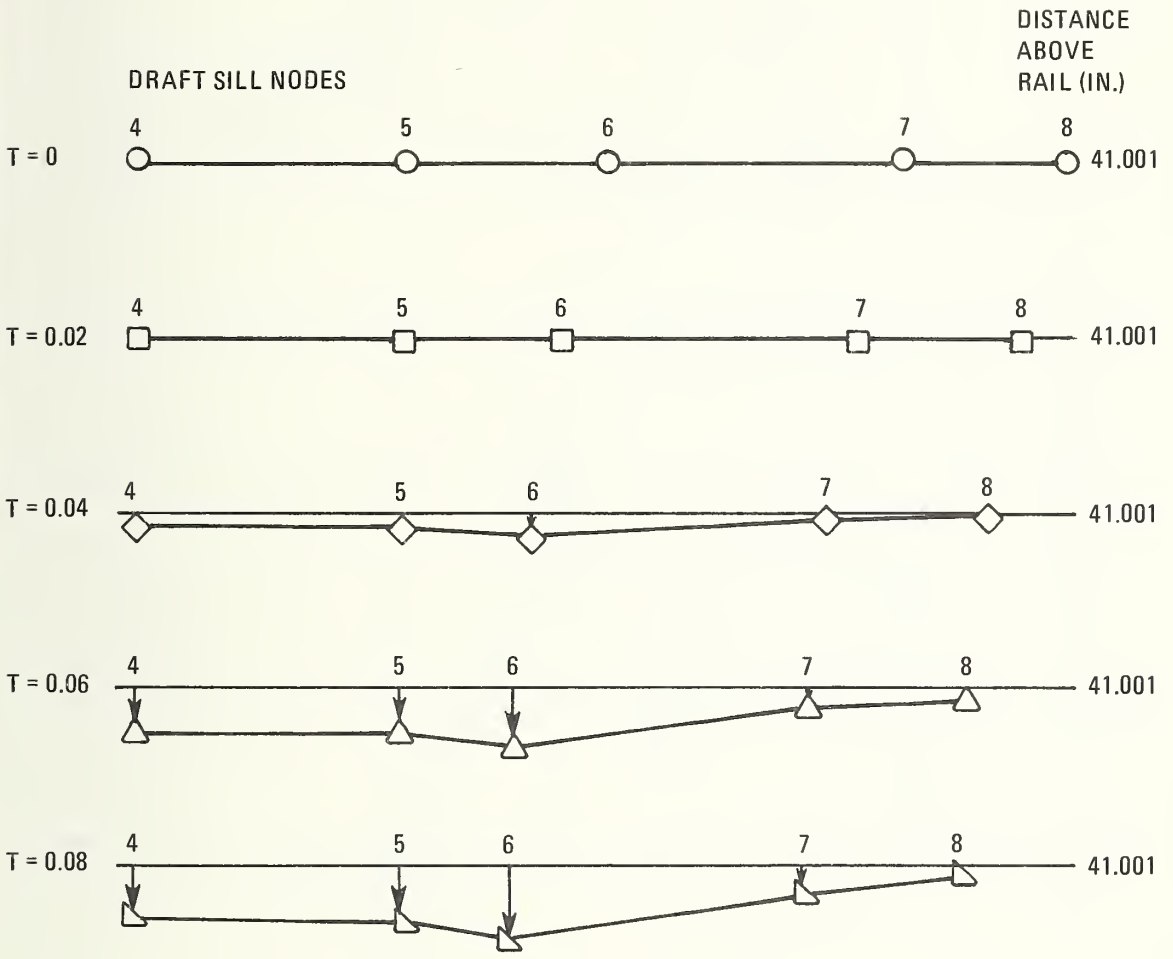

NOTES:
1. 1 INCH EQUALS 10 INCHES IN THE VERTICAL DIRECTION ↑ Z^+
2. 1 INCH EQUALS 20 INCHES IN THE HORIZONTAL DIRECTION → X^+
3. RUN 30-6
4. V_0 = 300 IPS

Figure 2–8. 30-Mass Model Coupler Impact: Draft Sill Deflections Versus Time

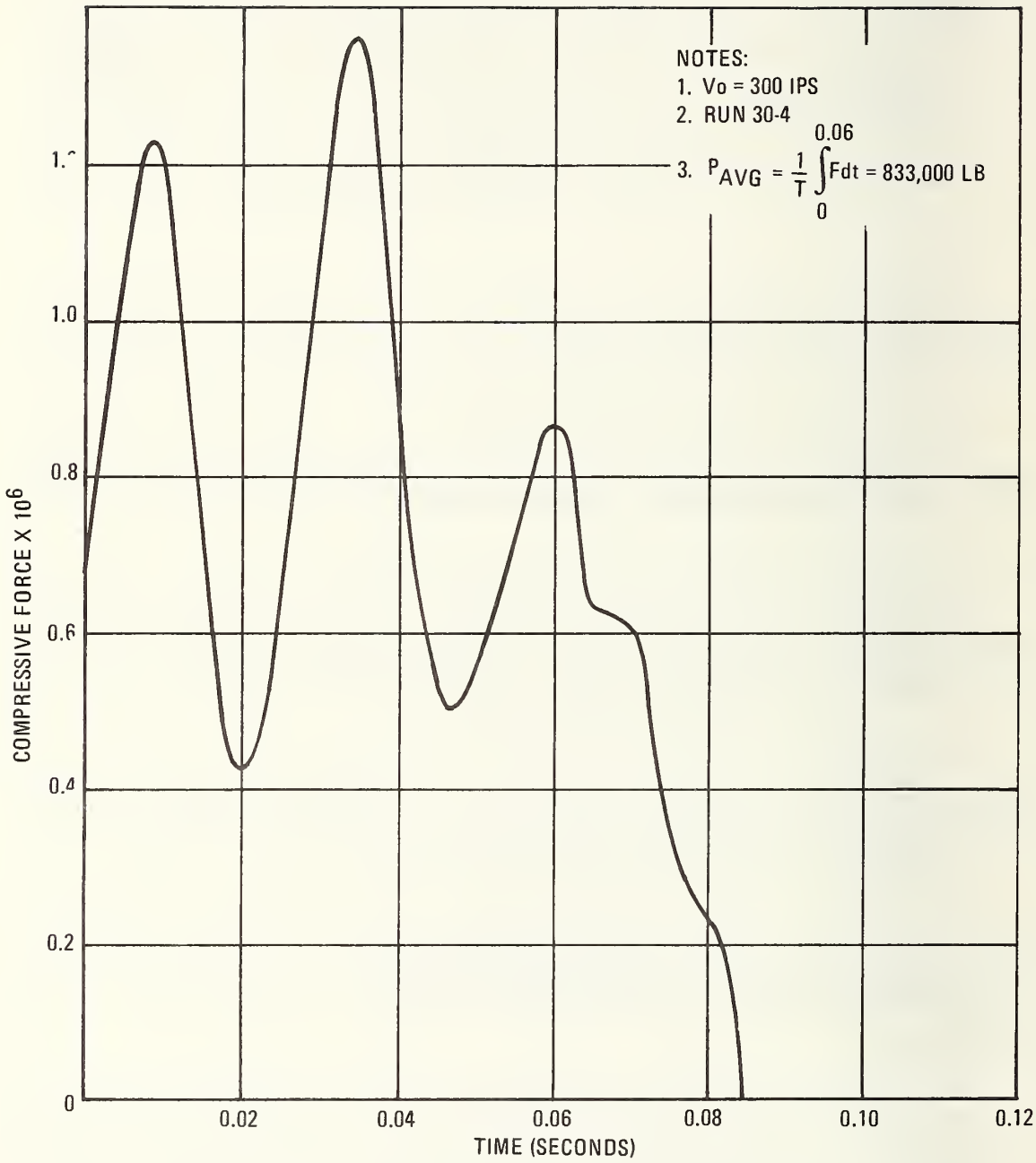

Figure 2–9. Anticlimber Contact: Axial Load in Element 4-5

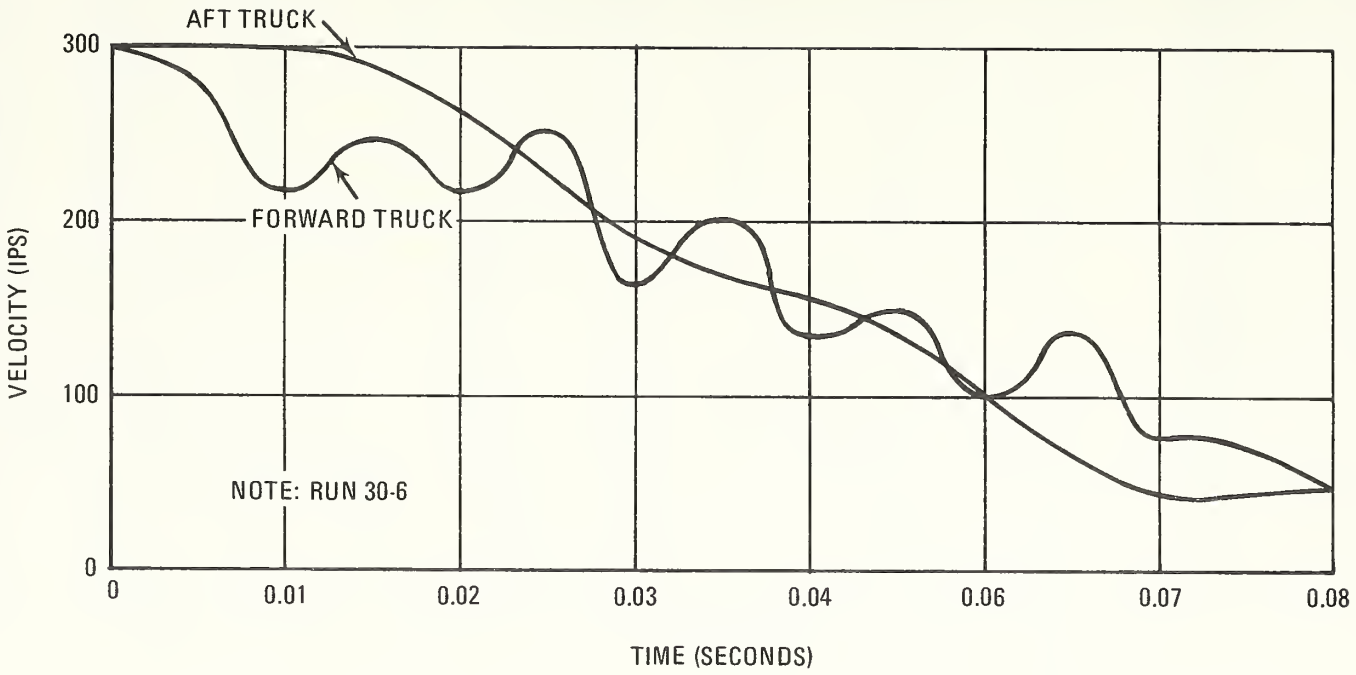

Figure 2–10. 30-Mass Model Coupler Impact: Truck Velocity Versus Time

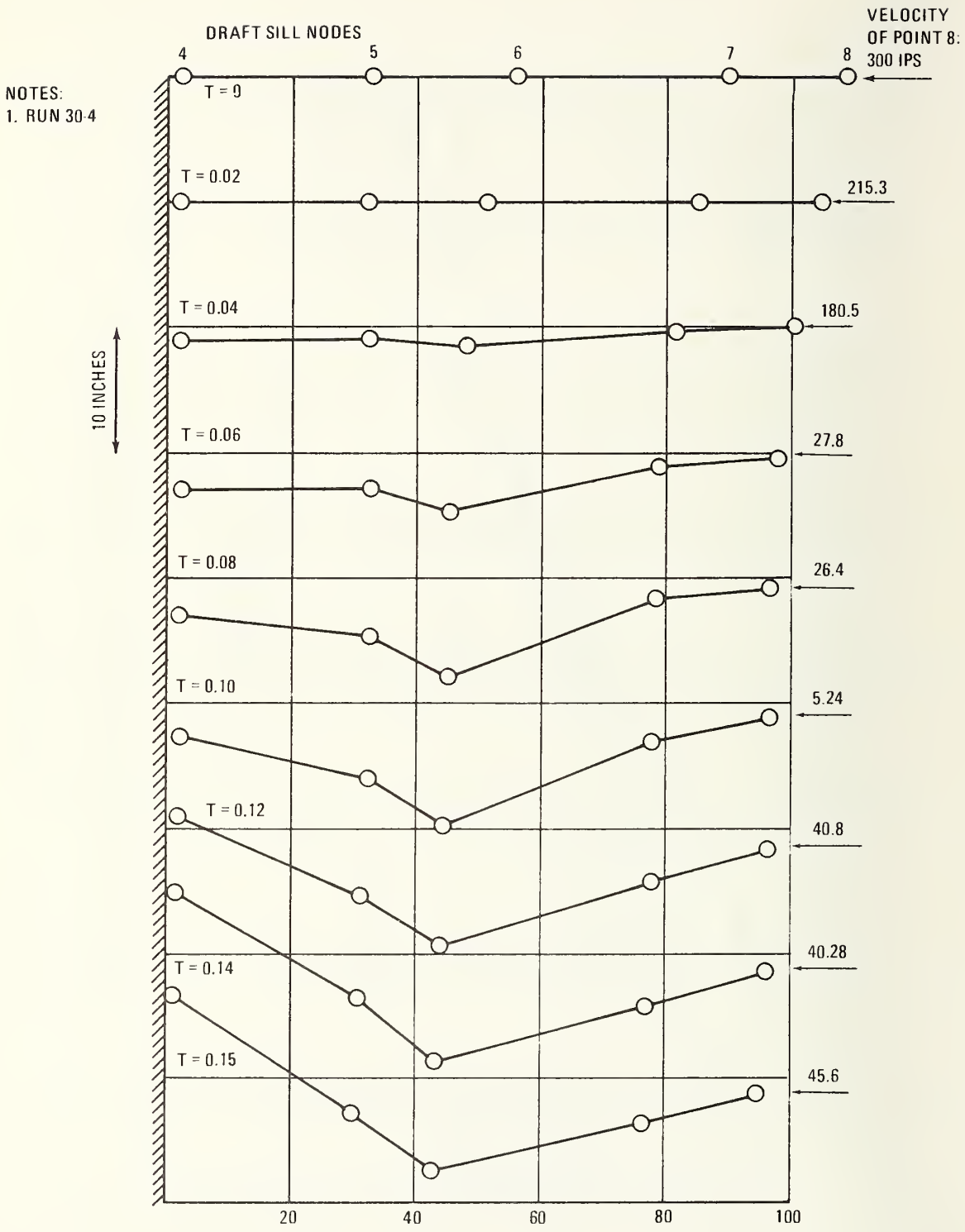

Figure 2–11. Draft Sill Deflections Versus Time

NOTES:
1. 1 INCH = 10 INCHES VERTICAL DIRECTION (+) (Y)
2. 1 INCH = 20 INCHES HORIZONTAL DIRECTION (+) – (X)

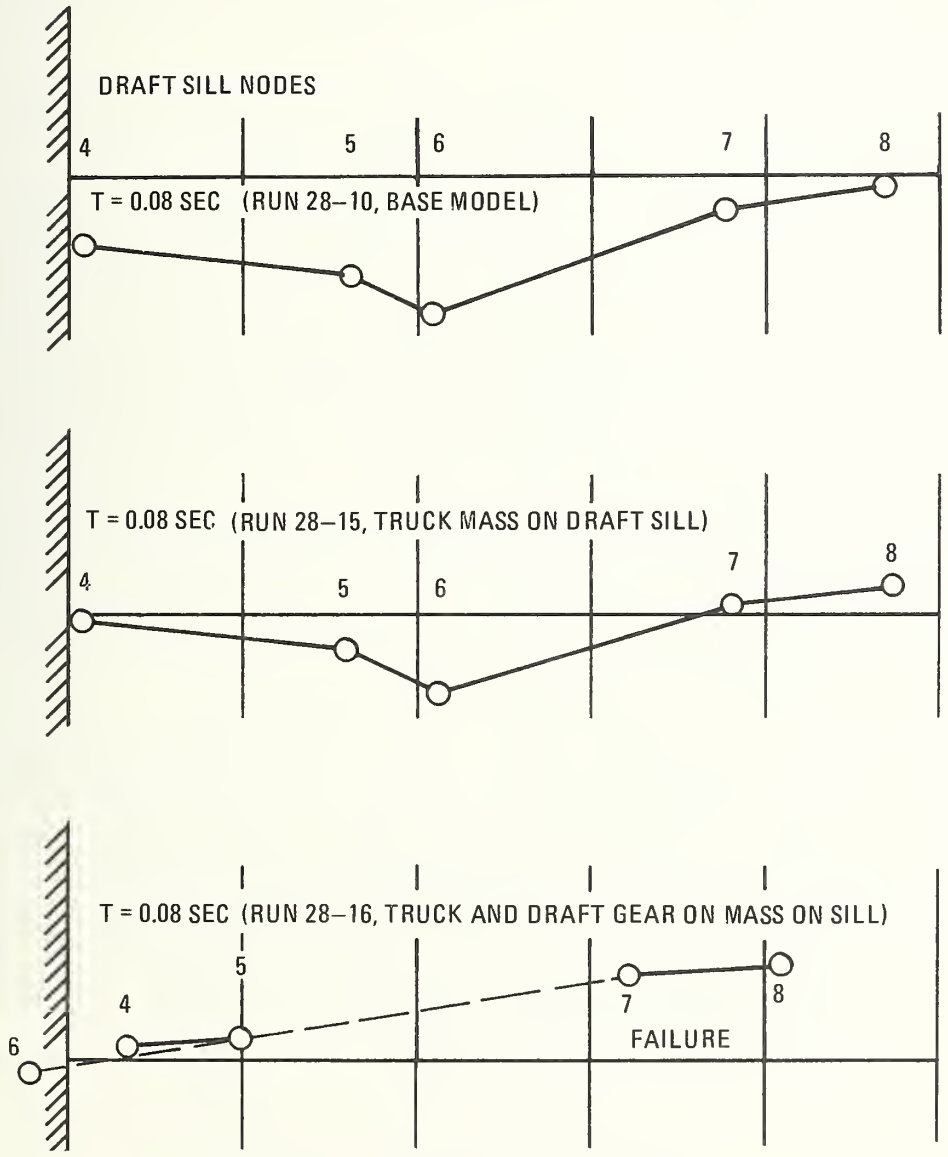

Figure 2–12. Anticlimber Hitting Barrier: Draft Sill Deflections for Different Mass Arrangements

Comparison of the draft sill deformation shows that draft sill behavior is essentially the same for both cases. This was surprising since in Run 30-4 the draft sill is given an impulsive moment by the coupler load. The effect of this coupler load is to counteract the inertial load of the coupler draft gear mass. As stated above, the average draft sill load for anticlimber contact was 200,000 pounds greater than the coupler/anticlimber case. The peak loads were similar with the anticlimber case being the greater.

The question as to why the draft gear buckles as it does has been investigated. It was thought that the underslung mass of the trucks was the cause. To investigate this the mass of the trucks was moved from nodes 23 and 24 to nodes 10 and 14. A comparison of the draft sill deflections is shown in Figure 2-12. As can be seen, the basic mode of deformation was not affected by the location of the truck mass. In Run 28-16 the mass of the draft gear and the coupler (nodes 3, 25 and 26) and the barrier, mass 1, were located in the plane of the underframe. This eliminated the moments due to the underslung inertial loads. The draft sill deflection is also shown on Figure 2-12 for this case. As can be seen, the mode of failure of the draft sill has changed from a beam column to a simple compression failure. This becomes significant in designing a draft sill that does not buckle.

The KRASH model does show the elastic response of the underframe during impact. Figure 2-13 shows the vertical bending of the side sill during impact of the draft sill. As can be seen, the response is a combination of the first vertical bending mode and a rigid translation and rotation. Node 9 experiences a maximum downward deflection relative to t = 0 second of 4 inches.

In the prevention of overclimbing, the draft sill and side sill behavior may become significant. The bending slope of the underframe at the anticlimber could contribute to the generation of significant vertical forces and pitching moments (about the car center of gravity). Even at small angles, the large axial impact loads could have vertical components exceeding the weight of the car. As regards the vertical displacements, the downward deflection of the underframe of the SOAC contributed to the failure of the gondola anticlimber and to the gondola car body being above (over) the end weldment of SOAC. Thus the vertical flexibility may be an important parameter in the problem.

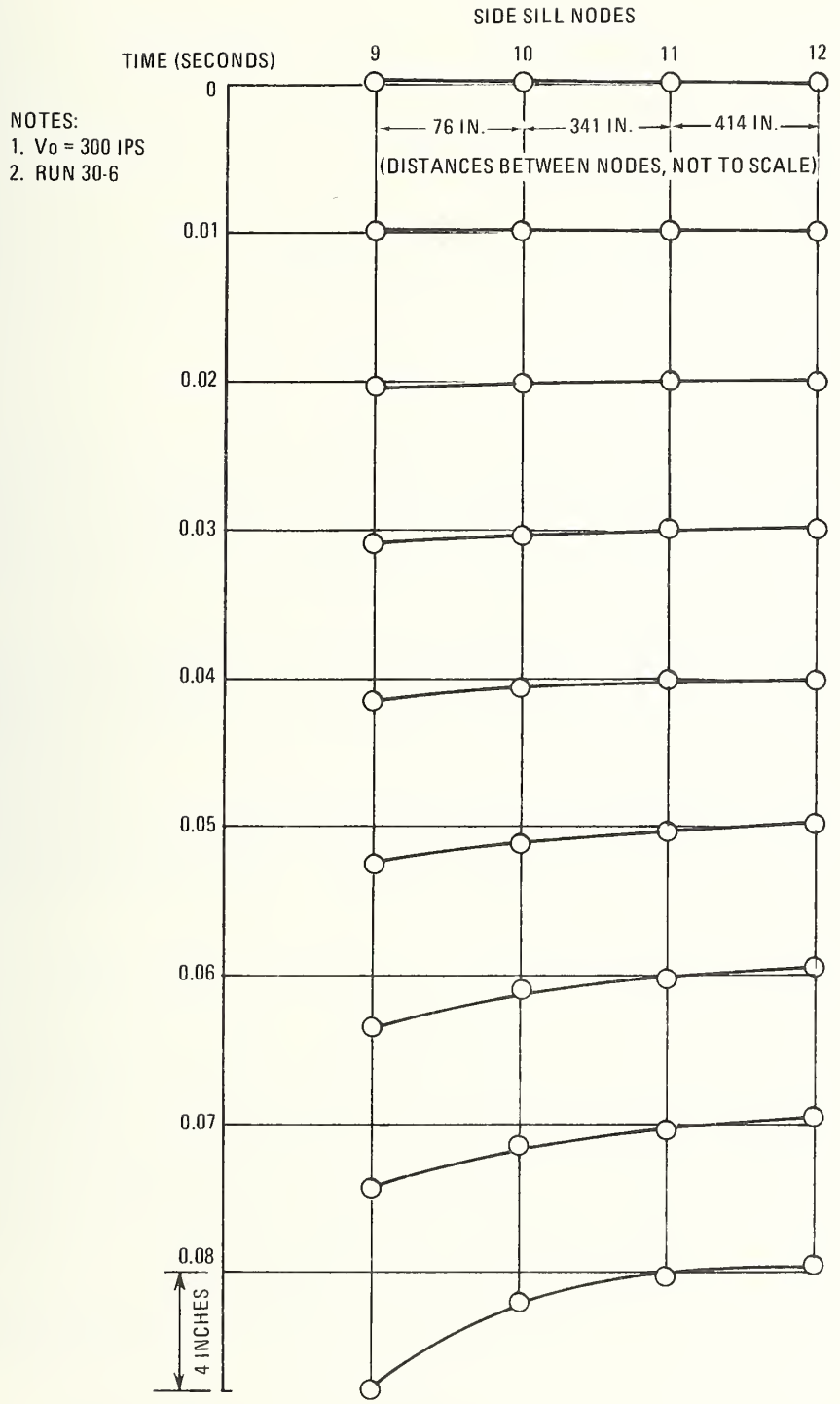

Figure 2–13. Side Sill Vertical Deflection for Coupler Impact Versus Time

3. REVIEW OF TEST AND CRASH DATA

A review of the R-44 static test data, the SOAC crash data, and the SOAC damage has been conducted. The static test data was reviewed to establish the ultimate strength of the car, the relative strengths of the car elements, and the distribution of loads in the elastic range.

The accident damage data was reviewed to determine how the various elements of the car performed in the crash. The review included both the sequence of events and the extent of the damage. An effort was made to establish the extent and mode of deformation.

These data are compared with the analytical results for the car model in a general crash and with the analysis of major structural elements. The data are also to be used in the analysis of specific crash conditions.

STATIC TEST DATA

The static test data was provided by the New York City Transit Authority. The data is proprietary to NYCTA and has been summarized for the purposes of this study. The R-44 car is structurally similar to the SOAC. Some modifications were made to the SOAC draft sill and to the SOAC bolster. However, the load distributions, particularly between the draft sill and side sills and between the side sills and the cove (sides and roof) in the car center, are applicable to the SOAC.

The R-44 car was subjected to four structural tests. The R-44 specification requires the following static tests (see Appendix D).

- Paragraph 3.12(e) calls for a vertically distributed load of 62,000 pounds--allowable stress is 50% F_{TY}.

- Paragraph 3.12(f) calls for a squeeze load of 250,000 pounds on the anticlimber of a light car--allowable stress is half yield and allowable deflection on the centerline between bolsters at the side sill is 0.205 inch maximum.

The first test car was subjected to the vertical load and then the squeeze load; the deflection was considered unacceptable by the buyer. St. Louis Car Company strengthened the shell and retested.

The retesting indicated an area of high stress, in the corner of a window, was not acceptable and was an area of excessive buckling. The buckling was noticed on the first test series and was strain-gauged for the second series. The area was reinforced and was not strain-gauged during the overload testing accomplished later. The draft sill stress level was acceptable based on a survey of material properties being supplied to St. Louis for the R-44 sills. This showed a F_{TY} level of 60,000 psi compared to the minimum of 50,000 psi assumed for the material.

At this time the buyer was concerned about buckling of the shell, and St. Louis Car was required to test to special overload conditions. These tests were conducted on a new shell with the reinforcements incorporated.

- The first test required a 225,000-pound buff load on the coupler with the car light, plus the 49,000-pound passenger load.

- The second test required an anticlimber load of 400,000 pounds on a light car plus 49,000 pounds; the allowable stress was raised to 80-percent yield, but the buyer stipulated that stresses in the order of 72- to 75-percent of yield would require retesting on another shell.

The data used herein is the test of the 250,000-pound squeeze load applied to the anticlimbers. The strain readings have been converted to axial loads in the structure, assuming the resistance is developed as in Figure 3-1. The results are summarized in Table 3-1. NYCTA used the tests for acceptance and suitability for service. Where secondary members showed high stresses or buckling, these areas were reinforced to resist imposed loads. The result was a total structure capable of resisting a relatively high end load.

The strength of the load-carrying structure was evaluated using F_{TY} = 50,000 pounds at STA. 200. STA. 200 was used because it is representative of the structure between the bolsters and because the strain data for this station was linear with applied load. As can be seen, an anticlimber load of between 730,000 and

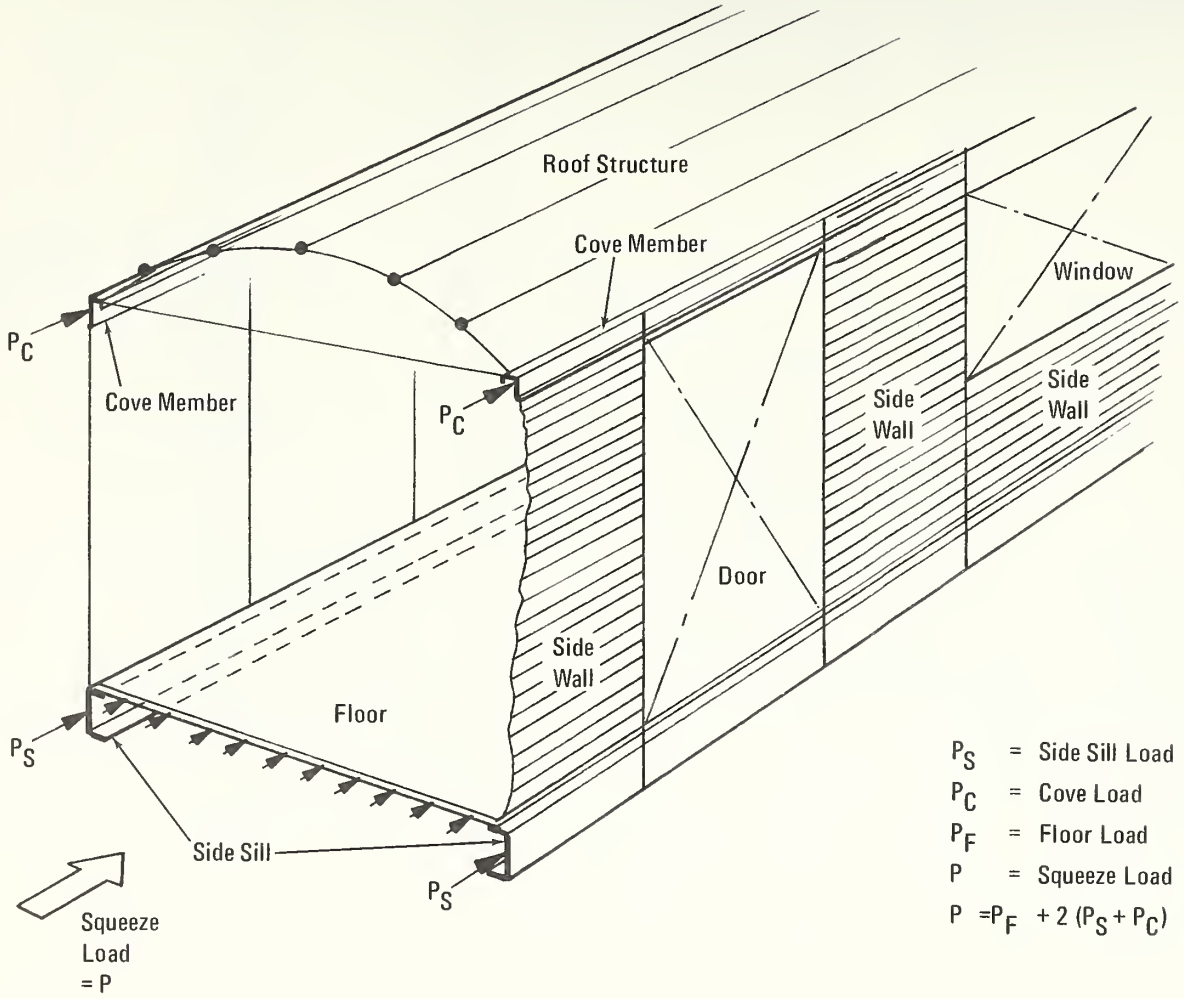

Figure 3--1. Location of Members Assured Active in Resisting Squeeze Load (R-44 Car)

TABLE 3-1. EVALUATION OF R-44 STATIC TEST DATA

Stress and Load Data for Members at Station 200:

Using data available for structural members:

Side Sill: Gages 9 and 10

Cove Member: Gages 43 and 47

Squeeze Load (lb)	Direct Stress (σ_A)	
	Side Sill	Cove
50,000	– 1,704	– 979
150,000	– 6,670	–3,263
250,000	–11,274	–5,511

Load Distribution Estimates:

In addition to the side sill and cove members the floor is capable of carrying direct loads.

Floor: 3/4-inch plywood with 0.02 steel skins top and bottom (bonded)
Attached to side sill area by 1/4-inch-diameter huck bolts at 6-inch pitch
Attached to cross beams at bolster area by 5/16-inch-diameter bolts at 3-inch pitch

Areas: Side Sill = 7.33 $in.^2$ per side
Cove = 1.05 $in.^2$ per side
Floor = 108 X 2 X 0.02 = 4.32 $in.^2$

Note: Floor area has capability of working up to yield because it is stabilized by being bonded to the 3/4-inch plywood. In addition, the contributions of secondary structure are attributed to the floor for the purposes of accounting for the load.

TABLE 3-1. EVALUATION OF R-44 STATIC TEST DATA (Continued)

Distributing Squeeze Loads:

(Floor Load Computed for Equilibrium)

Squeeze Load (lb)	Total Side Sill Load	Total Cove Load (lb)	Load in Floor (lb)
50,000	24,981	2,056	22,963
150,000	97,782	6,852	45,366
250,000	165,277	11,573	73,150

Note: The actual floor loads will be less than these values since the side walls, cutout surrounds (doors and windows), and the roof have been assumed ineffective.

Summary of Direct Stresses:

Squeeze Load (lb^2)	Direct Stress, σ_A ($lb/in.^2$)		
	Side Sills	Cove Members	Floor
50,000	– 1,704	– 979	– 5,316
150,000	– 6,670	–3,263	–10,501
250,000	–11,272	–5,511	–16,933

Percentage Load Distribution:

Squeeze Load (lb)	Load Distribution (%)		
	Side Sills	Cove Members	Floor
50,000	49.96	4.11	45.93
150,000	65.19	4.57	30.24
250,000	66.11	4.63	29.26

$$\text{End load (yield)} = \frac{50{,}000}{16{,}933} \times 250{,}000$$

$$= 738{,}203 \text{ lb}$$

$$\text{End load (ultimate)} = 1.4 \times 738{,}203$$

$$= 1{,}033{,}484 \text{ lb}$$

1,000,000 pounds might be sustained before yield in the major load-carrying structure is reached. Since yielding of secondary load paths will result in a redistribution of load, these values must be used cautiously. These results do show that a load which might cause local yielding in the draft sill could be carried successfully between the bolsters.

ACCIDENT DATA

An understanding of the SOAC accident at Pueblo and a reconstruction of the conditions throughout the accident were gained from the NTSB report 1 and from an independent study by Boeing Vertol, the results of which were made available to the NTSB.

From the Boeing study, the energy balance indicates that the SOAC hit the standing train at a velocity of between 26 and 40 mph with the most probable impact velocity being 35 mph.

The car collision sequence from the Boeing study is given in Appendix A. This sequence is a reconstruction based on the examination of the debris at the test site and an inspection of the damaged vehicles, and was established prior to the present study. The account is valuable for the identification of structural damage to both cars; it presents a good background for the study.

Of particular significance to the understanding of the crash damage are the heavy damage to draft gear of both the SOAC and the gondola, the failure of the gondola anticlimber, the detrucking of the gondola, the column collapse of the SOAC draft sill, the overclimbing of the SOAC anticlimber, and penetration of the SOAC by the gondola body. This damage is shown in Figures 3-2 and 3-3.

After the accident, the SOAC and debris were returned to Boeing Vertol for repair. A further examination of the damage to the SOAC structure was made. The draft sill deformation, the collision posts, side sills, weld joints, etc., were examined and photographed. These data provide insight into the SOAC crashworthiness capability.

The deformed draft sill pieces removed from the car are shown in Figures 3-4 through 3-6. Figure 3-4 shows two views of the section adjacent to the bolster. Here, a plastic hinge is

Figure 3-2. *Damage to SOAC*

Figure 3-3. *Damage to Gondola*

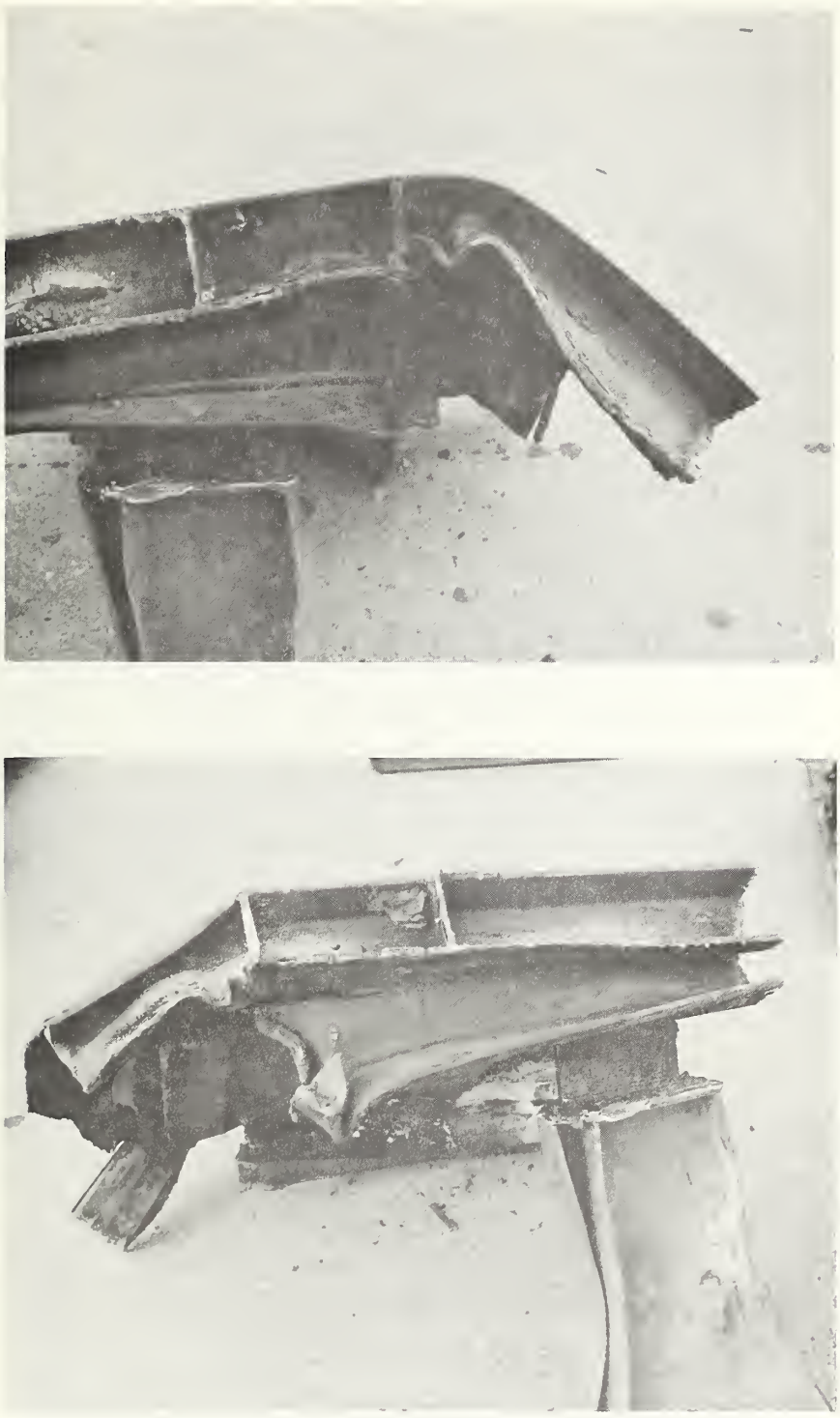

Figure 3-4 *Draft Sill, Section Adjacent to Bolster*

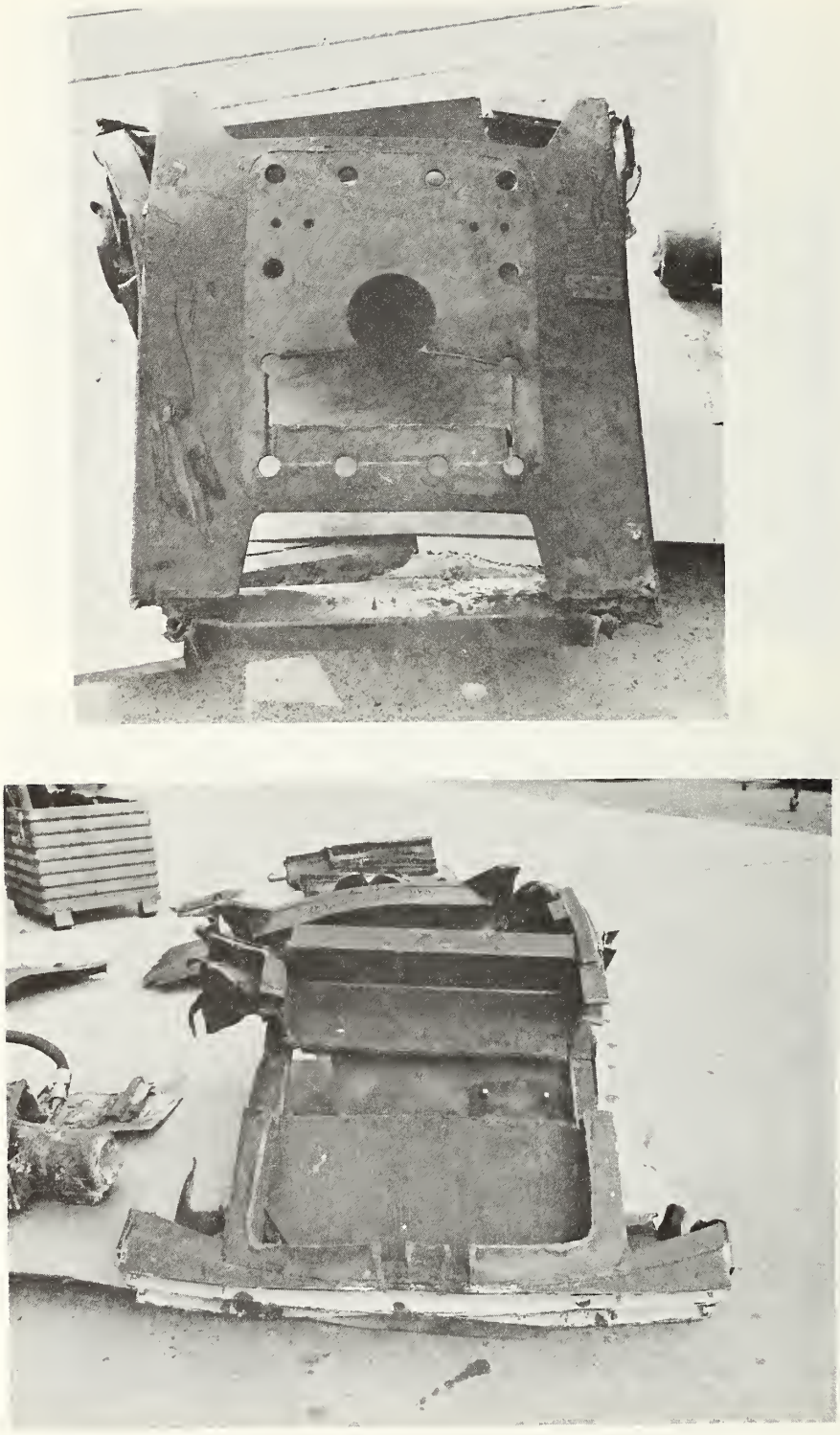

Figure 3-5. *Draft Sill Anchor Plate and Plastic Hinge*

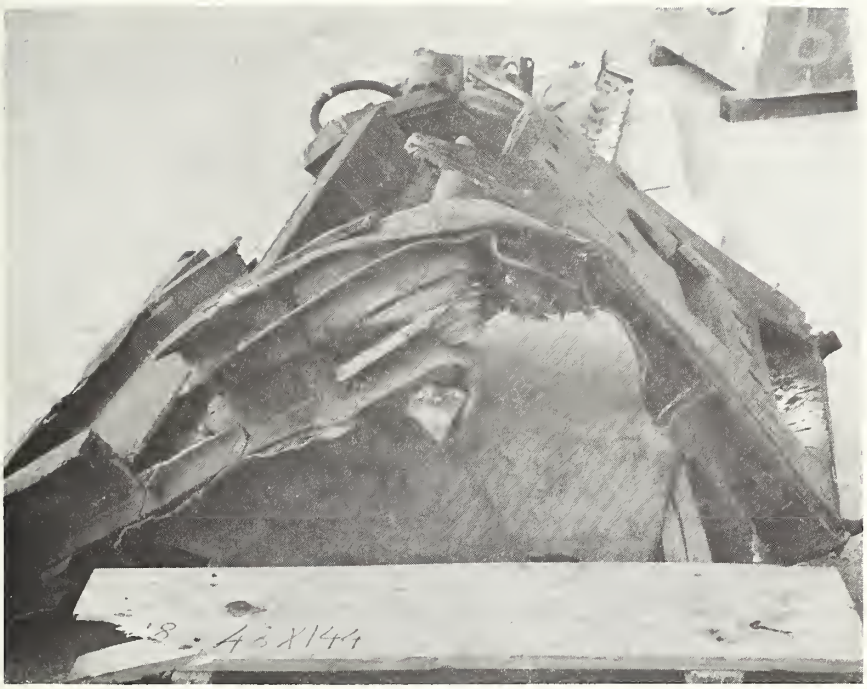

Figure 3-6. Second Plastic Hinge in Draft Sill

formed where structural changes occurred. The beam depth tapers from 6 inches at the bolster to 8 inches at the hinge. In addition the draft anchor plate (1/2-inch thick), shown in Figure 3-5 (top), joins the tapered section at the point of plastic deformation.

Figure 3-6 shows a second plastic hinge in the draft sill. In the second case, the failure probably initiated where the draft anchor plate meets the lower flange reinforcement and progressed aft as the weld between the draft anchor plate and the draft sill channels separated. The crimp then formed in the weakened draft sill in the vicinity of the anchor post. Figure 3-5 shows that, in addition to the plastic hinges, the draft sill experienced compression yielding over essentially the full length. Significantly the anticlimber, the backup plate, and the associated weldments remained intact even though some yielding is evident.

The collision posts are shown in Figure 3-7. As may be seen, they were attached to the car by weldments to the floor plate and by welds along the bottom edge. These posts failed by tearing of the floor plate and by rotation of the lower weld. It is obvious that the collision posts did not develop their full strength because the 3/8-inch plates show little deformation. Also, the failure of the attachment did little to absorb energy in the collision.

The coupler (which is discussed in Section 2) is shown in Figure 3-8. It took the initial impact. The shear pins failed and the coupler bottomed. The coupler shank failure is shown in the top picture, and damage to the vertical rotation stop is shown in the bottom picture.

The floor closing end sill and the light structure forming the platform extending forward to the anticlimber are shown in Figures 3-9 and 3-10. The end sill is made from two 8-inch channels welded to form a box beam. This beam spans from the side sill to the draft sill. It is the major transverse member forward of the bolster, and in conjunction with the floor plate, it transfers load from the draft sill to the side sill in end-on loadings.

As can be seen, the end sill did not undergo much deformation. The failure of the seam welds forming the box (Figure 3-10) and the failure of the joints to both the draft and the side sills is evident. The end sill did remain in effect long enough to cause the side sills to take a permanent set in torsion. A possible local failure sequence is failure of the end-sill draft-sill joint by shearing aft due to the anticlimber forces being transferred through the short longitudinal channel. After

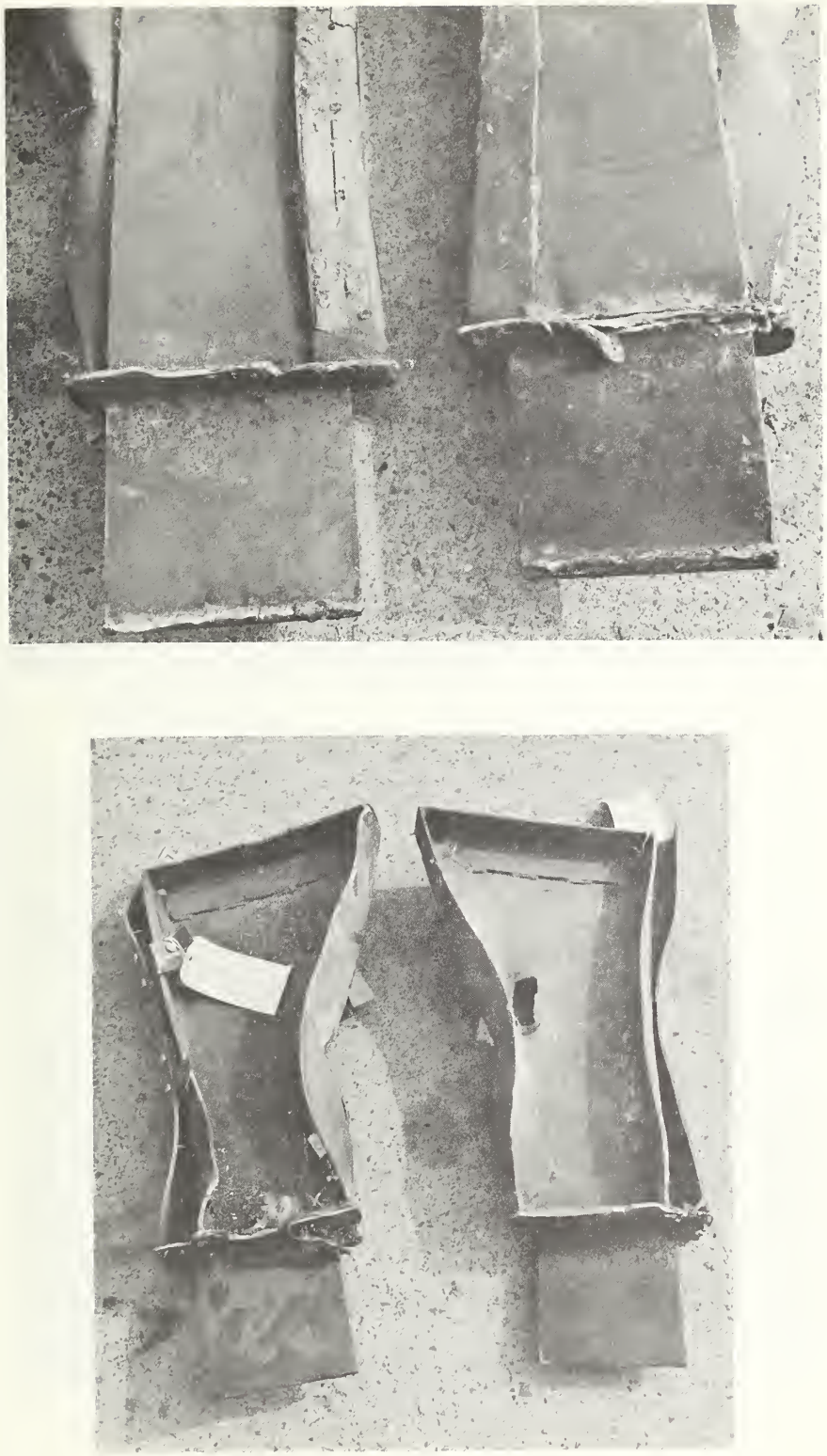

Figure 3-7. *Collision Posts*

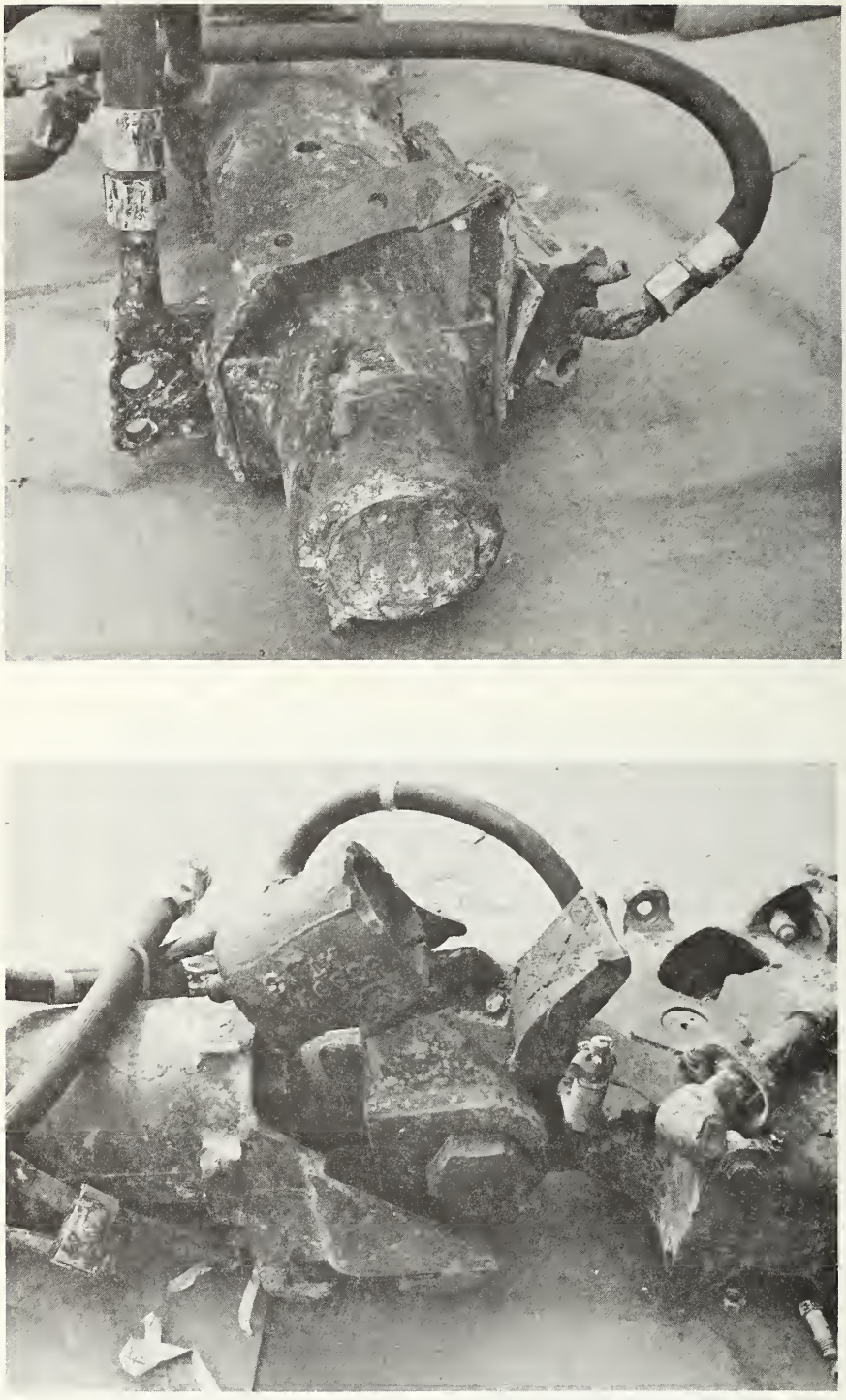

Figure 3-8. *Coupler*

Figure 3-9. *Floor Closing Sill*

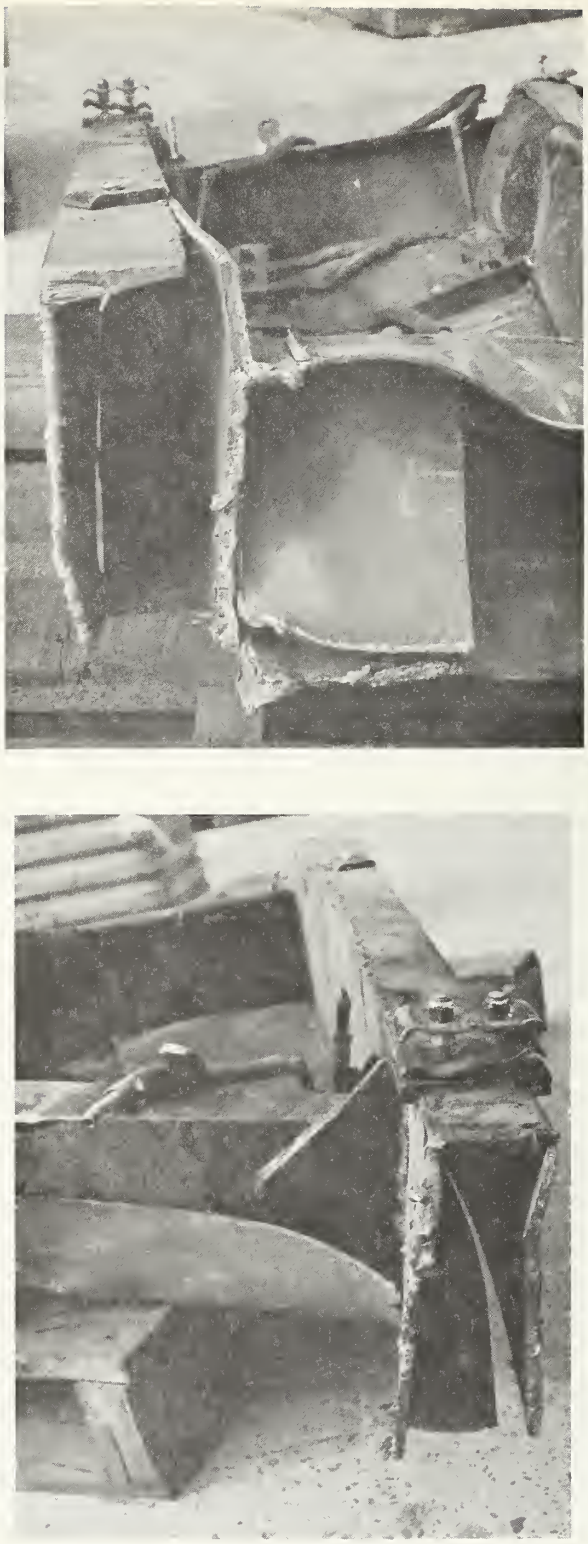

Figure 3-10. *Failure of Floor Closing Sill Seam Welds*

that joint ruptured, the torsion in the longitudinal channel occurred as the draft sill deformed downward and the side sills took their set.

The side sills, shown in Figure 3-11, deformed primarily in torsion. The permanent twist in both side sills is clearly evident. The left sill (bottom) appears to have set due to lateral bending. This bending may be due to a lateral shift in the draft sill pushing through the left end sill. Figure 3-12 shows the weldments for the end sill. These joints failed in the weak bending mode.

During the repair of the car, the forward bolster was checked for distortion and was found to have bowed upward. The forward beam of the bolster had a set at the car centerline of approximately 0.59 inch up relative to the side sills. The aft beam of the bolster had a set of approximately 0.17 inch up. Inspection of the side sills between the bolsters indicated that no detectable set was experienced in this area. Inspection of the sheet metal insulation pans in the car center section revealed that a compression set had occurred. The damage did not warrant replacement of the insulation pans. However, this type of set implies large deflections of the bolster relative to the side sills in the plane of the underframe.

The reinforced shear plates that transfer loads from the draft sill to the side sills formed deep permanent buckles, as shown in Figure 3-13. These plates were cut from the underframe during the repair. In the top picture the diagonal buckles indicate that, in the final phase of the collapse of the plate, the panel acted as one large unit with the reinforcing angles becoming less effective as the collapse progressed. These plates appear to have performed well.

ASSESSMENT OF CAR DAMAGE

In the accident the SOAC demonstrated strength in excess of design requirements and demonstrated full design performance of the anticlimber and support structure. However, even so, a general observation is that the SOAC did not utilize the material present in the car to its fullest capability to absorb energy. Specific items where the energy absorption could be improved include the following:

- Collision posts
- Side sills forward of bolster
- Draft sill cutouts
- Bolster cutouts
- Joint weldments
- Underframe arrangement
- Shear ties to the roof
- Redesigned bolster
- Purlin sections
- Corner post

These items are discussed and recommendation for improvements are treated.

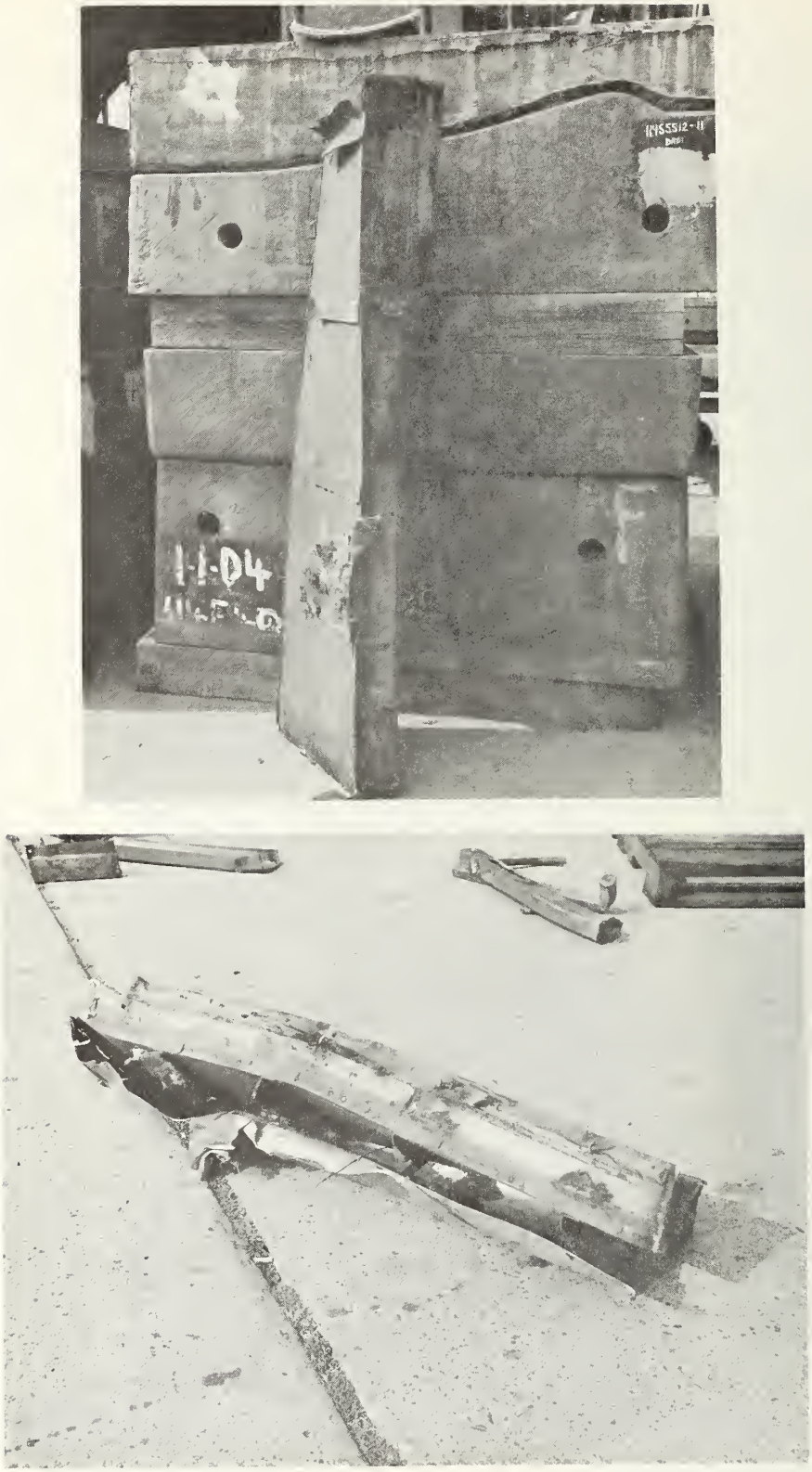

Figure 3-11. *Side Sill*

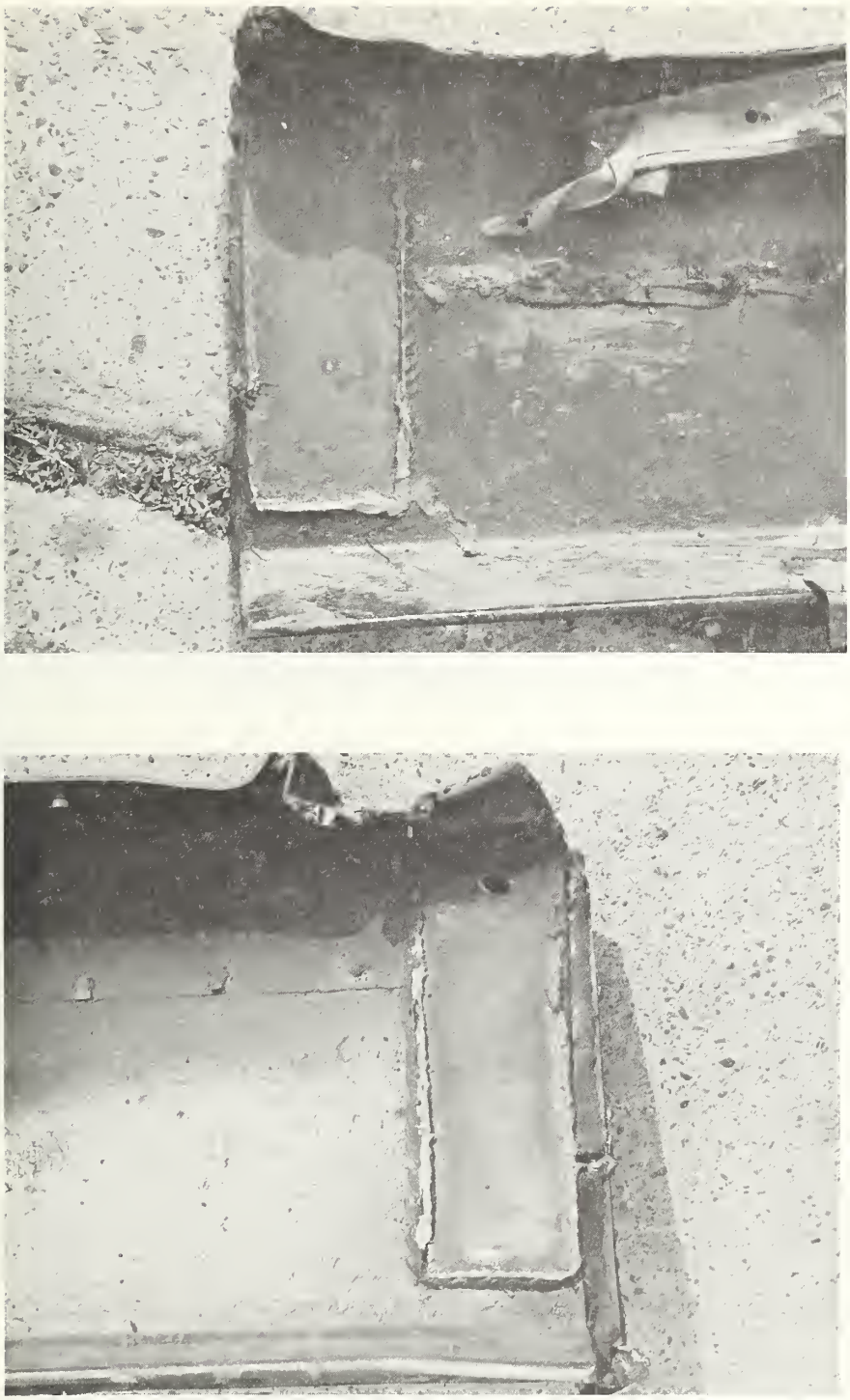

Figure 3-12. End Sill Weldments to Side Sills

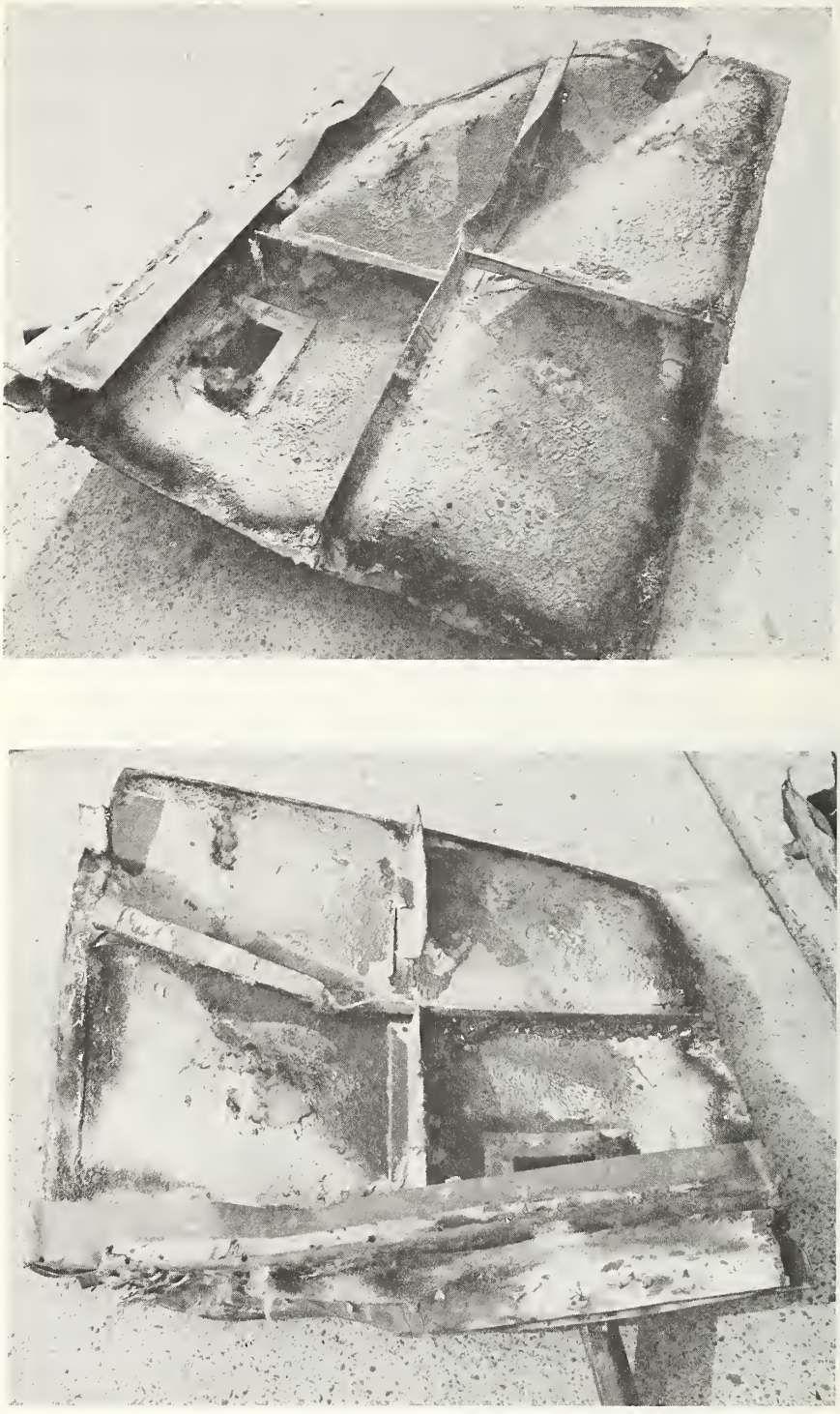

Figure 3-13. *Shear Plates*

Collision Posts

The collision posts for SOAC are cantilevered from the floor plate. These posts do not extend to the roof structure and so do not carry loads to the roof structure. The weld installation of the collision posts did not have sufficient strength to cause the underframe to develop its yield strength in the event of overclimbing. Further, the cantilever configuration precluded the rapid transfer of load to the roof structure.

Side Sills

The side sills forward of the bolster could have carried more of the crash buff loads. This was due in part to the inability of the floor closing sill and the end weldment to bridge loads from the anticlimber to the side sills, and in part to the reinforced shear plates which do not extend forward of Station 52. Further, the attachments of the floor closing sill, the end weldments, and the corner and side posts were designed for non-crash static strength requirements. Thus the side sill is not forced to absorb energy either in the anticlimber crash or in the case of overclimbing.

Draft Sill

The draft sill was designed to meet the static buff requirements. The structural section has discontinuities in the form of cutouts and section changes for equipment access and clearances. The addition of the draft anchor plate and the coupler carrier result in the neutral axis and column centroid introducing eccentricities which reduce the load capability. The draft sill did absorb energy in the crash; it developed a double plastic hinge and was plastic under axial load. It is not altogether clear that increasing the capability of the draft sill by itself would result in high energy absorption in a crash, since there is a strong likelihood that the deformation may then occur in the bolster. These elements should be tuned to maximize the energy absorption of the complete structure.

Review of the draft sill design indicates that a systems approach in which all the requirements are integrated into the design might result in a more serviceable draft sill with less weight and greater crash capability.

Weldments

The weldments used in the SOAC were adequate to sustain the specified design loads. As such the weldments would be considered satisfactory for normal car usage. However, review of the accident damage indicated that many of the welds failed without causing the development of the potential energy absorption in the structure. Cases in point are the collision posts, the end sill and floor closing sills, the floor beams, the shear plates, and the corner and side posts. The notable exceptions are the anticlimber with its backup structure and the draft sill.

Analysis of the joints that failed indicated that in the crash condition the joints were subject to combinations of loads that resulted in joint rupture before the inherent strength of the structure in these conditions was developed. For instance, the floor closing sills split along the seam weld, probably due to a combined bending and torsion as a result of the draft sill buckling. The side/floor closing sill joint probably ruptured in a bending stress distribution. It should be noted that the welds are considerably weaker in this condition than in shear.

There are many other examples, but the point is that the joints can be designed to develop the full strength of the members. With the exception of the anticlimber, no gussets or clips were used. In the case of the collision posts, more length of weld and plug welds could have been used to help provide the needed strength. A similar argument could be made for the corner and side posts.

Corner Posts

The corner posts appear to have been designed to provide support for the roof and for the fiberglass car end. There is a decided mismatch in the strength of the corner posts when compared to the side sill.

The corner post is supported in the fore and aft direction by the car sides. On the motorman's side there is a large window for approximately the upper half of the post. However the car sides, as shown in Table 2-1, provide little resistance. Thus the crashworthiness could be improved by increasing the size of the corner posts, the backup structure and the attachments to the roof, the belt rail, and the side sills.

Underframe Arrangement

The general arrangement of the underframe requires the transfer of load from the anticlimber/draft sill at the car ends to the side sills, the floor, and the roof in the car center section. In the car end, the draft sill axial loads are transferred to the side sills by shear plates and by the bending of the bolsters. In the car center, the side sill loads are partially transferred to the roof by shear through the sides of the carbody.

When compared to a center sill arrangement, this current arrangement has some advantages in the installation of equipment and may offer some weight advantage. It does impose load requirements on the floor shear plates, the bolster, and the car sides. The floor shear plates are critical in buckling, and even after developing a tension field, the welds failed. This failure forced the load through the draft sill and the bolster.

The bolster design contains cutouts for access and equipment installation. After the failure of the floor shear plates, the buildup of redistributed load would soon result in deformation of the bolster in fore and aft bending. The bolster did deform in a combination of torsion and vertical bending in the SOAC crash.

In summary, the SOAC demonstrated the full design performance of the anticlimber and support structure in the acccident. This performance could have been improved even further through control of the failure modes from basically the same structure. The design features discussed in this section could lead to this improvement.

4. FORCE DEFORMATION CHARACTERISTICS

FORCE DEFORMATION CHARACTERISTICS

The force deflection curve for static load application can be generated from the results given previously. In these load applications the failure mode follows a minimum energy path through the elements in the car and continues as the stronger elements fail. The final portion of such a curve shows the compression of compacted material as in bulk modulus testing.

In the real life crash the externally applied loads are reacted by the decelerating masses and result in a continually changing load distribution throughout the car. In the static force deformation simulation it is assumed that all the mass is concentrated at the car center. This is a simplification of a complex phenomenon which has value in understanding the gross behavior of cars.

For impact study purposes, the structure is symmetric about the car center. Thus the deflection will account for the contribution of each end of the car. The curves presented here are for the deflection of one car end. When a car is loaded from both ends the data must be treated as springs in series. For trainline acceleration studies, the deflection contribution of couplers is important. For instance, if the couplers maintain a 5-inch separation between anticlimbers of adjacent cars, after the first car crashes, the last car in a ten-car train would travel 45 inches before anticlimber contact. The introduction of the phase lag has important implications for the acceleration distribution in the train.

In the formulation of meaningful force deflection curves for the SOAC, the results of the elemental analyses summarized in Table 2-1, and the results of the dynamic simulation using the KRASH Program presented in Section 3 and the static test results and the review of the SOAC accident data presented in Section 3, should be used as a basis for the hypothesizing of a rational scenario.

Referring to the summary of the elemental analyses in Table 2-1, it may be seen that the underframe elements constitute both the primary load carrying and the principal energy absorption capacity. In particular, the draft sill and the side sills act in this manner. The relative load and energy-absorbing capacity of the other elements is seen to be of secondary importance. This is particularly true when the weldment rupture criteria summarized in Table 2-2 are considered. Thus, for anticlimber-to-anticlimber impacts, the deformation of the cars will be less than for the case of one impacting car overriding another.

The role of the draft sill is supported in the dynamic impact analysis using KRASH. Here 90 percent of the strain energy is absorbed by the end weldment and the draft sill. KRASH computes kinetic energy for each mass and the strain energy for each element. The value of 90 percent is obtained from elements (4-5), (5-6), and (6-7) of the draft sill, and from elements (4-9) and (4-13) of the end weldment. These elements were subjected to large plastic deformations accompanied by the absorption of strain energy. It should be noted that 10 percent of the strain energy content was in the elastic region, particularly for elements aft of the forward bolster. These dynamic analyses also confirmed the early failure of key joints as in the end sill to the draft sill and in the corner posts to the side sills.

The static test data indicate the car center probably is able to resist loads of at least 738,000 lbs. without yielding. Further, depending on the sequence of yielding and rupture failures, the car's center might support static loads in excess of 1,000,000 lbs. This higher load capacity is due in part to better distribution of loads between the side sills, coves, and floor. (The Floor in this study collects all secondary load paths.) The static tests also indicate the loads are not significantly transferred from the draft sill to the side sill in the car end.

The accident data also support the role of the draft sill and the significance of the welded joint rupture behavior. The correlation with the accident data is presented in Validation of the SOAC Collision Dynamics, Section 5.

The first case is for the application of a static load through the coupler faces at each end of the car until the coupler shear pins fail, followed by application through the anticlimber until "complete destruction" of the car is obtained. The end force that may be sustained is based on the sectional properties of the car with the weakest section failing first.

The application of this approach to simplify the crash dynamics has the effect of limiting the "resolving power" of analysis. The conclusions that can be drawn must be confined to the processes that involve "gross" properties of the car and respond as the car's center of mass. The scenario for the construction of this curve, shown in Figure 4-1, is as follows:

a. Coupler contact is made and coupler load increases until coupler shear pins fail; the coupler telescopes (by design) until anticlimber contact is made;

b. Load reaches value to start collapse of the draft sill; draft sill deflects until side sills and car shell are contacted;

c. Side sills are contacted, floor and end sill weld ruptures, side post welds rupture, forward floor buckles, sides, coves and roof buckle; side sills buckle inward about weak axis; load increases approximately 100,000 lbs.;

d. Failing elements maintain approximately constant load until bolster is contacted;

e. Car center yield strength is realized and rises to a short column ultimate (factor assumed = 1.2); and finally,

f. Bulk compression of all material.

Also shown in Figure 4-1 is the Cassidy and Romeo prediction[2] for the R-44 Car for the end squeeze. The Calspan results were obtained from consideration of "static" properties of the R-44 Car. The sequence of events hypothesized for the R-44 is considerably different than that used for SOAC. This is due in part to the SOAC accident and static test data which were not available to the Calspan study.

The results in terms of energy absorption and in terms of load levels are actually in fair agreement. Some differences do appear in the shape of curves at large deflections. This becomes significant for the higher energy conditions such as closing speeds of 80 MPH, and for long trains even at lower speeds. However, either curve may be taken as representative of the SOAC/R-44 for comparison to other cars analyzed in the same manner.

The resistance of the SOAC for the case of overriding (that is, one car impacting another car with sufficient vertical misalignment to prevent anticlimber contact) is shown in Figure 4-2. This case demonstrates the lack of resistance of the car in the override mode as compared with the anticlimber-to-anticlimber crash. In particular, the survivable volume reduction in the car ends is readily seen. The full strength of the underframe is not developed until the truck bolster of the overriding car contacts the anticlimber/draft sill of the overridden car.

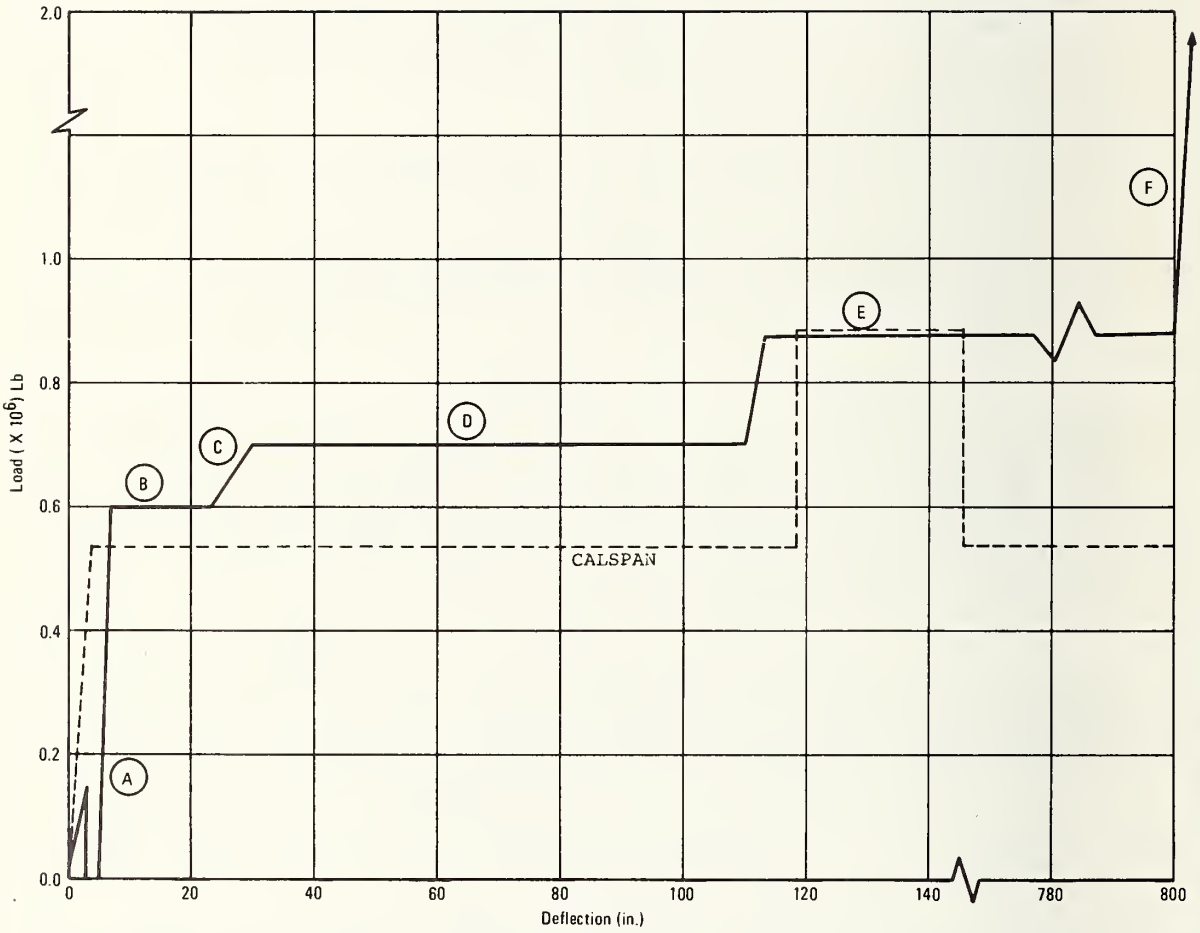

Figure 4—1. Crush Force Versus Deflection for Car Squeeze with No Overriding

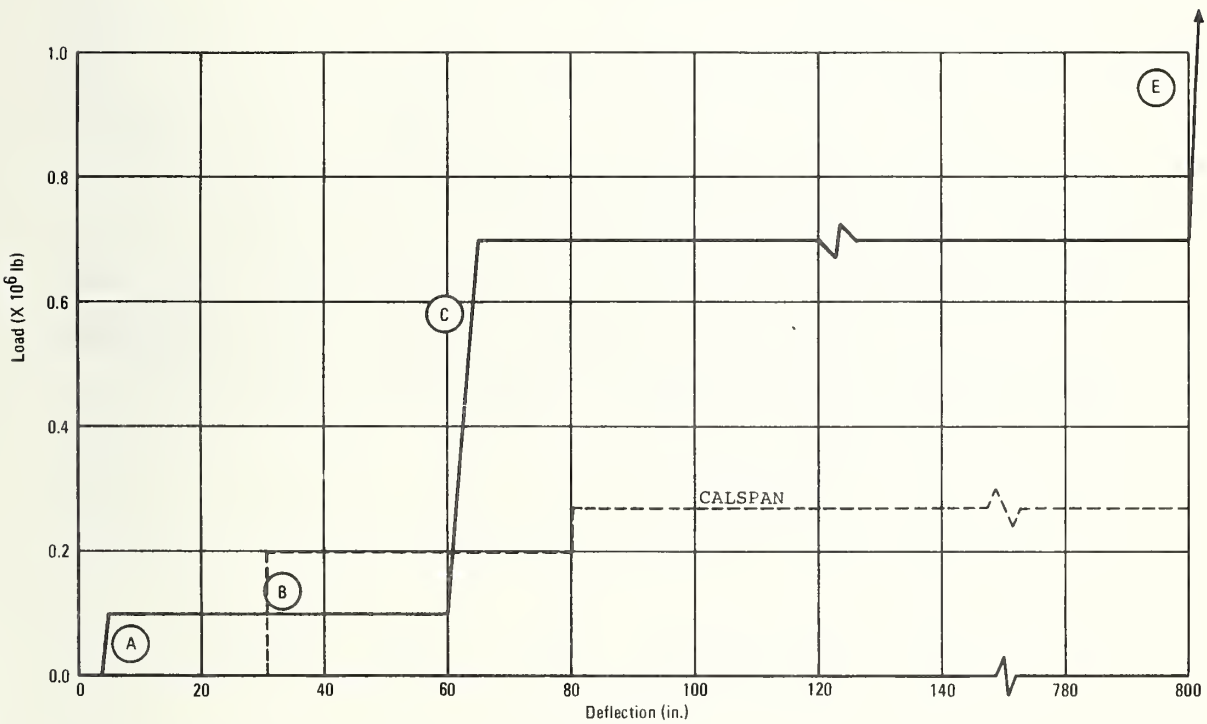

Figure 4–2. Crush Force Versus Deflection with Overriding

For the overriding case the scenario is as follows:

a. Target (car) contacts fiberglass shell; collision post welds fail; car sides, coves and roof pick up load;

b. Target penetrates car at constant load until truck bolster contacts anticlimber;

c. Car center strength developed; and

d. Bulk compression.

In Figure 4-2 the Calspan R-44 results for overriding are shown. Some major differences here are seen, for the SOAC contact with the car body occurs earlier than for the R-44. This is probably due to the SOAC car body extending further forward due to styling and the absence of walk-through capability that is present on the R-44. The large rise in force given for SOAC at 60 inches deflection is associated with the assumption that the car trucks make underframe contact causing a change of load distribution to include the underframe. This implies that the trucks remain attached. This behavior would reduce penetration and could modify the assessment of crashworthiness for the overriding cases.

ASSESSMENT

The previous effort has produced a detailed analysis of the SOAC structure using both static and dynamic considerations. The results of static tests on a similar structure (R-44 Car) and the accident of August 11, 1973 have been reviewed. Using these data, force deflection curves for the SOAC have been formulated and presented.

In assessing the force deflection characteristics presented in Figures 4-1 and 4-2, it should be remembered that these curves become highly subjective, particularly at large crush distances. Insofar as they represent the car, the curves give a measure of the capability of the car to protect the passengers and help to define the passenger environment.

The force deflection curves are used in the solution of the spring coupled equations of motion for the impact of one consist with another. In this role, the properties of the curves have significance in the manner in which they affect the car crush, the time variation of the displacement, velocity, and acceleration of the individual car mass centers, and the relative displacements and velocities of the passengers.

Three basic properties of the curves are important to the crash dynamics. These are the shape as given by slopes and general form, the peak magnitude, and the area under the curve.

The shape of the curve is significant for those cases where the frequency of the dynamic mode of response of the cars is sufficiently high to be excited by the frequency content of the force. This match of frequency contents is more significant for the lower closing velocities than for the higher closing velocities. The train action characteristic frequencies are on the order of 4 Hz. The 4 Hz frequency was observed from the acceleration response of the individual cars in a four-car train impacting a four-car train analysis using the force deflection curves of Figure 4-1.

Thus for force rise times less than 0.2 second, the slope of the curve for low velocities does not exert much effect. Even at 20 MPH closing speed, the cars are advancing at 352.96 inches per second and the time to reach the first peak force is approximately 0.025 second, or one tenth of the train

action characteristic time (.25 second). As the closing speeds are reduced, the rise time will more nearly approach this characteristic time. Thus the slopes are important for the cases involving low closing velocities.

The maximum force affects the peak accelerations experienced in the primary crash at the cars center-of-gravity (C.G.). The human tolerance levels[6,7] to fore and aft accelerations indicate that 40G's for under 0.1 second will not result in injury for a properly supported occupant. This would indicate that a 100,000-pound car could experience 4,000,000 pounds of force for short times (0.1 second) without damaging the properly supported occupant. The SOAC level of 700,000 pounds would impose about 5.35G'S at the C.G. of the 131,000-pound car. Consequently, the magnitudes of the forces are considered to be well within acceptable ranges.

It should be noted that practical railcar structures should not exhibit a sudden loss of load-carrying capability. Such a feature is associated with elastic stability of column elements or the sudden rupture of principle elements in major load paths. The elastic buckling stability of major elements is avoided by providing sufficient support that the elements behave as short columns. The sudden rupture is avoided by the selection of ductile materials and by the proper design of joints.

Perhaps the most significant characteristic of the force deflection curves is the area under the curve. This area is a measure of the energy-absorbing capability of the car body structure. The energy absorbed increases with the crush distance. The larger the area under the curve, the higher the closing velocity for a given crush distance, or for a given closing velocity the less will be the crush.

Since the crush is directly related to fatalities it is desirable to reduce the crush. Comparing Figures 4-1 and 4-2 it may be seen that the override case will incur much larger crush distances than the end-on case. This may require improvement in the SOAC, as discussed in Section 9.

The next effort is directed toward the crash damage that would be sustained by SOAC trains in service and the injury potential to passengers. These studies will apply the methodology development by Calspan to assess the crashworthiness of the SOAC. In these studies, the sensitivity of injury potential as measured by a Severity Index to variations in the

---

6. U.S. Army Air Mobility Research and Development Laboratory, Crash Survival Guide. 71-22. Revised October 1971.

7. Society of Automotive Engineers, Human Tolerance as Related to Motor Vehicle Design, Information Report, SAEJ885A. 1964; revised 1966.

energy absorption (area under the curve) of the force deflection curve, closing velocity, relative velocity of the passenger to the car structure, length of the path of the passenger before second impact, and the cushion of the impacting surface will be treated.

5. CRASHWORTHINESS METHODOLOGY

Presented in this section is a summary of the methodology for the assessment of crashworthiness developed by Cassidy and Romeo.[2] TSC has directed Boeing to use the Calspan methods to provide a common basis for comparison of the SOAC results with those of the Calspan Study. Much of the material that follows is taken directly from the Cassidy and Romeo report and is given in quotations.

The Calspan methodology provides a procedure relating the structural properties of the rail vehicles to the collision dynamics. From the collision dynamics, the passenger may become a fatality through reduction of survivable volume (crush), or through secondary collisions with the car interior or other passengers. For the secondary collision, the Severity Index (SI) quantifies the passenger injury experience and relates the numerical measure to classes of injuries.

The collision dynamics are obtained from the solution of the equations of motion for each train. The program for this procedure is described in some detail.

CASUALTY QUANTIFICATION

The Severity Index and its application is discussed in Reference 2-2. The Severity Index is given by,

$$SI = \int_0^T A_p^{2.5} dt$$

where Ap is the acceleration in g's and T is the duration of the impact.

In the secondary collision, the passenger is assumed to be subjected to a constant deceleration (a perfect absorber). The velocity of the passenger relative to the interior and the distance to arrest the velocity (cushion) then determine Ap.

$$Ap = \frac{V_R^2}{2dg}$$

where V_R is the velocity between the passenger and the car
d is the cushioning distance
g is acceleration due to gravity

The relationship between the Severity Index and injury experience is given in Table 5-1.

TABLE 5-1. ABBREVIATED INJURY SCALE

SEVERITY CODE	SEVERITY CATEGORY/INJURY DESCRIPTION	POLICE CODE	CALSPAN SEVERITY INDEX (SI)
0 (Zero)	NO INJURY	0 or D	LESS THAN 250
1	MINOR	C	250 TO 500
	GENERAL ---Aches all over. ---Minor lacerations, contusions, and abrasions (first aid--simple closure). ---All 1° or small 2° or small 3° burns. HEAD AND NECK ---Cerebral injury with headache; dizziness; no loss of consciousness. ---"Whiplash" complaint with no anatomical or radiological evidence. ---Abrasions and contusions of ocular apparatus (lids, conjunctiva, cornea, uveal injuries); vitreous or retinal hemorrhage. ---Fracture and/or dislocations of teeth. CHEST ---Muscle ache or chest wall stiffness. ABDOMINAL ---Muscle ache; seat belt abrasion; etc. EXTREMITIES ---Minor sprains and fractures and/or dislocation of digits.		
2	MODERATE	B	500 TO 1000
	GENERAL ---Extensive contusions; abrasions; large lacerations; avulsions (less than 3" wide). ---10-20% body surface 2° or 3° burns. HEAD AND NECK ---Cerebral injury with or without skull fracture, less than 15 minutes unconsciousness; no post-traumatic amnesia. ---Undisplaced skull or facial bone fractures or compound fracture of nose. ---Lacerations of the eye and appendages; retinal detachment. ---Disfiguring lacerations. ---"Whiplash" - severe complaints with anatomical or radiological evidence. CHEST ---Simple rib or sternal fractures. ---Major contusions of chest wall without hematharax or pneumothorax or respiratory embarrassment. ABDOMINAL ---Major contusion of abdominal wall. EXTREMITIES AND/OR PELVIC GIRDLE ---Compound fractures of digits. ---Undisplaced long bone or pelvic fractures. ---Major sprains of major joints.		
3	SEVERE (Not Life-Threatening)	B	1000 TO 1500
	GENERAL ---Extensive contusions, abrasions; large lacerations involving more than two extremities, or large avulsions (greater than 3" wide). ---20-30% body surface 2° or 3° burns. HEAD AND NECK ---Cerebral injury with or without skull fracture, with unconsciousness more than 15 minutes; without severe neurological signs; brief post-traumatic amnesia (less than 3 hours). ---Displaced closed skull fractures without unconsciousness or other signs of intracranial injury. ---Loss of eye, or avulsion of optic nerve. ---Displaced facial bone fractures or those with antral or orbital involvement. ---Cervical spine fractures without cord damage. CHEST ---Multiple rib fractures without respiratory embarrassment. ---Hemotharax or pneumothorax. ---Rupture of diaphragm. ---Lung contusion. ABDOMINAL ---Contusion of abdominal organs ---Extraperitoneal bladder rupture ---Retroperitoneal hemorrhage ---Avulsion of ureter ---Laceration of urethra ---Thoracic or lumbar spine fractures without neurological involvement. EXTREMITIES AND OR PELVIC GIRDLE ---Displaced simple long-bone fractures, and/or multiple hand and foot fractures ---Single open long-bone fractures. ---Pelvic fracture with displacement ---Dislocation of major joints ---Multiple amputations of digits ---Lacerations of the major nerves or vessels of extremities		

TABLE 5-1. ABBREVIATED INJURY SCALE (Continued)

SEVERITY CODE	SEVERITY CATEGORY/INJURY DESCRIPTION	POLICE CODE	CALSPAN SEVERITY INDEX (SI)
4	SERIOUS (Life-Threatening, Survival Probable)	B	1500 TO 2000
	GENERAL ---Severe lacerations and/or avulsions with dangerous hemorrhage ---30-50% surface 2° or 3° burns. HEAD AND NECK ---Cerebral injury with or without skull fracture, with unconsciousness of more than 15 minutes, with definite abnormal neurological signs, post-traumatic amnesia 3-12 hours ---Compound skull fracture CHEST ---Open chest wounds; flail chest; pneumomediastinum, myocardial contusion without circulatory embarrassment; pericardial injuries. ABDOMINAL ---Minor laceration of intra-abdominal contents (to include ruptured spleen, kidney, and injuries to tail of pancreas). ---Intraperitoneal bladder rupture. ---Avulsion of the genitals. ---Thoracic and/or lumbar spine fractures with paraplegia EXTREMITIES ---Multiple closed long-bone fractures. ---Amputation of limbs		
5	CRITICAL (Survival Uncertain)	A	OVER 2000
	GENERAL ---Over 50% body surface 2° or 3° burns. HEAD AND NECK ---Cerebral injury with or without skull fracture with unconsciousness of more than 24 hours; post-traumatic amnesia more than 12 hours, intracranial hemorrhage; signs of increased intracranical pressure (decreasing state of consciousness, brady-cardia under 60, progressive rise in blood pressure or progressive pupil inequality). ---Cervical spine injury with quadriplegia. ---Major airway obstruction. CHEST ---Chest injuries with major respiratory embarrassment (laceration of trachea, hemamediastinum, etc.). ---Aortic laceration. ---Myocardial rupture or contusion with circulatory embarrassment. ABDOMINAL ---Rupture, ovulsion or severe laceration of intra-abdominal vessels or organs, except kidney, spleen or ureter. EXTREMITIES ---Multiple open limb fractures.		

SEVERITY CODE	SEVERITY CATEGORY/INJURY DESCRIPTION	POLICE CODE	CALSPAN SEVERITY INDEX (SI)
6	FATAL (Within 24 Hours)	K	OVER 2000
	---Fatal lesions of single region of body, plus injuries of other body regions of severity Code 3 or less. ---Fatal from burns regardless of degree.		
7	FATAL (Within 24 Hours)	K	OVER 2000
	---Fatal lesions of single region of body, plus injuries of other body regions of Severity Code 4 or 5.		
8	FATAL	K	OVER 2000
	---2 fatal lesions in 2 regions of body.		
9	FATAL	K	OVER 2000
	---3 or more fatal injuries. ---Incineration by fire.		
99 X	SEVERITY UNKNOWN		
	---Injured, but severity not known.		
98 Z	PRESENCE UNKNOWN		
	---Presence of injury not known.		

"The passenger fatalities and injuries resulting from a given rail crash can be estimated by summing the number of occupants whose severity indices exceed a given value and the number of occupants who occupied the portion of each rail car which is crushed. Such estimates are calculated below for rated maximum passenger loads as a worst case condition."[2]

The assumed conditions for a passenger catapulted into an obstruction (second-collision) are the same as used in Reference 2 and are presented in Table 5-2. Also shown in Table 5-2 are the passengers assumed to be subject to these conditions.

TABLE 5-2. SECOND-COLLISION CONDITIONS

CONDITION	PASSENGER SPACING (FREE-SPACE DISTANCE), S, IN FEET	IMPACTED-OBJECT PASSENGER CRUSH DISTANCE, d, IN INCHES	CONDITION
1	2	1	19
2	2	2	19
3	4	1	18
4	4	2	18
5	12	1	138
6	12	2	138
7	24	1	-
8	24	2	-

passengers per foot of occupied portion of car
$\rho = 4.7$

"These numbers attempt to distribute the passengers with regard to the relative number of fore- or aft-facing or side-facing seats and standing positions in each car."[2]

In SOAC the number of seated passengers facing fore or aft is 26, 48 are side-facing, and 275 are standing. This is the same distribution used by Calspan for the R-44.

"Stated numerically, the fatalities can be estimated from:

$$N_f = N_{1st} + N_{2nd}$$

$$N_f = \sum^{n} \rho\,(\delta - \delta_\mu) + \sum^{n} \left(n_1 \rightarrow 10 \right)_{SI \geq 2000}$$

where N_f is the total number of fatalities per crash,

N_{1st} is the number of first-collision crush fatalities,

N_{2nd} is the number of second-collision fatalities,

ρ is the passenger density per foot of car length

δ is the car crush distance

δ_μ is the crush space unoccupied

and $n_1, n_2, \ldots n_n$ are the number of passengers per car in each of the second-collision conditions in the region of the car which is not crushed.

In a similar manner, the injuries per crash can be summed from

$$N_1 = \sum^{n} (n_1, \ldots n_n)_{SI = 500 \rightarrow 2{,}000}$$

where $n_1 \ldots n_n$ are the number of passengers in each second-collision condition who experience severity indices between 500 and 2,000".

Tabulations of these summations are presented in Sections 7 and 8, which indicates first- and second-collision fatalities and injuries per car and total fatalities and injuries per train.

"The one single point which probably cannot be expressed enough with regard to these tables and subsequent comparisons is that these fatalities and injury estimates are only the most gross estimates of what might actually occur in real-life crashes. Although we have tried to use state-of-the-art knowledge with regard to the crash analyses, it must be remembered that the number of variables which enter into estimates such as these simply do not allow high degrees of confidence in the qualitative results. A review of the construction of the crash-injury mathematical model must be made to appreciate this point.

With these reservations in mind, it is possible to examine these tables and make meaningful comparative evaluations concerning the relative problems concerned with car crush versus second-collision, effect of crash velocity, effect of car position in the train, and so on."[2]

COLLISION DYNAMICS

A simple train collision model developed at Boeing to simulate the forces, deformations, velocities, and accelerations of a multi-car consist impacting another multi-car consist has been used to define the passenger crash environment.

Each car of each consist is treated as a separate degree of freedom in the direction of travel see Figure 5-1. The external forces acting on each car are taken to be the "spring" forces arising from the relative distance between the CG's of the car with the adjacent car and the braking forces. At the instant of impact, each car is assigned an initial velocity and a brake force. The initial displacement of the force deflection curve (spring) is taken to be zero. The differential equations of motion for each degree of freedom are then integrated to give velocities and displacements.

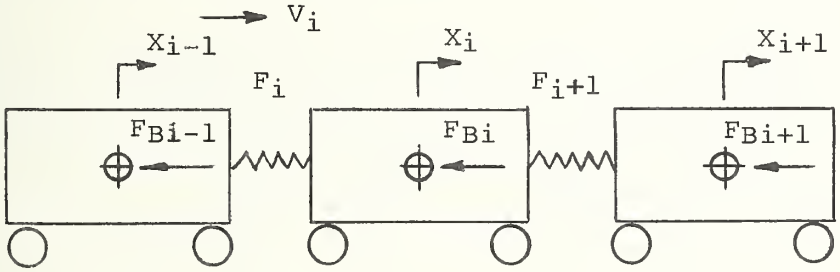

Figure 5—1. Multi-Car Consist Impact Model

The equations for the general car are:

$$-M_i\ddot{X}_i - F_i\left|(X_i - X_{i-1})\right| - F_{i+1}\left|(X_i - X_{i+1})\right| - F_B = 0$$

Where M_i = mass of ith car
F_i = force deflection curve between the ith-1 car and the ith car as a function of the relative displacement between cars
F_{i+1} = Force deflection curve between the ith car and the ith+1 car as a function of the relative displacement
$\ddot{X}_1$ = acceleration of the ith car
$(X_1 - X_{i-1})$ = relative displacement of the ith car to the ith-1 car

FB = Braking Force acting at car CG and opposed to the velocity.

Force Computation

The force, Fi, is a continuous piece-wise linear function of the relative displacement between cars. The force deflection curves for each adjacent single car are combined as "springs in series" to provide the function Fi. In the computer program the function,F, is specified in terms of rates and the applicable linear ranges.

In the computation of F, the current relative deflection is compared to the reference deflections at the break points in the force deflection curve to identify the applicable rate. The value of the force is computed as shown in Figure 5-2.

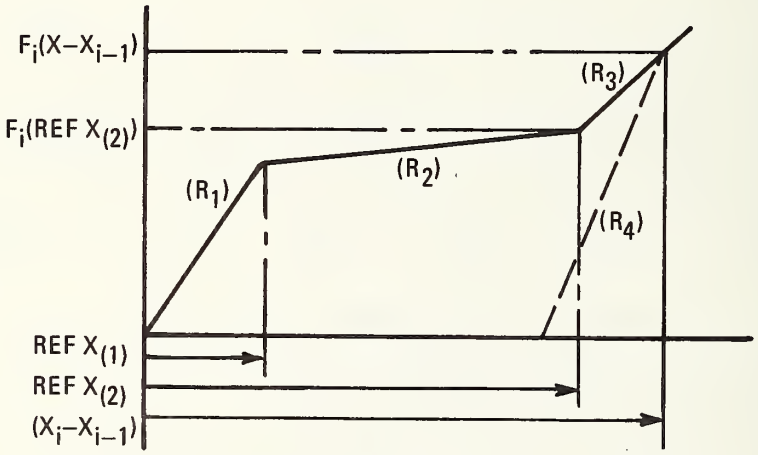

Figure 5–2. Force Value Computation

To extend the validity of the solution, logic was added to the program to include springback in the plastic region, $(X_i-X_{i-1}) > REF\ X_{(1)}$, and for the condition where the springs are in tension. For the springback case, the logic tests the current deflection against maximum deflection. If the current deflection is less than maximum deflection, and the elastic region is exceeded, and the maximum deflection is greater than REF $X_{(1)}$, then the amount of rebound is compared with the reference

deflection for the elastic region i.e., Ref $X_{(1)}$. If the rebound is less than the magnitude of Ref $X_{(1)}$, the rate R (4) is computed and Fi evaluated. If the rebound is greater than ref $X_{(1)}$ then Fi = 0.

For the case where the "spring" is in tension and the elastic region not exceeded, corresponding to situation where the coupler shear pins are intact, the tension force is applied. However should the elastic region be exceeded as for the failure of the shear pins then Fi = 0.

Brake Forces

A simple representation of braking is included in the equations of motion. Logic is provided to distinguish between impending motion and motion. Where motion is present, $|V|>0$ then FB has the input magnitude and the proper sign to oppose the motion.

For the case of impending motion, V=0, FB is compared to the net spring forces acting on the car. If FB is greater then the net spring forces then FB = Fi. If FB is less than the net spring forces FB is set to oppose the impending motion.

The role of braking forces in this simple model is to increase the forces between the impacting cars and the struck cars. The presence of braking results in larger crush distances than for when braking is absent. In the cases treated in the SOAC study the differences in crush are small since the breaking force is approximately 3% of the crush force.

The presence of braking does hasten the attainment of slide out equilibrium. This may be described as a condition where all the cars in each consist have attained the same velocity. In a conservative system, the final velocity is one-half the initial velocity for equal masses.

Integration Methods

The integration method assumes the acceleration of a car is constant over the time interval. The increment in velocity is then given by acceleration X time increment. The velocity increment is then added to the previous velocity to give current velocity. The displacement is found in a like manner where the incremental displacement is given by Velocity X time increment. Some error is present in the displacement since a

time increment squared term is omitted. For the time increment used (.0001 sec.), the error is very small.

CORRELATION WITH CALSPAN RESULTS

The assessment of crashworthiness of the SOAC was to be conducted using the Calspan computer model for train collision in accordance with the provisions of this contract. However, at the convenience of the Government, Boeing Vertol was instructed to proceed with the application of the Boeing computer model previously described.

In order to establish a common basis for comparison of the crashworthiness studies a correlation calculation was performed. The R-44 force deflection curve discussed and shown on Figure 1-2 was used in the Boeing model but with the SOAC mass properties. The case treated was the 40 MPH crash of a 4-car train with a standing 4-car train.

The results are shown in Figure 5-3. The car crush distance for the first (impacting) car is shown as a function of time after impact. As may be seen, the agreement both as to shape and magnitude is good. From this, one may conclude that the models produce comparable results and that real differences are small.

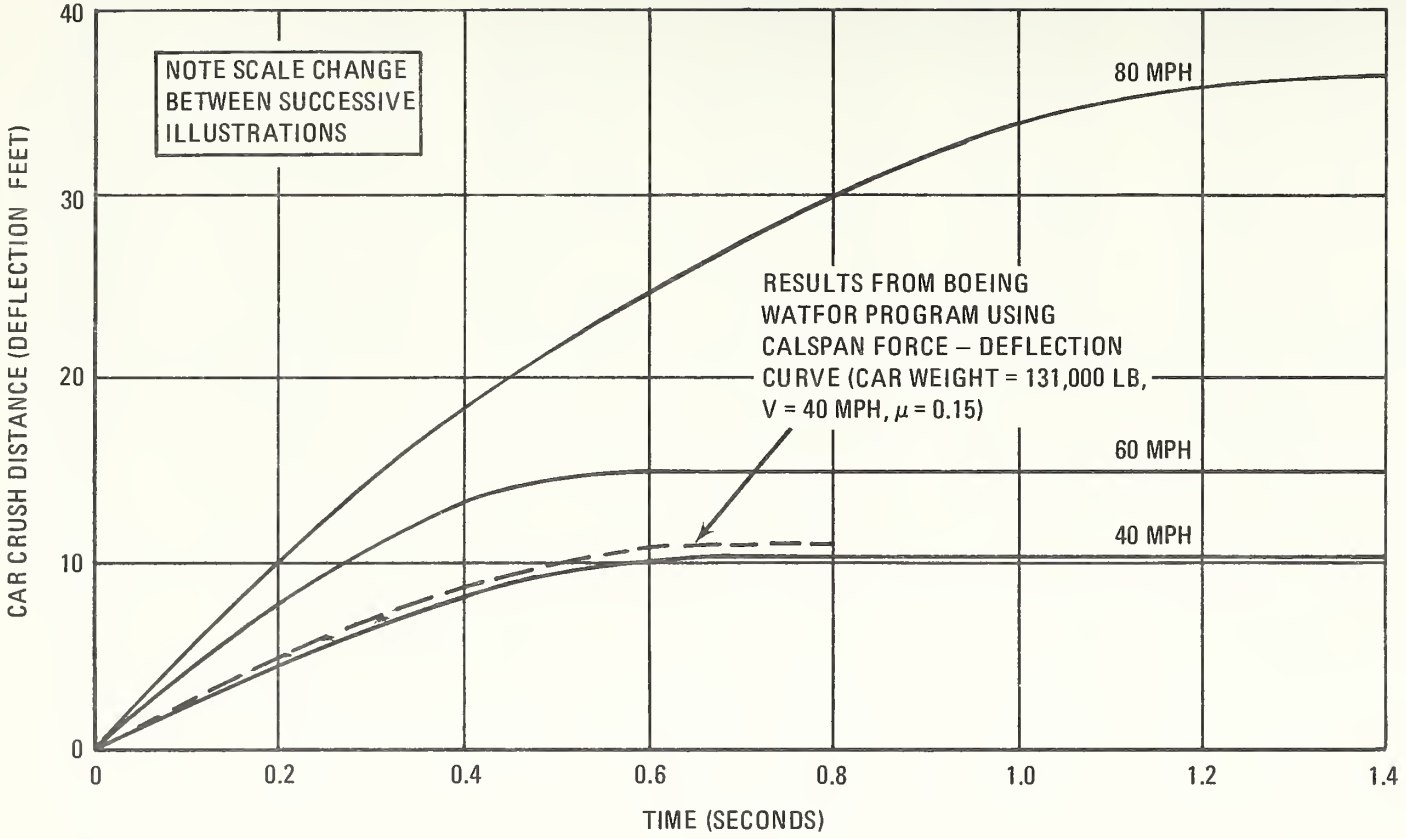

Figure 5–3. Effect of Closing Velocity on Crush Distance of First Car (Two Trains of Four R-44 Cars Each)

VALIDATION OF THE SOAC COLLISION DYNAMICS

In this section the validation of the SOAC collision dynamics is presented. The validation is based on comparisons of the analytical crush data to the accident data, and on comparisons of force levels used in the "Calspan Method" to the KRASH models. The latter comparison is supported by an energy balance. From these comparisons, it is concluded that the SOAC collision dynamics as given by this method is a fair first order representation of the crash.

A collision dynamics case was run for the accident. The locomotive at 88,000 pounds and the gondola at 46,000 pounds were impacted by 2 SOAC's ballasted to 105,000 pounds each. The force deflection curve of Figure 4-1 was assumed to apply to the SOAC-SOAC, and the SOAC-Gondola interfaces. A simple 333,333-pound per inch spring was used between the Gondola and the locomotive.

The results showed that there was no damage between the locomotive and the gondola. Between the SOACs the crush was indicated to be 11.7 inches on the two cars after failing the shear bolts in both couplers. Assuming a 2 inch elastic deflection, the results indicate about 5 inches of crush per SOAC. Between the SOAC and the gondola approximately 50 inches of crush (25 inches per car) after the coupler shear pin failures as predicted.

The deformations observed in the accident substantiate the above values. There was no damage on the locomotive or the forward end of the gondola. The shear pins on both couplers in the SOAC-SOAC interface failed and the anticlimber showed some "dents" but there was no other damage. Compared with the small crush predicted this is good agreement.

The forward draft sill of the lead SOAC was driven aft of the end of the side sills. This is a distance of approximately 30 inches. The crush on the anticlimber supports and plates of the gondola was estimated to be 36 inches. These values compare favorably with the 25 inches predicted by the analysis.

As shown below, the crush of the SOAC carside by the detrucked gondola carbody would contribute about 12% of the total strain energy of the crash.

The strain energy absorbed by the Gondola and by the SOAC may be obtained from the conservation of momentum. A reckoning of the energy and an energy balance is given in Appendix E.

Referring to Appendix E, the kinetic energy that must be converted to strain energy in the SOAC accident is approximately 3.45×10^6 lb-ft.

The major energy absorption mechanisms for the SOAC were the deformation of the draft sill and the crushing of the left side wall, cove, and roof. The major energy absorption mechanisms for the gondola were the deformation of the anticlimber supports and the tearing and deformation of the plate under the rear of the car. The energy balance is based on a "best" estimate of the events.

These mechanisms account for 90% of the energy to be absorbed. The draft sill contribution is sensitive to the plastic hinge angle. For instance, a change from 45° to 60° changes the energy absorbed by the draft sill from 16×10^6 to 24×10^6 in. lbs. Also, the energy due to the gondola anticlimber support deformation may be questioned. One may trade the sensitivity of the draft sill calculations against the anticlimber support mechanisms without affecting the conclusions. There are no other sources of strain energy sufficient to account for the change in kinetic energy.

The KRASH model was used to simulate the SOAC accident. The purpose of this simulation was to further confirm the crash dynamics and to compare the accident simulation to the earlier barrier crash studies. The model is shown in Figure 5-4. In this model the gondola is represented by mass 2, the locomotive by mass 1 and the trailing SOAC by masses 31 and 32. Since the simulation is directed to the structural behavior of the SOAC, the properties of the locomotive and the gondola are represented only approximately. The link connecting the locomotive and the gondola is a linear spring approximating the combined stiffness of the locomotive and the gondola.

The element 2-4 connecting the SOAC anticlimber and the gondola is a non linear spring as shown in Figure 5-5. The load is linear until 300,000 lbs corresponding to the resistance of the anticlimber supports given in Appendix E. The 300,000 lb level is assumed to apply for approximately 28 inches of deflection. At 31 inches the SOAC seating against the gondola draft anchor is assumed and the gondola resistance is taken as linear thereafter.

The mass of the trailing SOAC is divided between mass 31 and Mass 32 to facilitate the transfer of inertial load to the first SOAC. The force deflection for elements 12-31 and 16-32 are given by one half of the complete SOAC values shown in Figure 4-1.

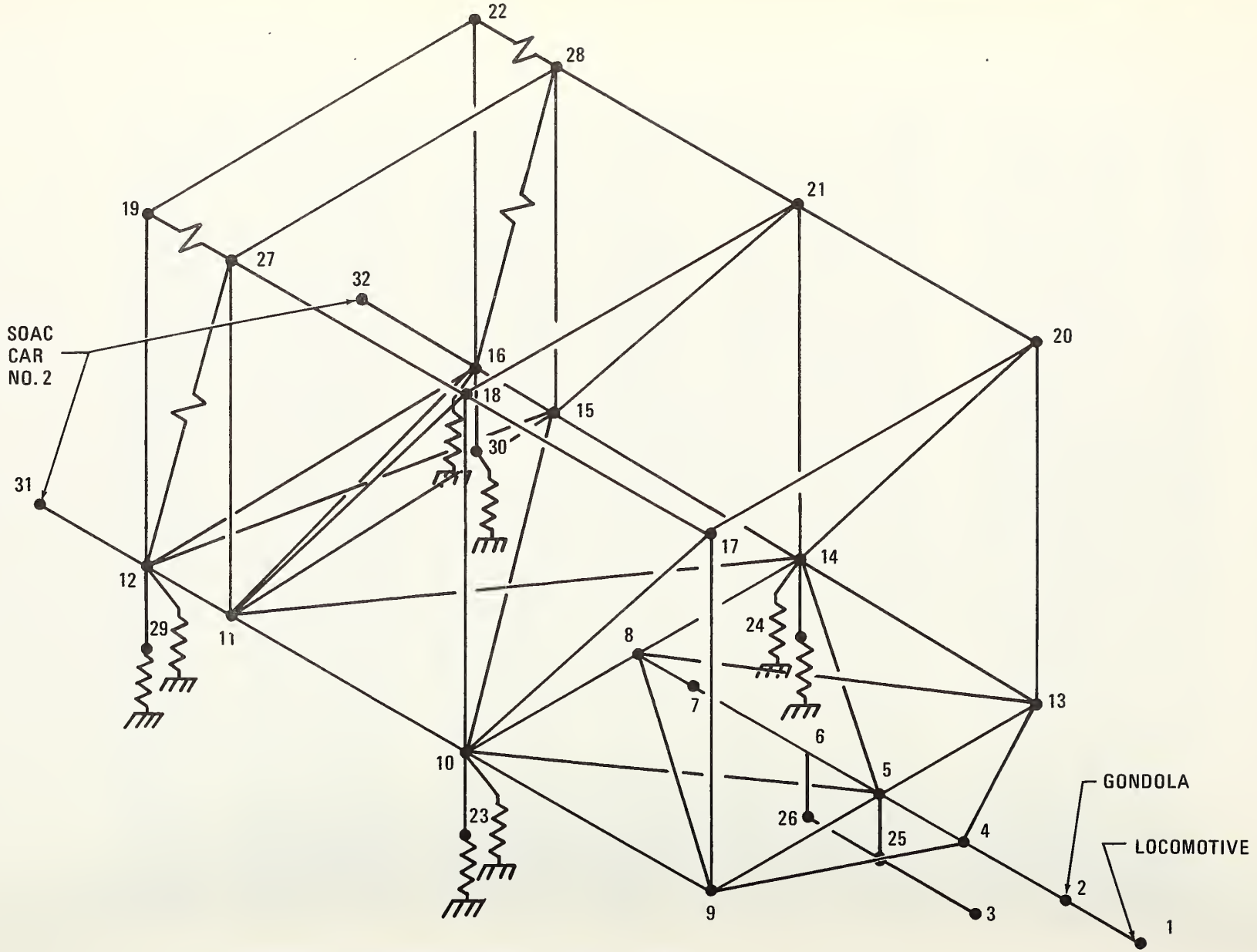

Figure 5–4. Simulation Model for SOAC Accident

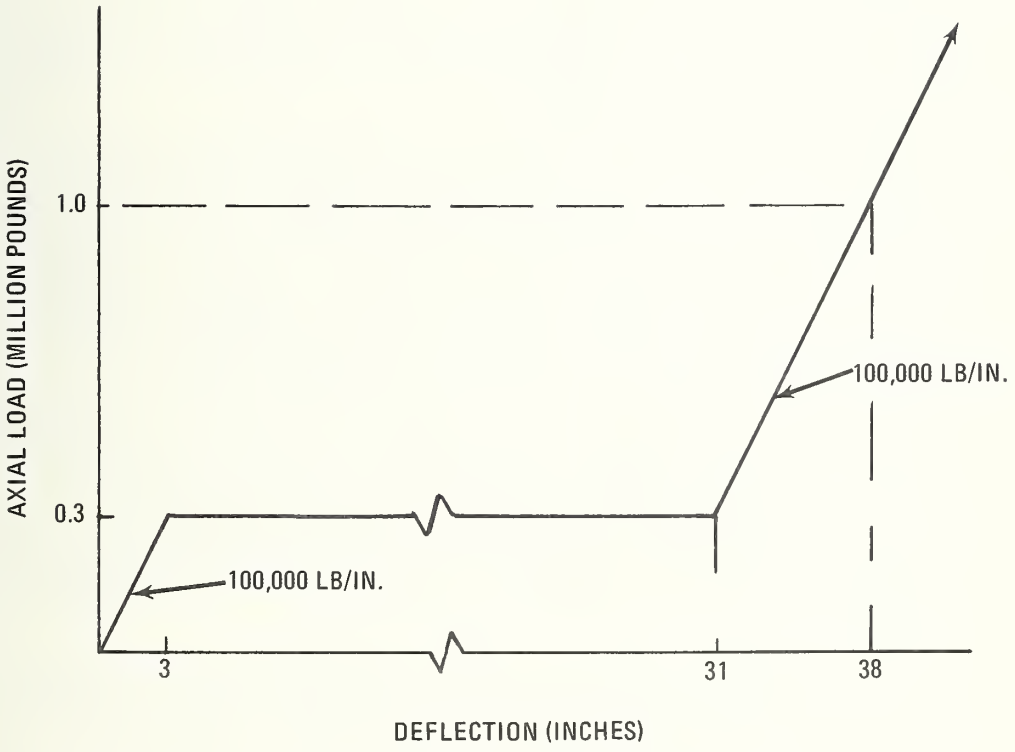

Figure 5–5. Accident Simulation Force Deflection Curve for Element 2–4.

To simulate the crash the gondola (Mass 2) and the locomotive (Mass 1) were given zero initial velocity while all other masses had 35 mph (620 in. per sec.) initial velocity. The first computer studies indicated that the model was collapsing prematurely. Consequently, beam elements were added to represent the structure more completely. Diagonal elements to resist the shear loads in both the underframe and the car sides and to provide more realistic support against element column buckling were incorporated into the model. Also, a slightly better representation of the shear plates in the car end was added.

The attempt to simulate the accident with this model met with qualified success. The major deficiency concerned the impulse to the standing train. In particular, the axial loads in elements 1-2 and 2-4 built up to a level sufficient to buckle the draft sill before the standing train reached the velocity indicated by momentum relations.

This implies that the compliance of the gondola and of the locomotive was too stiff. For instance, the single spring-single mass representation of the gondola and of the locomotive responds more rapidly than a distributed mass spring system. The system spring rates could be adjusted to permit a better approximation to the actual impulse. Alternatively, the model could be changed by adding more springs and masses. Both of these alternatives require a more detailed analysis of the gondola and locomotive than available for this study.

Useful results were obtained from this simulation. The accident structural failure mode for the SOAC was duplicated by the model, insight into the load distribution in this type of collission was provided, and a better understanding of modelling techniques and requirements for improvement was obtained. Also, a comparison of the barrier studies with the accident simulation was made.

The duplication of the failure mode is shown in Figure 5-6. As may be seen the draft sill failure mode compares favorably with the accident damage. The plastic hinges at node 6 and 7 bear a similarity to those shown in Figures 3-4 and 3-6. The weld ruptures of the corner posts and of the floor closing sill seen in the accident were obtained in simulation. The axial load distribution in the SOAC at the instant just prior to buckling of the draft sill for the simulation is shown in Figure 5-7.

The load on the face of the anticlimber, mass 4, is a compressive load of 1,045,180 lbs. The load in the anticlimber back up structure, element 4-5, is 802,305 lbs compression, being reduced by the inertial loading of mass 4. The backup structure is capable of carrying 1,200,000 lbs without

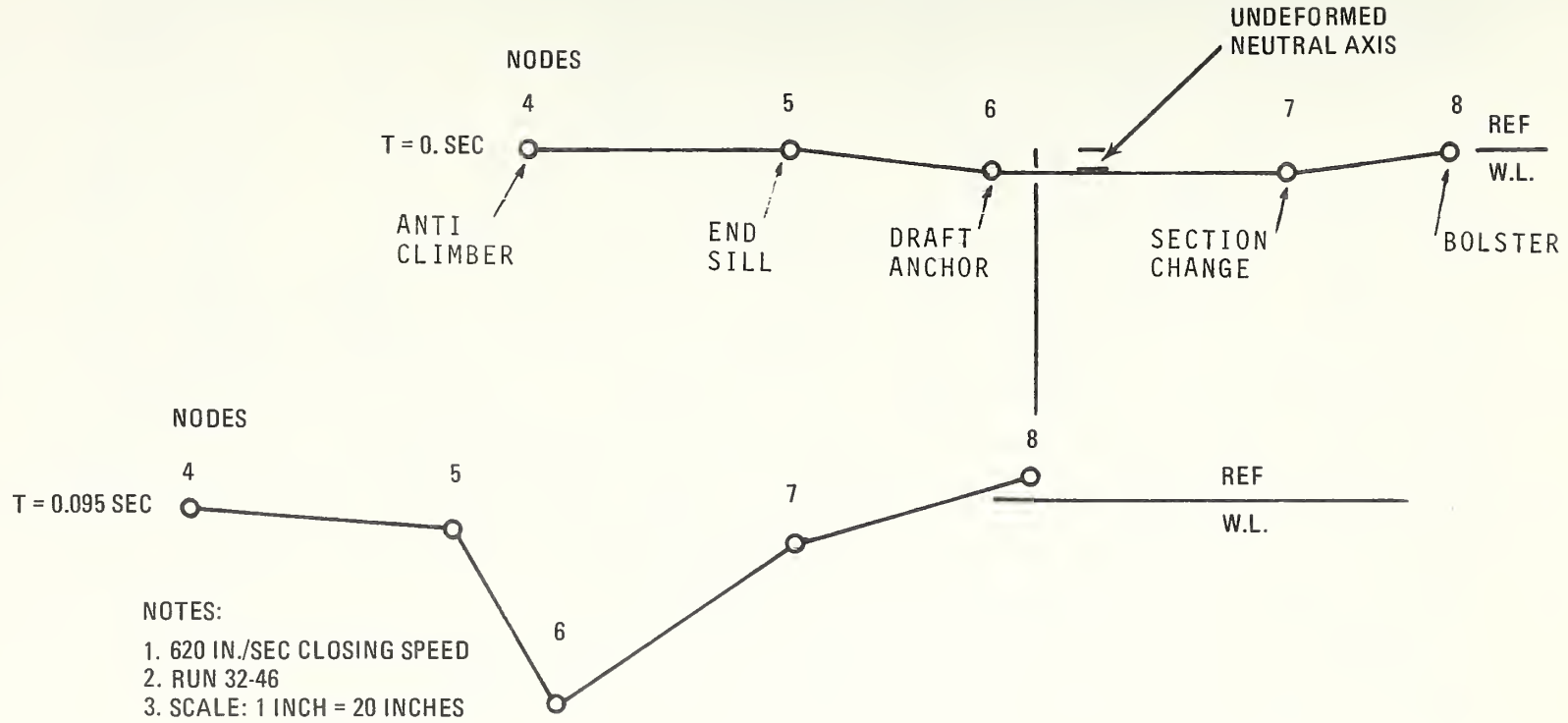

Figure 5–6. Draft Sill Deflection for SOAC Accident Simulation

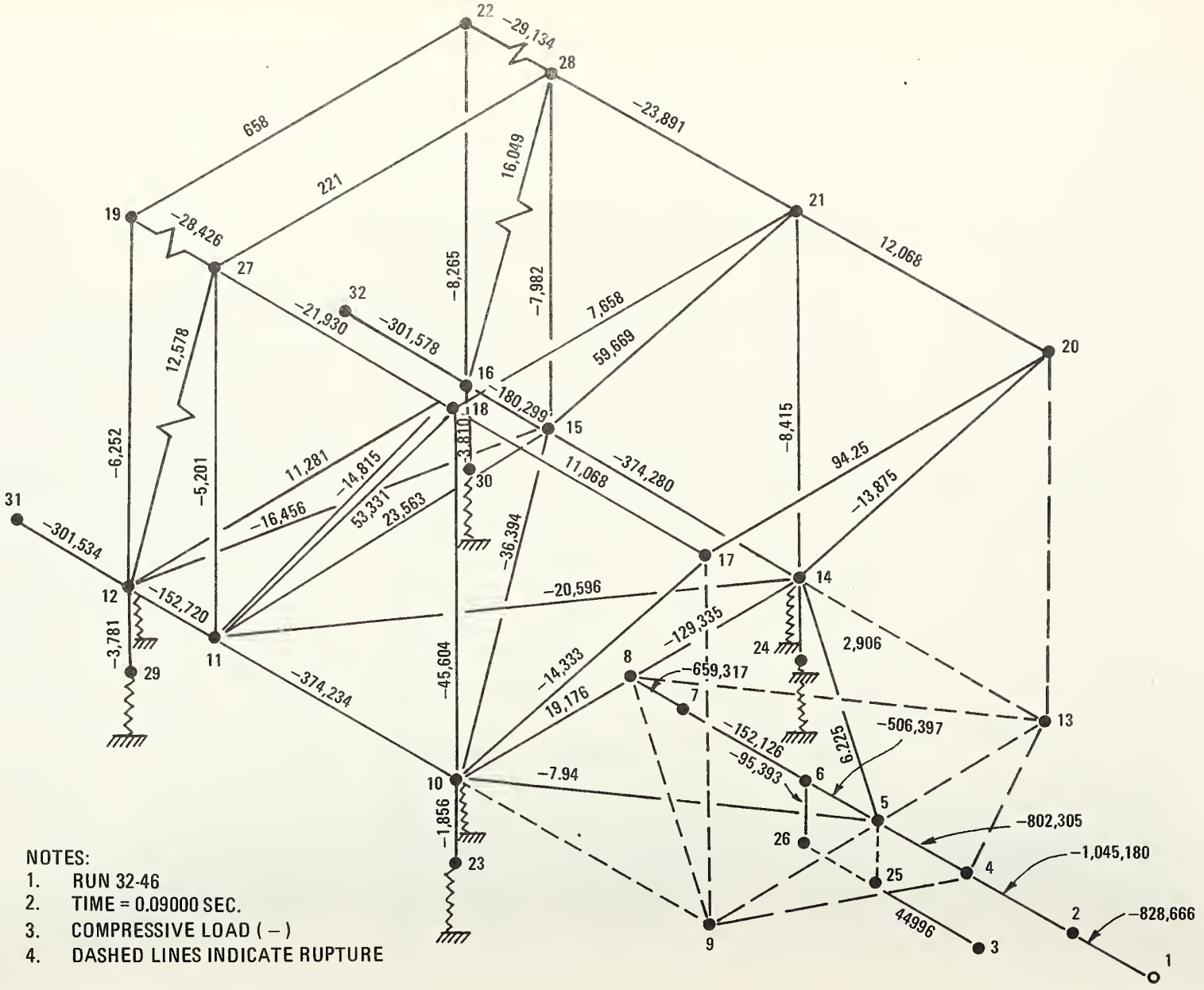

Figure 5–7. Axial Load Distribution Immediately Prior to Collapse of Draft Sill

yielding. Element 5-6 is loaded axially to compression yield and is also subjected to bending moments due to neutral axis eccentricity and the inertial loads on the draft gear. A plastic hinge is forming at node 6. The load shown in element 6-7 has started to fall off due to the inertial loading of mass 6 and the deflection of element 5-6.

The loads exerted by the trailing SOAC on the first SOAC are shown in elements 12-31 and 16-32. As can be seen, the trailing SOAC experiences a deceleration of approximately 5.75 gs at the instant draft sill collapse.

The first SOAC car center sees the loads in the side sills (10-11 and 14-15) and in the coves (18-27 and 21-28). The side sills are 3% above the compression yield load. However, as shown in the static tests the side sills would obtain relief due to other load paths such as the floor. These other paths are not reflected in this model. It is of particular significance that the car center did not fail and that the dynamic loads were such as to cause the failure to occur in the car end.

Comparisons of the results from the barrier studies with the results for the SOAC accident indicate that the car end behavior may be studied using a barrier model. This offers advantages in economy of analysis and of computer effort. The failure of the draft sill in both cases was governed by the rise in resistance at the face of the anticlimber by the inertial loading due to the masses of the draft gear and the local underframe, and to the structural details.

From the "free body" analysis of the draft sill, the static force to yield the draft sill is 500,000 pounds. From the KRASH analysis, the average force in the draft sill is 620,000 pounds for 0.06 second (Figure 5-8).

Further, the KRASH model analysis depicts the structural deformations experienced by SOAC in the accident. The analysis presents a rational behavior of the structure under dynamic loading in which the modes for failure and rupturing of elements is in good agreement with the observed accident damage.

Since the assumptions for the force deflection curve of the Method in reference 2 are based on a "squeeze" condition, the force deflection curve, Figure 4-1, at a 700,000-pound value for the carbody is a fair representation of SOAC. The solution of the collision equations gives reasonable values of crush for the Gondola and SOAC, and for the second SOAC with the first SOAC. On this basis the representation is validated.

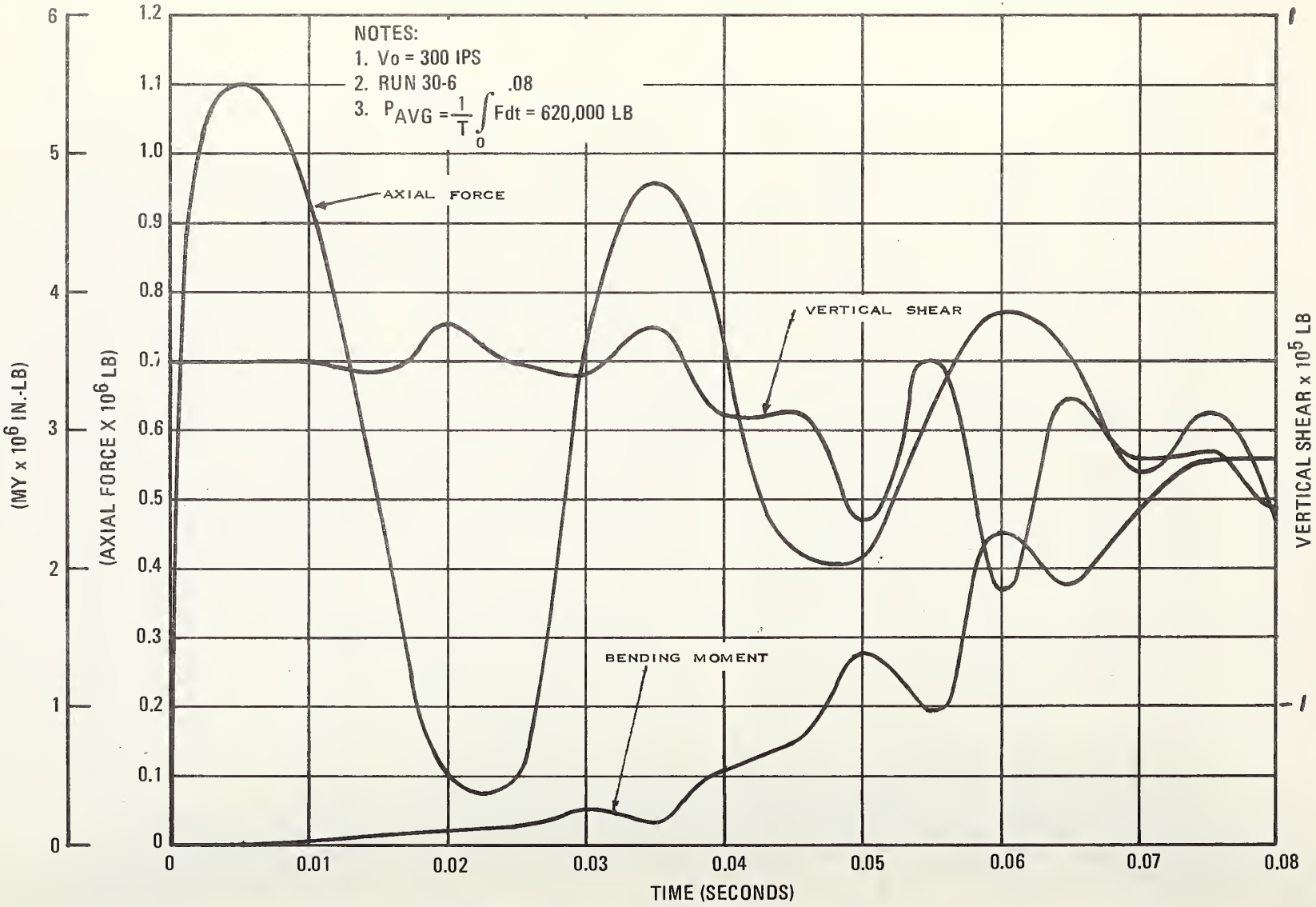

Figure 5–8. 30-Mass Model Coupler Impact: Loads in Element 4-5

6. PARAMETER SENSITIVITY STUDIES

In this chapter, some of the basic properties of the parameters defining casualties are studied to determine the nature of the problem and the relative significance of the individual parameters.

The collision of a 4-car SOAC train with a 4-car SOAC train was investigated. Data are presented for an end-on collision and the situation where the lead car of the moving train overrides the standing train.

The range of closing velocities investigated was from 20 mph to 80 mph for the end-on collision and from 20 mph to 40 mph for the overriding case. These ranges appear reasonable in terms of probable operating conditions for the urban mass transit car, particularly for end-on collision.

The overriding case is strongly dependent on the assumptions leading to the scenario, but presents even higher casualty results than the end-on case. The results of both reference 2 and the present study support a conclusion that overriding must be prevented. The reference 2 results show more damage than the present SOAC study. Consequently the closing velocity range for overclimbing was not extended to the 80 mph shown for the end-on collision.

In the study of the collision dynamics the results are essentially symmetrical about the plane of impact. Some skewness is introduced by the presence of having the brakes set on all cars, but this is a small effect. Therefore all data should be considered applicable to the "mirror image" car in a standing train.

Car crush as used here is a measure of the casualties encountered in the initial crash. Car crush is also a measure of the cost of repairs determining whether the car is returned to service or scrapped.

The relative velocity, displacement, and the cushion relate to second-impact. These variables enter the crashworthiness in terms of the SI value they produce.

EFFECT OF CLOSING VELOCITY ON CRUSH

Figure 6-1 shows the crush at each end of the lead car of the advancing 4-car train for the end-on crash as a function of time for each closing velocity. As may be seen, the maximum crush distance is a function of the kinetic energy, i.e., V^2. At 80 MPH the crush is 410 inches, representing a reduction in survivable car volume of approximately 80%. At 20 MPH the crush at each end is 24 inches. It may be observed that the loss of 24 inches from each car end does not result in a serious loss of occupied volume. Thus the 20 MPH case is a good lower value for the study.

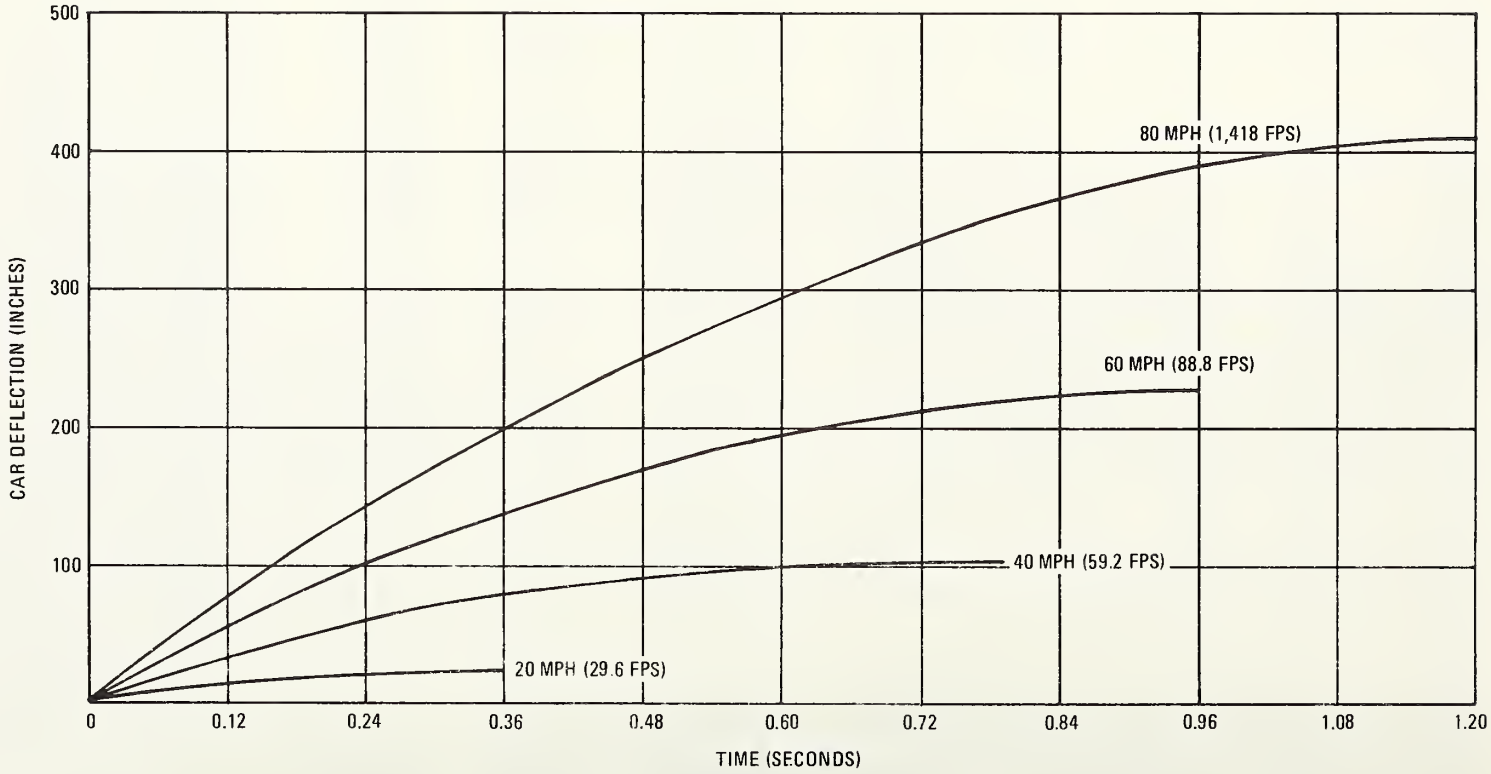

Figure 6–1. Total Crush Deflection of Car No. 5 Versus Time (for Two 4-Car SOAC Trains)

In Figure 6-2 is shown the crush of the second car in the advancing train. Notice the scale change between Figures 6-1 and 6-2. The final crush for 80 mph is seen to be 54 inches, and decreases as the velocity decreases. A comparison of the curves in Figure 6-1 with those in Figures 6-2 and 6-3 shows some effect of train action and of the coupler characteristics. A time delay (shift) is observed at the inception of the car end deformation for the cars remote to the plane of impact. At time = 0.12 seconds for the 80 mph closing velocity: Car 5 (first car in impacting train) has crushed 80 inches at each end while Car 6 has failed the coupler shear pins and is seating the draft gear against the draft anchor. Car 7 (third car in the impacting train) has deformed only 0.25 inches at each end. While Car 5 is undergoing a large crushing action, Car 6 is under essentially no load, and the Car 7 coupler has not even failed the shear pins. Consequently, the initial significant structural deformations occurring in Car 5 are essentially independent of the trailing consist.

The crush histories for the third car in the advancing train are shown in Figure 6-3. For this car the effects of the crash on the deflection have almost been eliminated. The final crush for closing velocities of 40, 60 and 80 mph are seen to be approximately the same (21 inches). The 20 mph case shows 18 inches crush. The crash dynamics of this car are strongly influenced by the coupler characteristics. From the viewpoint of the primary crash injury the crush is insignificant. The fourth car receives even less damage and the results are not presented.

The distribution of crush for the cars in the consist is of particular interest. The crush is incurred primarily in those cars at the plane of impact. The crush rapidly decreases to a "minus damage" category for cars remote from the plane of impact. This pattern also was observed in Tables 3-3 through 3-8 of reference 2 for all of the cars in that study; those consists each had different strength levels.

The reference 2 results show that even for 8-car trains and closing speeds of 80 mph the pattern was valid. For the larger consists and the higher speeds the penetration of the first car was increased and the penetration of the second car was beginning to be significant. However, the brunt of the energy absorption was taken by the first car.

The implications of this observation are significant for crashworthiness. It clearly identifies the problem to that of reducing the penetration of the first car. This focuses attention on the force deflection requirements of the car. Since buff strength is a measure of the level of the force deflection curve, the importance of properly specifying a buff strength compatible with the accident environment becomes apparent.

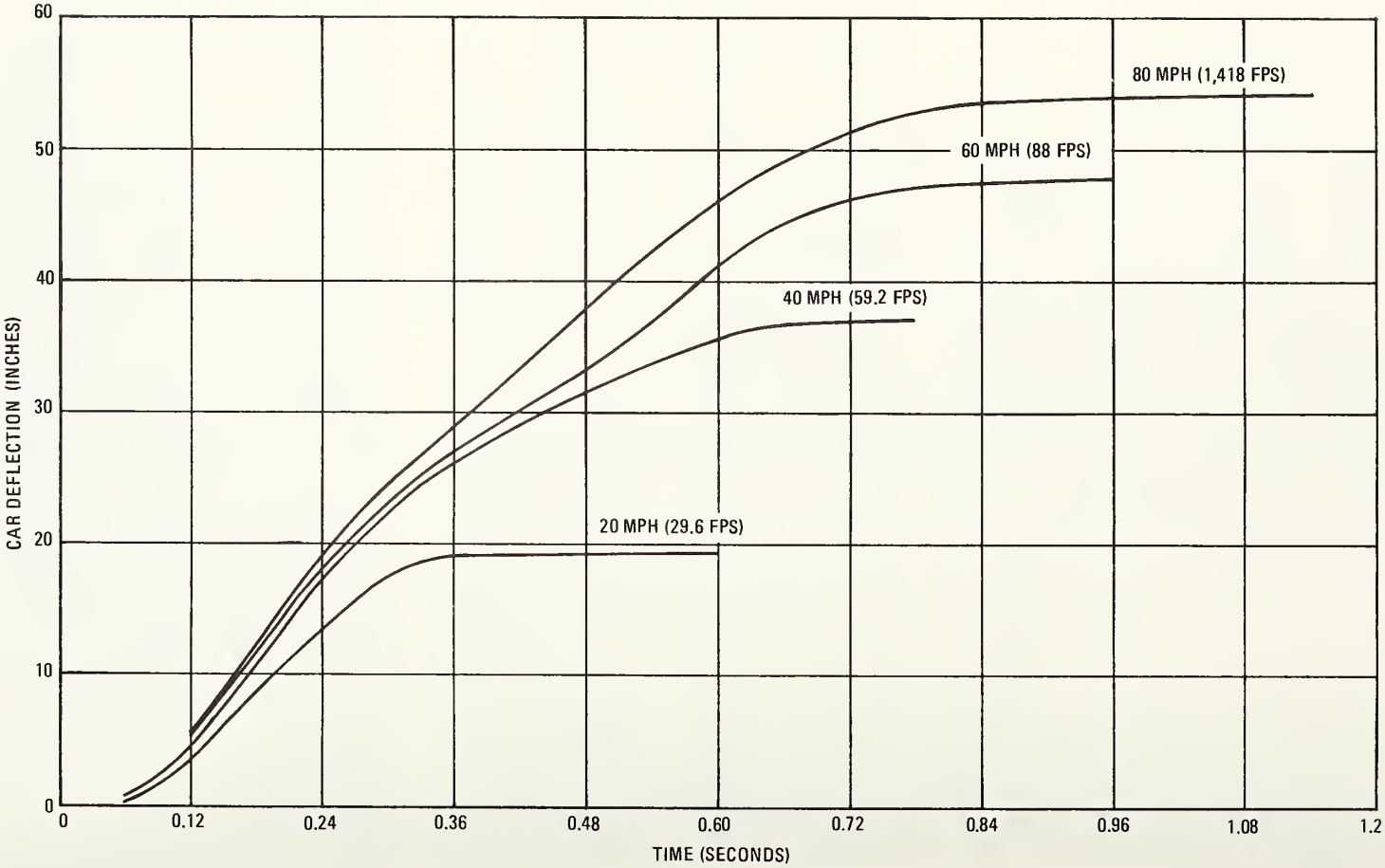

Figure 6–2. Total Crush Deflection of Car No. 6 Versus Time (for Two 4-Car SOAC Trains)

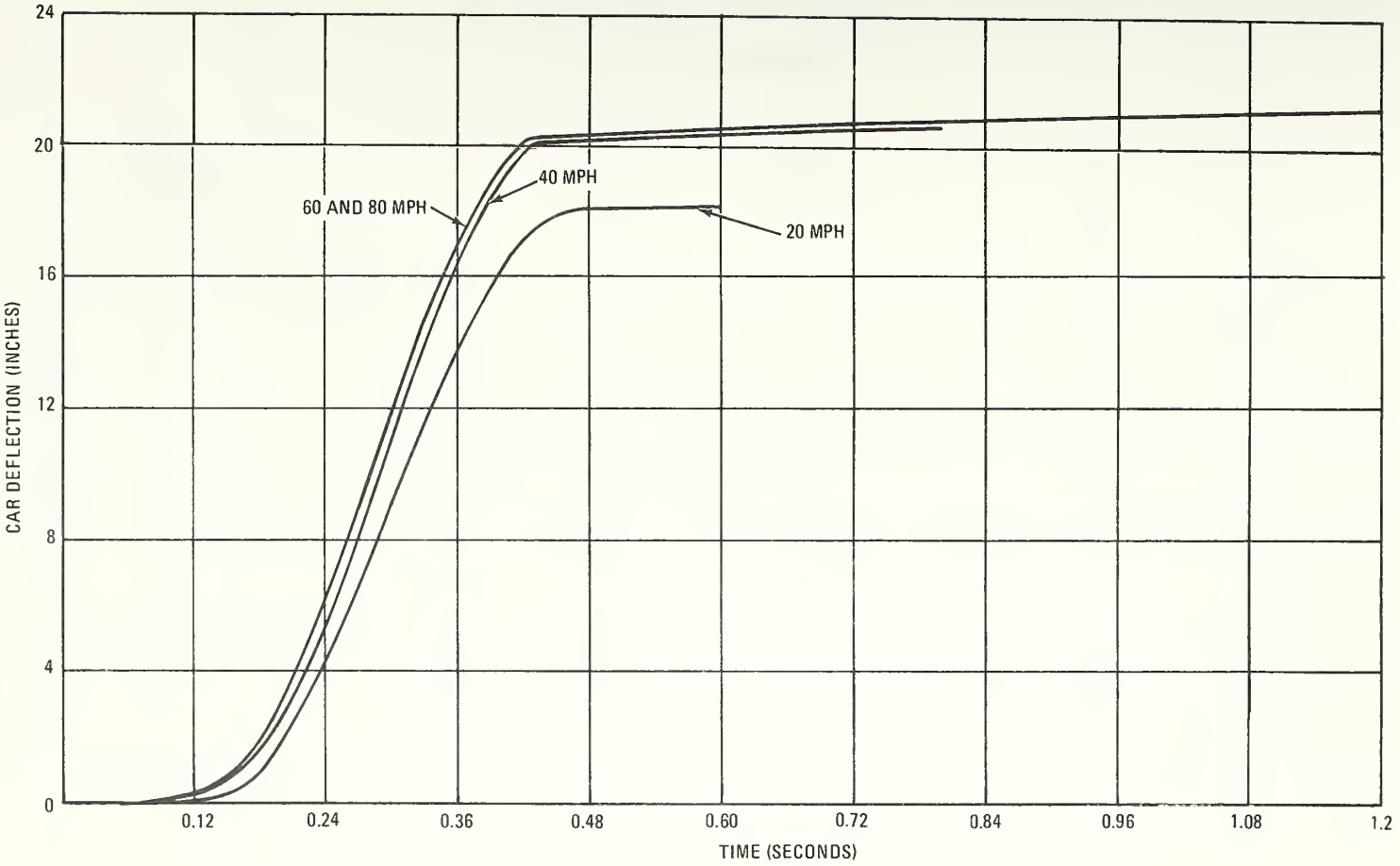

Figure 6–3. Total Crush Deflection of Car No. 7 Versus Time (for Two 4-Car SOAC Trains)

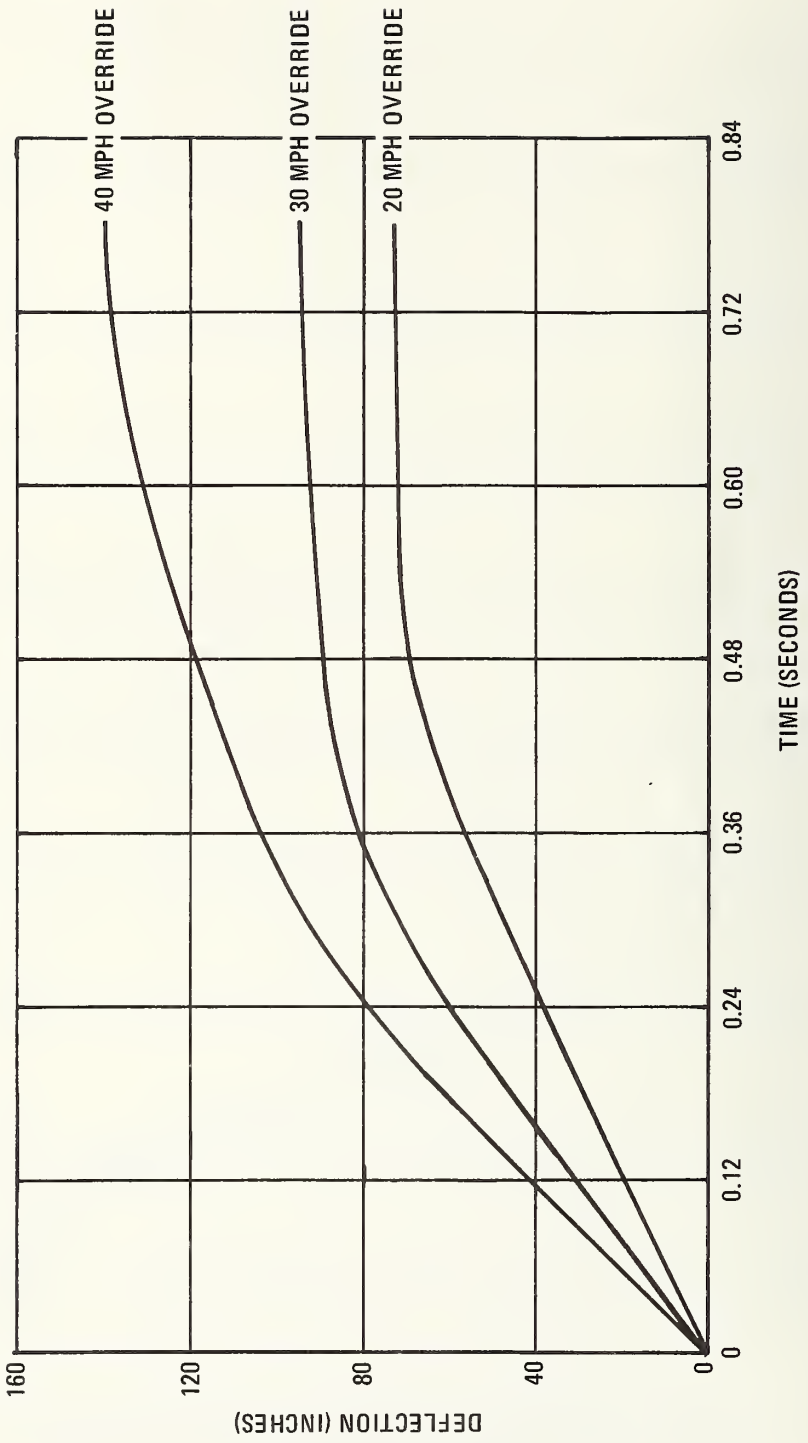

Figure 6–4. Deflection of Car No. 5 with Car Override

The override case uses both the force deflection curves of Figures 4-1 and 4-2 in the collision dynamics. It is assumed that the lead cars of each train experience the force deflection given by Figure 4-2 where the initial resistance is presented by the car sides and roof. The remaining cars in the trains experience the force deflection characteristics of Figure 4-1, i.e., end-on crash. This assumption is rational since these cars are coupled and will tend to experience anticlimber engagement.

The crush history for the lead car in the advancing train for override is presented in Figure 6-4. The maximum crush is 140 inches. Comparison of these results with those in Figure 6-1 for the end-on crash shows at 40 mph the override case has 40 inches more crush than the end-on crush. Also, the crush is not proportional to kinetic energy. This reflects the engagement of the trucks with the opposing underframe.

To illustrate the effect of not having the trucks engage the opposing underframe the reference 2 solution for the R-44 car is shown in Figure 6-5 for 80 mph closing velocity. As may be seen, the car crush is 1.75 times as great as for the end-on case. The crush in the lead car is excessive. The survivable volume in the lead car has been reduced by approximately 87 percent.

On this basis, at 40 mph and no truck engagement override, a crush of 105 x 1.75 = 182 inches would be experienced. Comparing this to the case of truck engagement (140 inches of crush) shows the reduction of 42 inches on intrusion. Thus, using the trucks as a second line of defense appears to have a benefit.

EFFECT OF CLOSING VELOCITY ON PASSENGER RELATIVE VELOCITY

The passenger relative velocity (VP) as discussed in Section 5 is used as the initial conditions for the calculation of the accelerations experienced by the catapulted passenger at impact (second-collision).

It is assumed in the calculation of the relative velocity that the passenger has the initial velocity equal to the car closing velocity. As the car decelerates, the passenger will move relative to the car and will have a velocity relative to the car. The magnitude of the relative velocity is a function of relative distance the passenger has been catapulted and is also a function of car location.

For the purposes of this study the relative distance represents passenger spacing and has been taken to be 2, 4, 8, 12, 16, 24 and 32 feet. The large values are not always obtained.

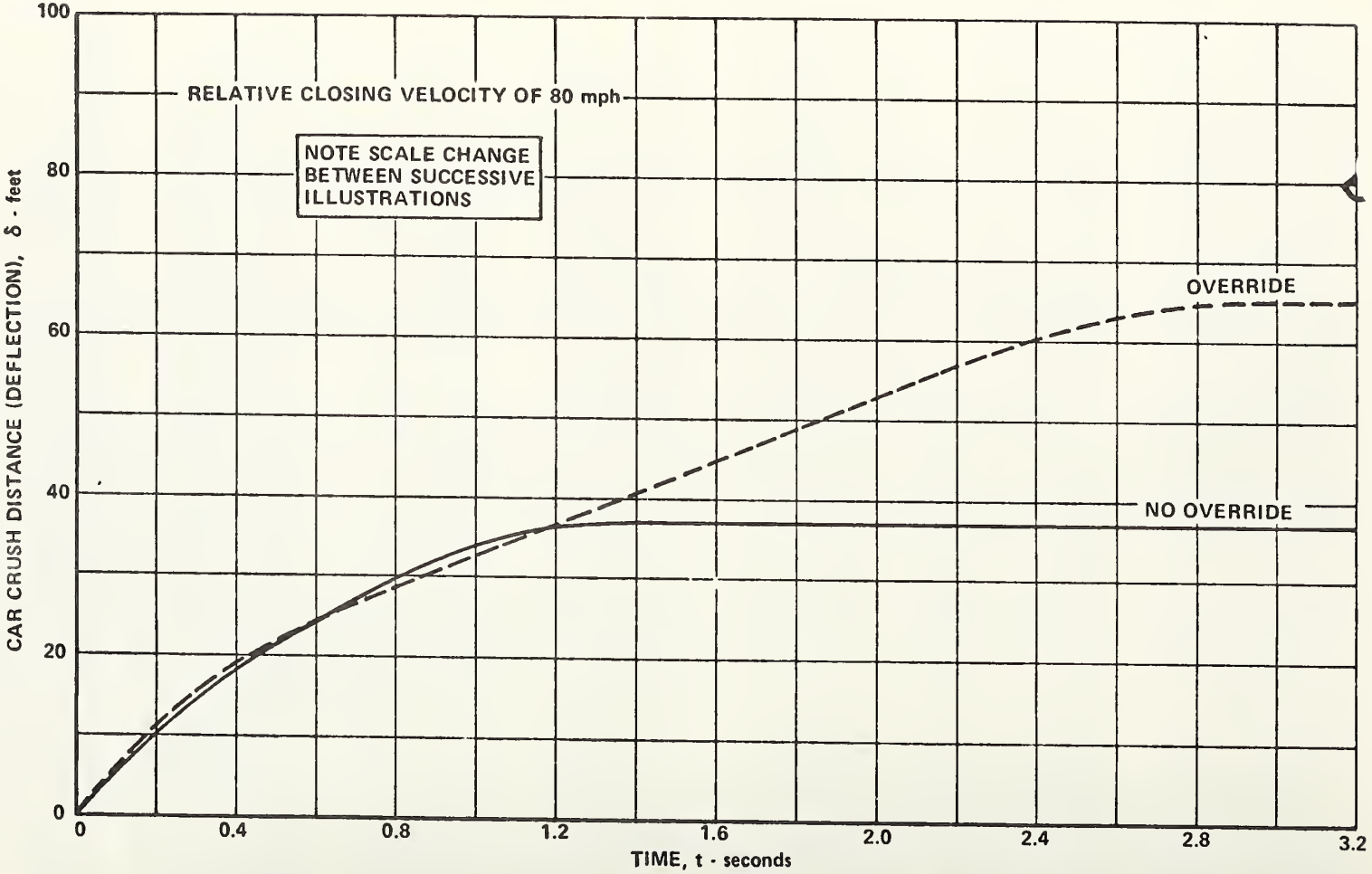

Figure 6–5. Effect of Override on Crush Distance of First Car (Two Trains of Four R-44 Cars Each)

In the collision dynamics program the relative velocity and displacement are computed for each car at each time increment. The computer tests the relative displacements of each car for 2^N where N = 1, 5 and stores the relative velocity associated with the displacement. SI is then computed for predesignated cushion distances.

Consequently, the passenger relative velocity is a key parameter in casualty determination. In Figure 6-6 is presented the passenger relative velocity for the end-on collision as a function of closing velocity. Graphs are shown for each car in the advancing train.

It may be seen that the passenger displacement (XP) has a strong effect on the relative velocity for passenger impact. As discussed later, the SI is strongly affected by VP. Thus to reduce SI the VP should be as low as practical.

Shown on Figure 6-6 is the train closing velocity and the final velocity according to simple momentum theory. Simple momentum represents the maximum VP that might be obtained if train action is not present. As may be seen train action only becomes significant to VP at the lower closing velocities, and is experienced first by the longer XP.

Where no solution is presented all cars of both the trains had reached equilibrium slide-out velocity and the computations were terminated. This eliminates values for longer XP. It is not a serious omission, because in real life, at low V_O, the passengers may take action to change the process and the larger XP itself becomes speculative.

For the short values of XP like 2 and 4 feet, VP is approximately independent of both VO and car location. Some small reduction is seen in the second car. For the longer values of XP, like 12 feet and greater, the VP increases with car location, i.e., as one goes away from the plane of impact the long XP yield higher VP.

These results give rise to the following observations:

- VP is strongly controlled by XP.
- VP is approximately independent of VO.
- VP is approximately independent of car location.
- The effect of train action on VP is more important for low speed impacts, for the remote cars, and for the large XP.

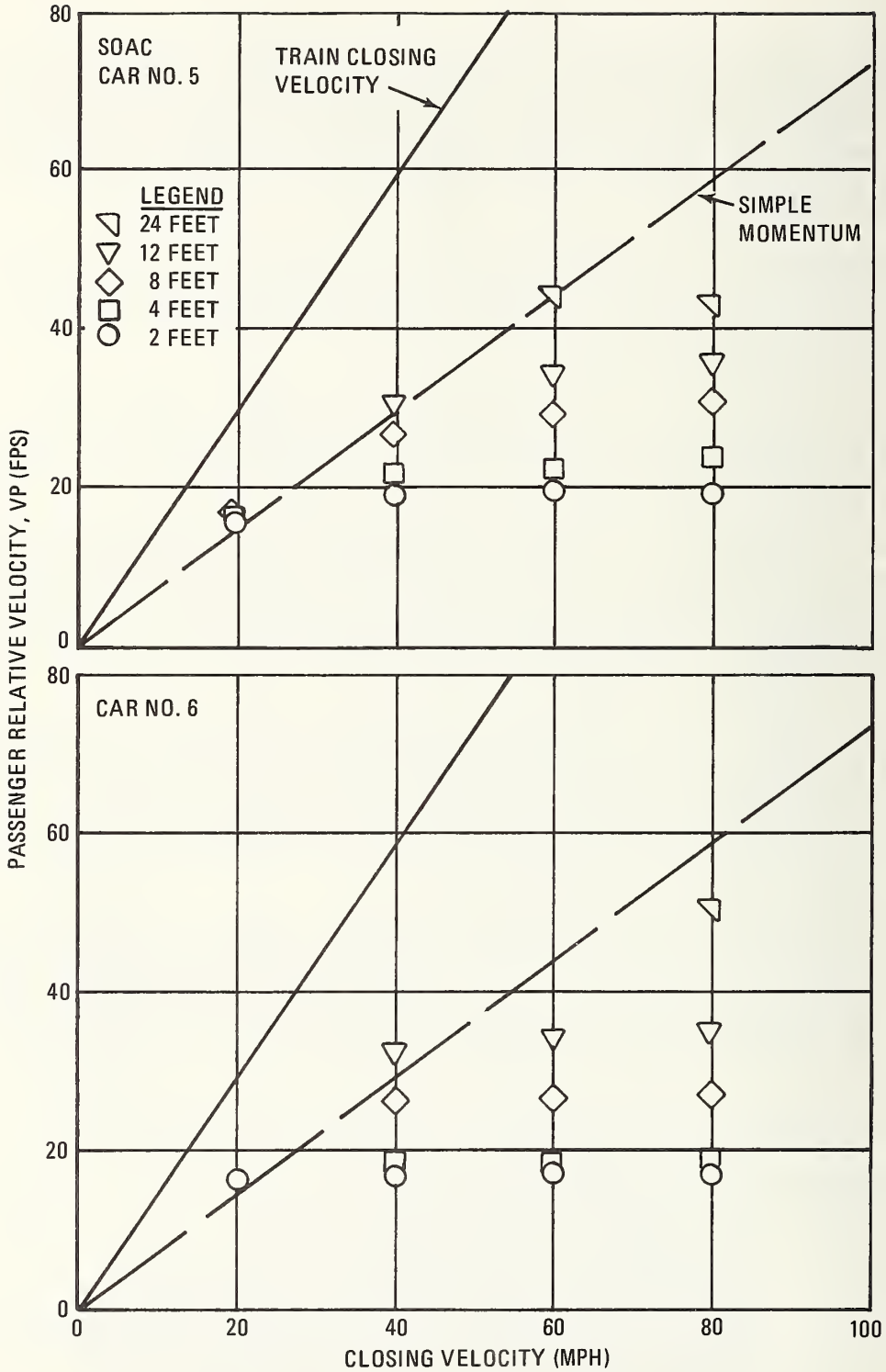

Figure 6–6. Passenger Relative Velocity Versus Train Closing Velocity (Sheet 1 of 2)

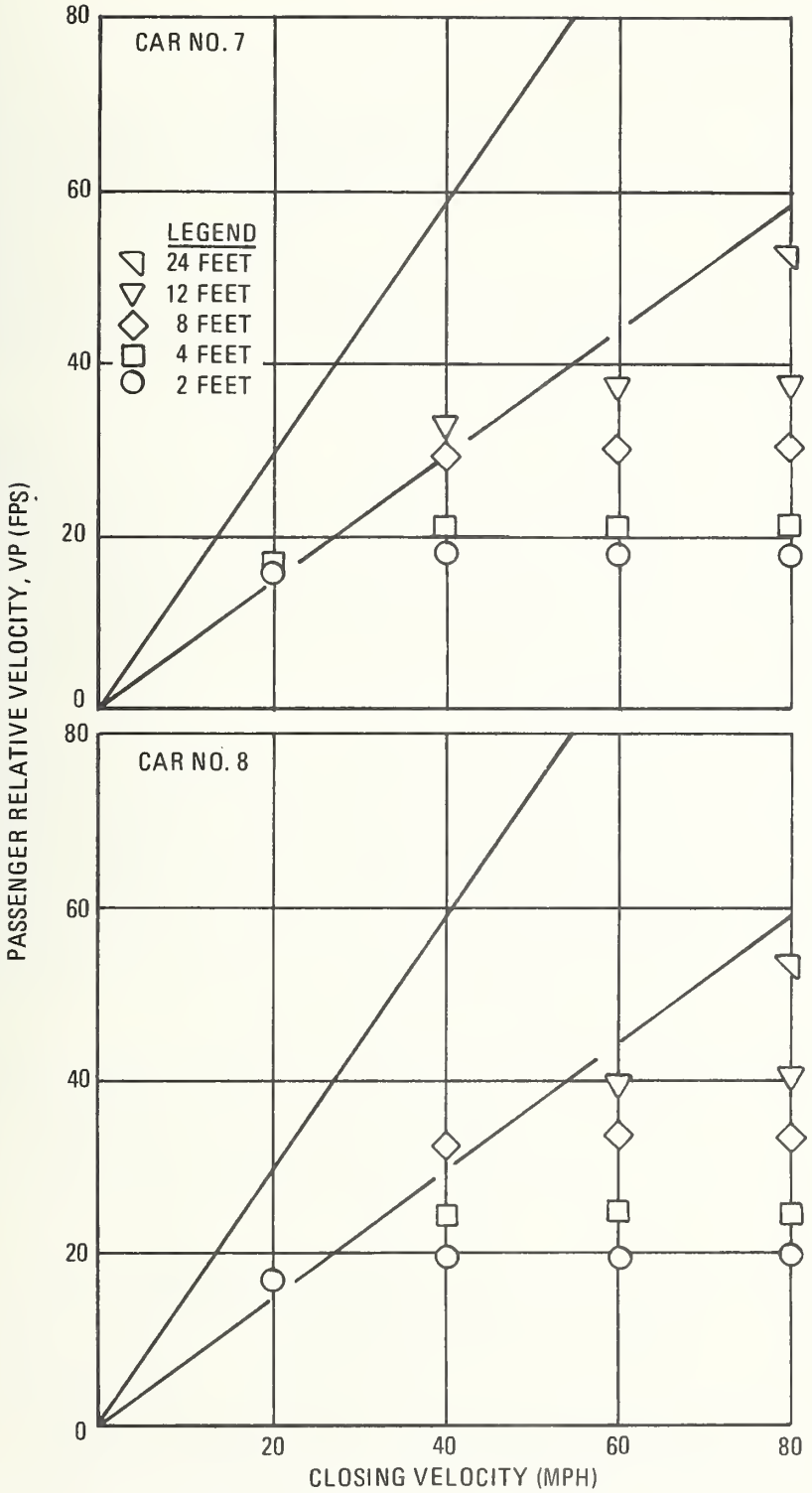

Figure 6–6. Passenger Relative Velocity Versus Train Closing Velocity (Sheet 2 of 2)

SEVERITY INDEX (SI) SENSITIVITY

As discussed in Section 5 the casualties due to second impact are quantified by the SI. SI as used in this study is a function of VP and cushion (D). The relationship for SI as a function of VP and D is shown in Figures 6-7, 6-8 and 6-9.

Basic properties of SI are that for a constant D, SI increases with VP, and for constant XP, SI decreases with D. In order to give a proper prospective to SI, the injury tolerance levels discussed in Section 5 are shown on Figure 6-7. SI greater than 2000 is defined as fatal. Thus the region of interest is where SI is less than 2000 (Table 5-1).

This enables one to bound the problem of protecting passengers. For instance, if passengers are permitted to have VP greater than zero (VP = 0 is defined as the restrained passenger) and a practical limit of D taken as two inches, then the maximum survivable (non-fatal) VP is 38 feet/second. Referring to Figure 6-6, then XP is limited to approximately 12 feet. Should D be one inch, then VP = 30 feet/second and the value of XP is approximately 6 feet. Detailed trade studies using these data are presented in Section 7.

Referring to Figure 6-8, SI versus VP is shown for constant D, in distinction to logarithmic presentation shown in Figure 6-7. The rate of change of SI with VP is readily discernible in this presentation. The rate of change (sensitivity) of SI increases for a given D as SI increases. For instance, small changes in VP will change a fatal impact into a survivable impact, if D = .25 inches and VP = 13 ft./sec. the fatal SI is achieved. Should VP be reduced to 11 ft./sec. SI = 950 and a moderate injury is sustained. This sensitivity of severe SI to VP will be seen in more detail in Section 7.

In Figure 6-9 is given SI versus D for constant VP. The survivable limit is shown as the cross-hatched line at SI = 2000. The sensitivity of SI to variations in D is a maximum at the high values of SI. Thus for VP = 20 mph and D = 1 inch a fatal impact is reduced to a moderate injury by increasing D to 1.5 inches.

Figure 6-9 also shows another important property of SI; that is, as VP is increased, an increase in D is less effective in reducing SI. Consider VP = 35 mph and VP = 20 mph. For VP = 35 mph an increase in D of 1 inch to D = 5.25 changes SI from fatal 2000 to a severe injury of 1500, while at VP = 20 mph the increase in D of 1 inch to D = 2.0 change SI from a fatal 2000 to a moderate injury of 700.

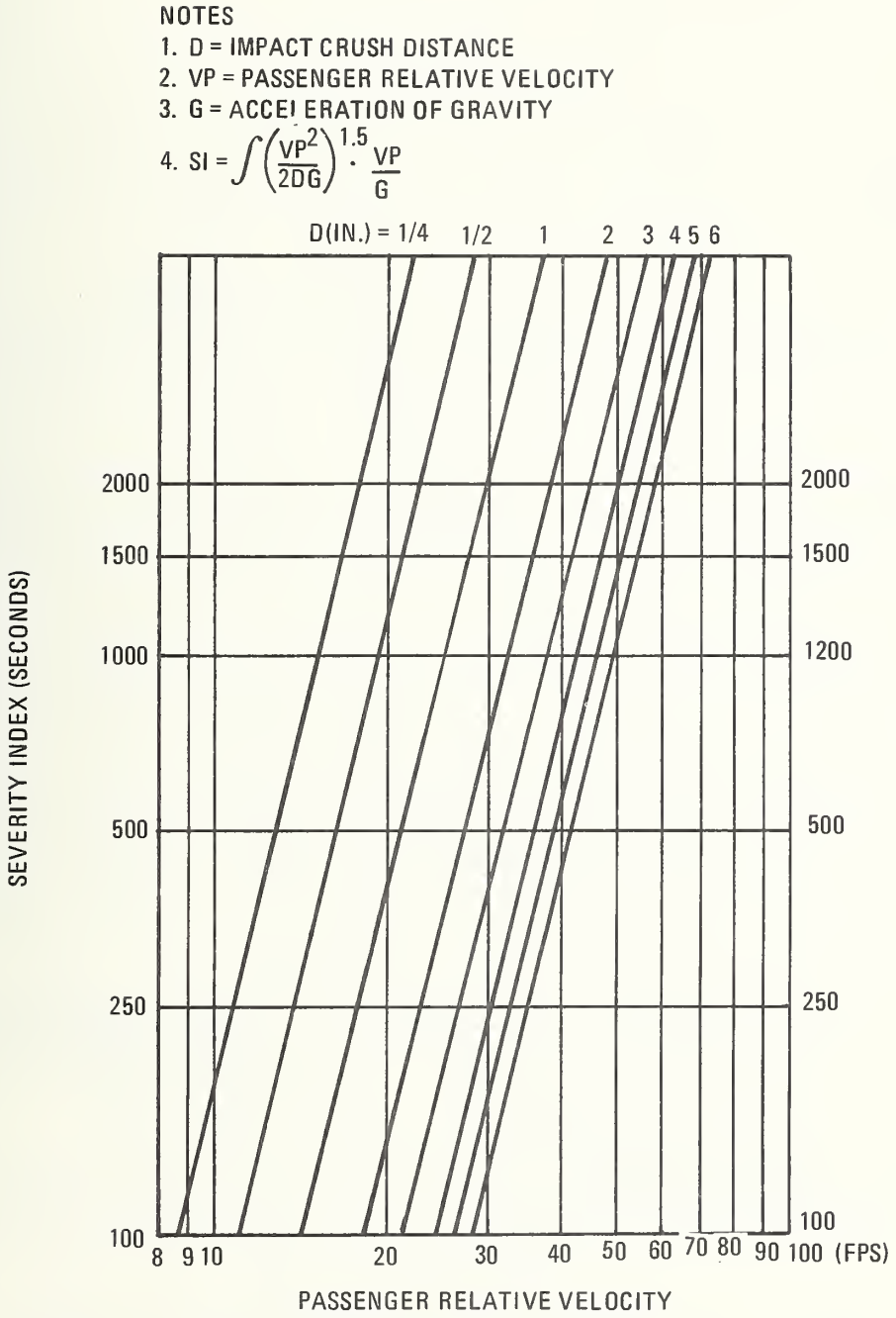

Figure 6–7. Severity Index Versus Passenger Relative Velocity for Constant Cushion Crush Distances

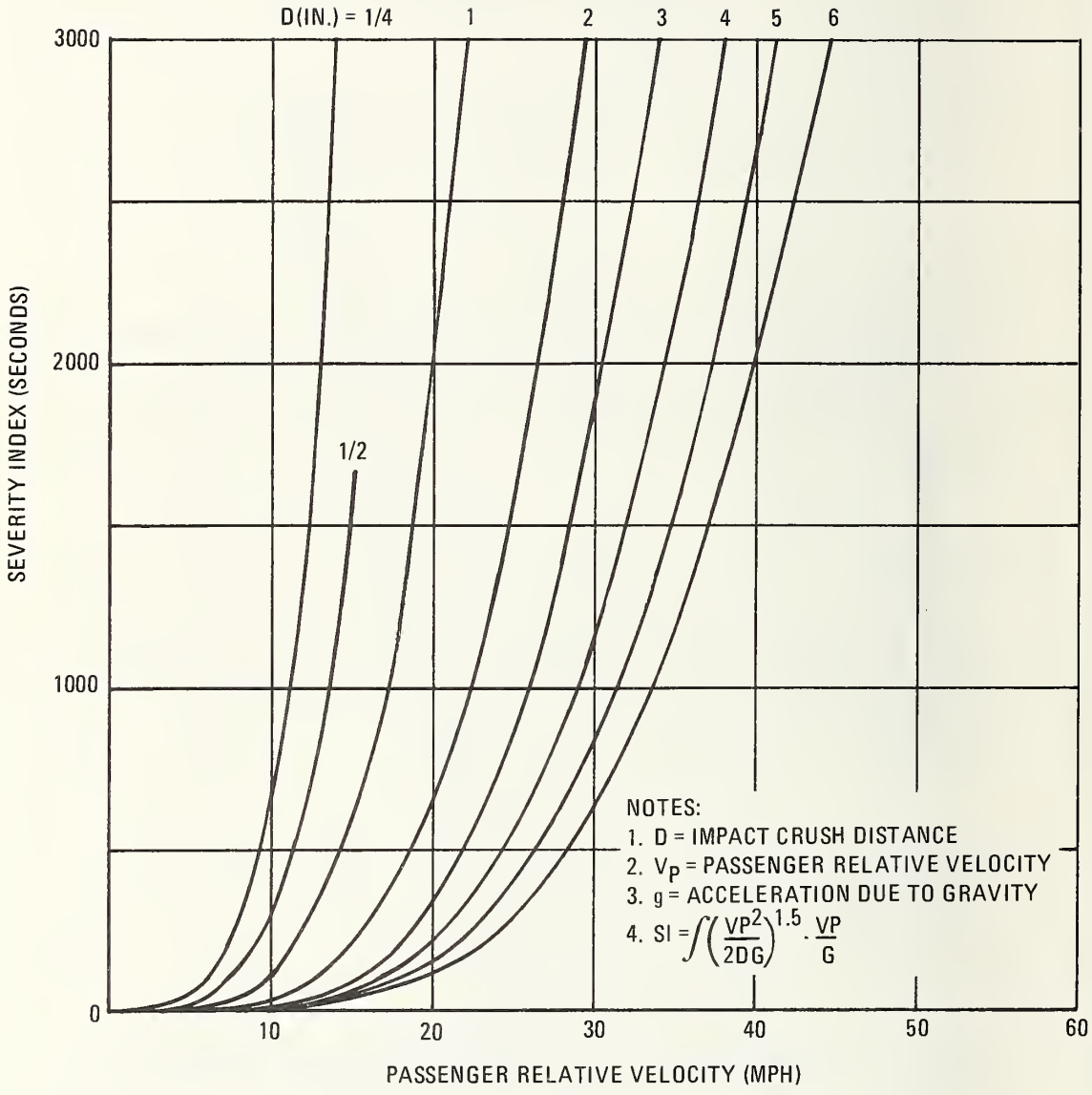

Figure 6–8. Severity Index Versus Passenger Relative Velocity for Constant Cushion Crush Distances

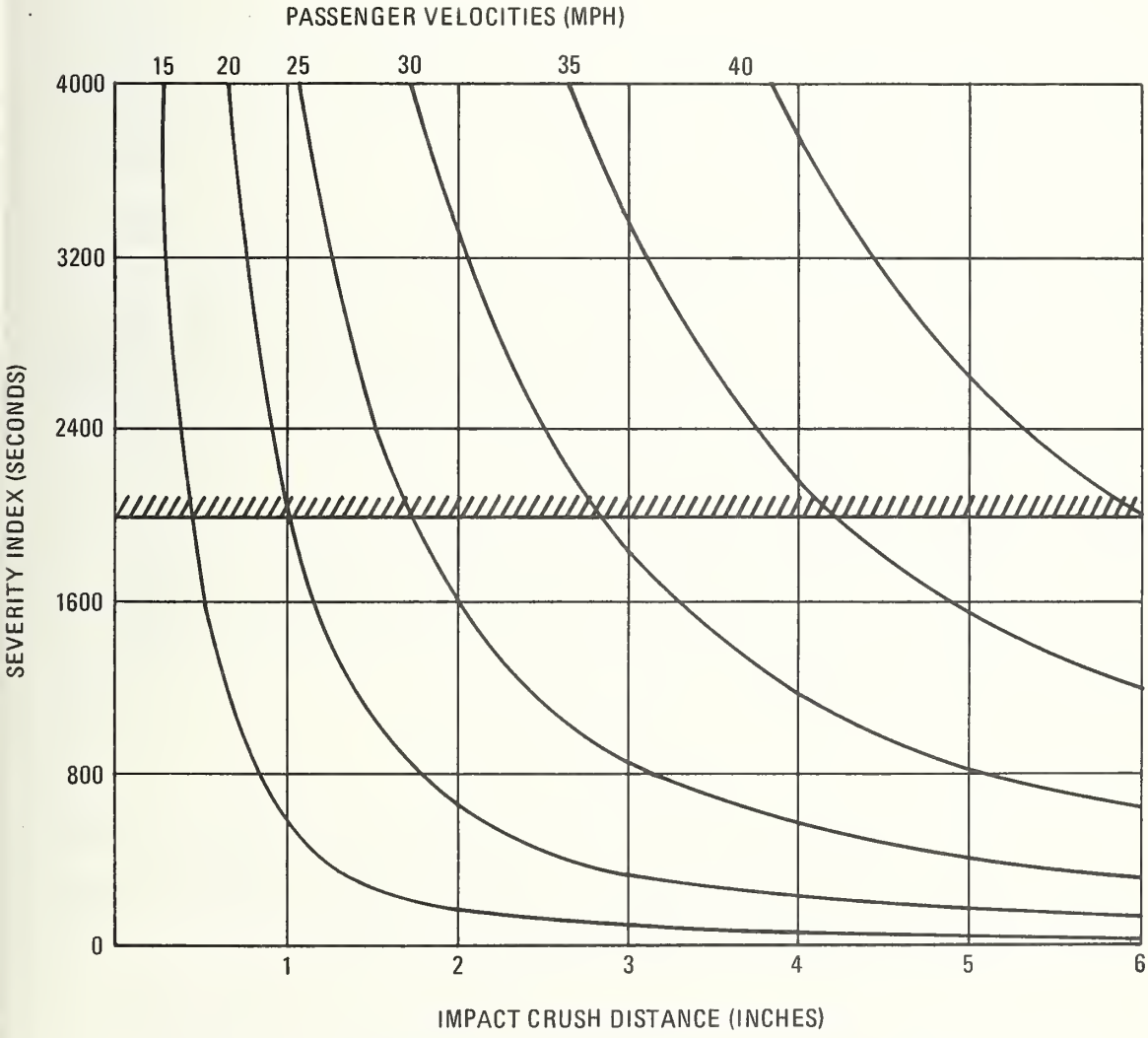

Figure 6–9. Severity Index Versus Impact Crush Distance for Constant Passenger Velocities

Perhaps the more significant relationship is illustrated in Figure 6-9 by considering the effect of a hard car interior ($D < .50$) and a soft car interior ($.5 < D < 2.0$). For the hard car, fatalities are obtained for VP greater than 15 mph. By softening the car interior (D = 2) the non-fatal VP is extending to approximately 27 mph. Thus marked reductions in injury may be achieved by moderate changes to the car interior, other factors held constant.

CAR STRENGTH

The effect of car strength on the collision dynamics has also been treated using VO = 40 mph. The force ordinates of the force deflection curve, Figure 4-1, were multiplied by a factor ranging from .5 to 4.0 and the collision equations were solved for the end-on collision. The crush of the lead car of the advancing train is shown in Figure 6-10 as a function of time.

The value of .5 represents a light construction with a limit buff load of 250,000 pounds, while the 4.0 case represents a strong design with a limit buff load of 2,000,000 pounds. As might be expected, the final crush values vary inversely to the strength factor. Some departures may be noted. The crush for 1.0 is 100 inches and instead of the expected 50-inch crush for 2.0 the crush is 32 inches. These departures are attributed to the action of coupler and the depth of penetration experienced. The SI's associated with these solutions are used in the studies presented in Section 7.

The results shown in Figure 6-10, taken with the results discussed under "Effect of Closing Velocity on Crush", earlier in this chapter, illustrate a fundamental concept for crashworthiness. Simply stated, the kinetic energy lost is equal to the integral of the product of the resistive force and the incremental deflection:

$$\frac{1}{2} M (V_O^2 - V_F^2) = \int_O^X F dx$$

For a first approximation, the force deflection shape for SOAC, Figure 4-1, may be considered to be rectangular. Thus for constant resisting force, the car crush is proportional to the kinetic energy, and for constant kinetic energy, the crush is inversely proportional to the resisting force.

The simple relationship assumes significance for crashworthiness when the relationship between the ultimate buff strength of the car and the resistive force is considered. The magnitude of the resisting force is directly related to buff strength of the car. Thus to reduce the car crush significantly the buff strength must be increased significantly.

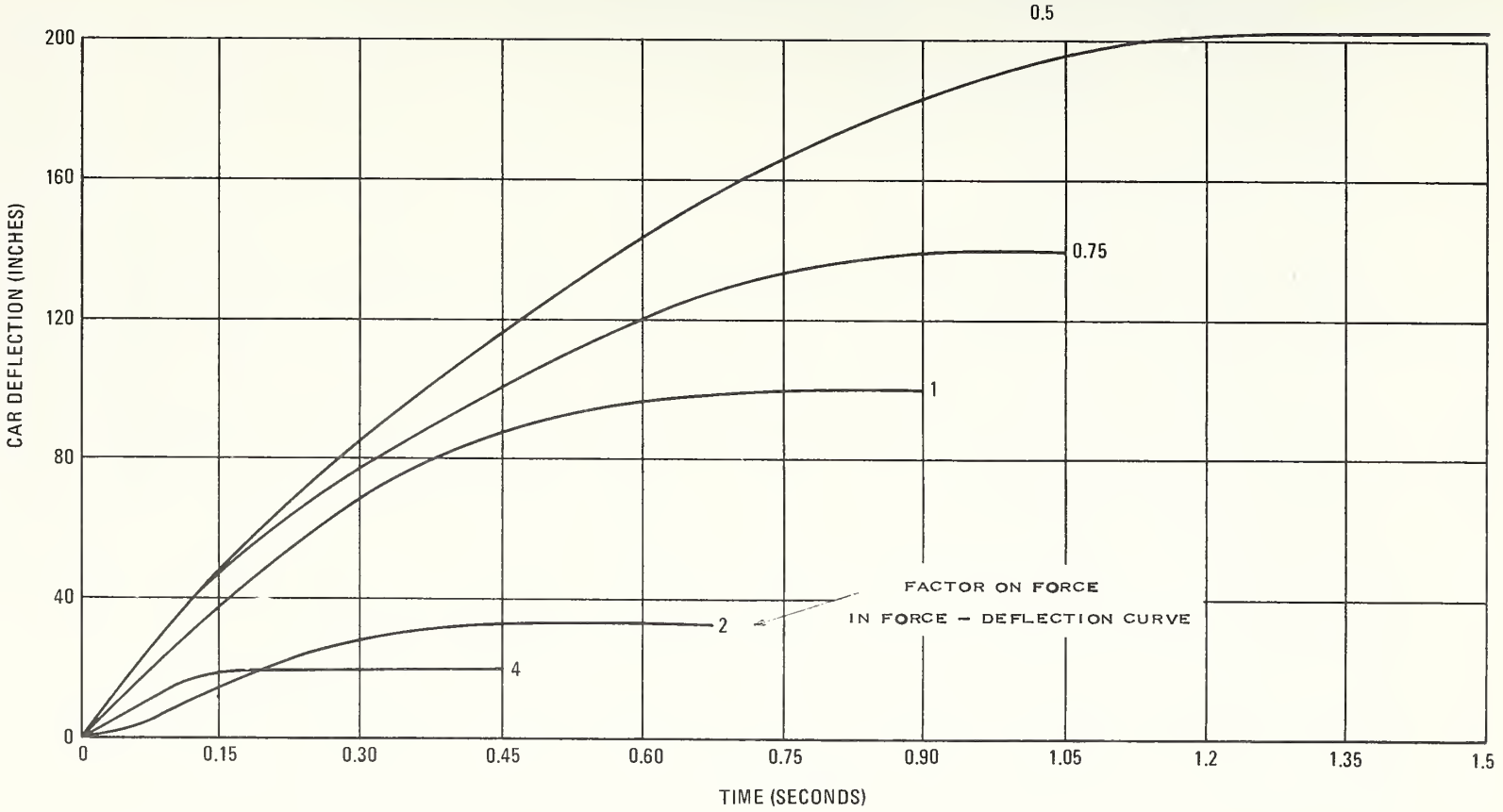

Figure 6–10. Effect of Car Strength on Crush Deflection (Car No. 5, V_o = 40 MPH)

RESTRAINED PASSENGER

An interesting aspect of SI is also in these studies. If the passengers were fixed to the car center of gravity and were to experience only the deceleration of the car center of gravity and no other secondary decelerations, how would they fare? The value of the integral form of SI has been calculated for each time by the computer program during the crash. The SI for the car center of gravity (XP = 0) is shown in Figure 6-11. As may be seen, the SI obtained is well within the no-injury level of 0-250. The increase in SI after t = 0.075 second is due to the longitudinal accelerations experienced as cars vibrated back and forth. Thus, if other aspects of injury mechanisms such as onset rate are not important, the use of restraints would eliminate injuries. The practical application of this information is a problem for the future.

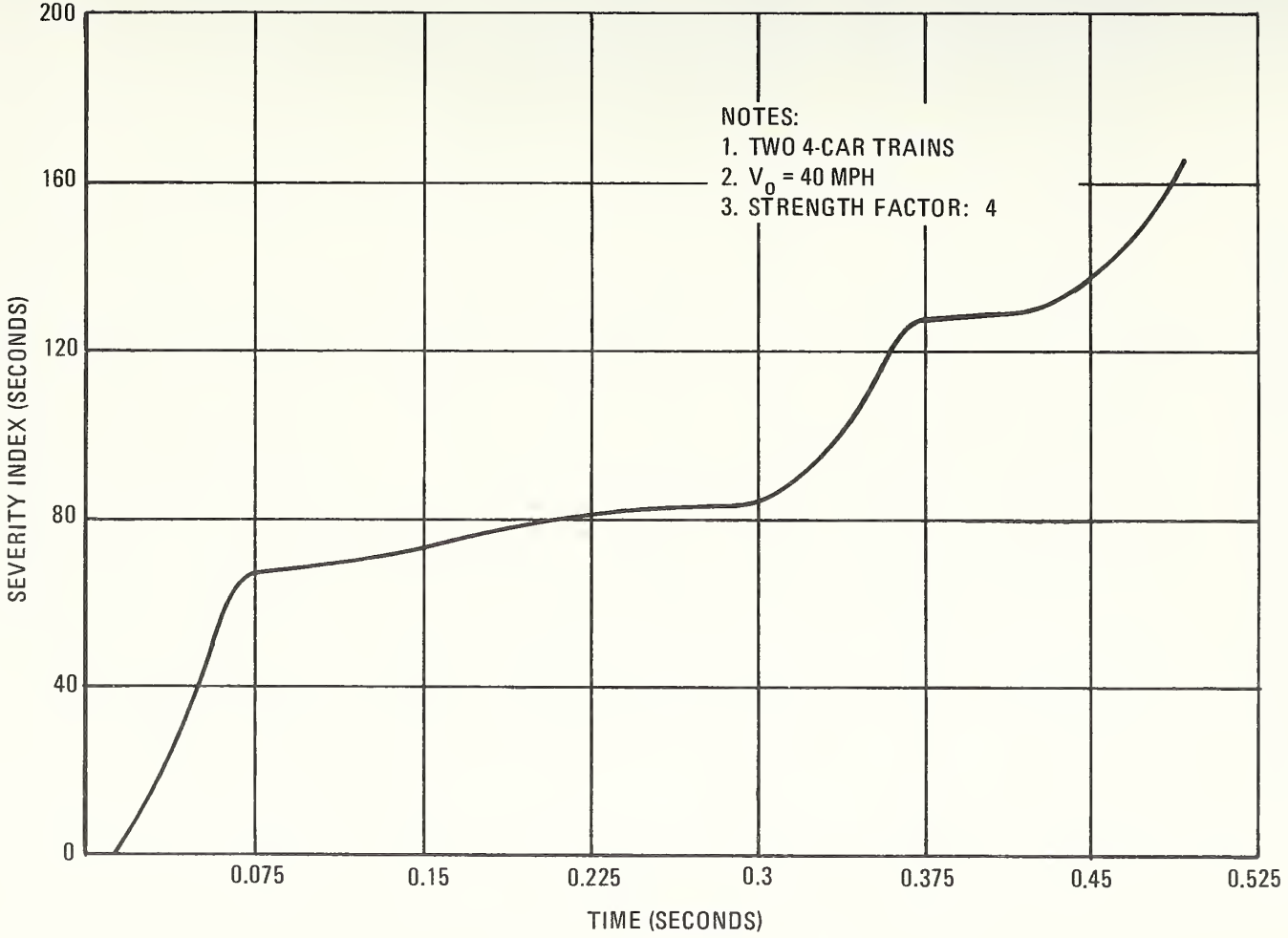

Figure 6–11. Severity Index for Center of Gravity of Car No. 5

7. CRASH CASUALTY SENSITIVITY STUDIES

The effect of the variables discussed in Section 6 were investigated as terms of the overall number of and severity of, injuries incurred in a collision of two 4-car SOAC trains. The methodology employed in determining injury levels (SI) for passengers is the same as that used in reference 2 as shown in Section 5. The passenger spacing (XP) and corresponding impacted-object crush distances (D) are also patterned on distances (D) of 1 and 2 inches in reference 2 and referred to as a "soft" interior, a second case with D's of 1/4 and 1/2 inch ("hard" interor) was also evaluated. These (XP) and (D) values for the high density SOAC are shown in Figure 7-1.

The following range of variables were examined for the hard and soft interior cars:

1) Collision Speed: Train closing speeds of 20, 40, 60 and 80 mph were evaluated for the baseline case.

2) Structural Stiffness: Multiples of 0.5, 0.75, 2.0 and 4.0 times the basic SOAC structure are evaluated.

3) Passenger Spacing: To determine sensitivity to variations in passenger spacing the high density seating arrangement was reconfigured to an all forward-facing arrangement.

COLLISION SPEED SENSITIVITY - STANDING PASSENGERS

As in reference 2, standing passengers were treated in the same manner as seated passengers in calculating the SI except that X_p was assumed to be 12 feet. This resulted in a large number of serious injuries at speeds of 40 mph and greater. Figure 7-2 shows the total number of critical and fatal (C&F)(1824) injuries. The figure shows that in the hard interior car all standees who were not in the area of the car which was crushed (first collision) received C&F injuries when catapulted into an obstruction (second collision).

In the soft interior car more than half of the standees suffered C&F injuries due to being catapulted. Based on the CTA collision of October 30, 1972, the number of C&F injuries projected by the SI is excessive. The reason for this large disparity is not completely understood; however, some of the factors which may tend to mitigate the severity of the injuries to standing passengers in real crashes are:

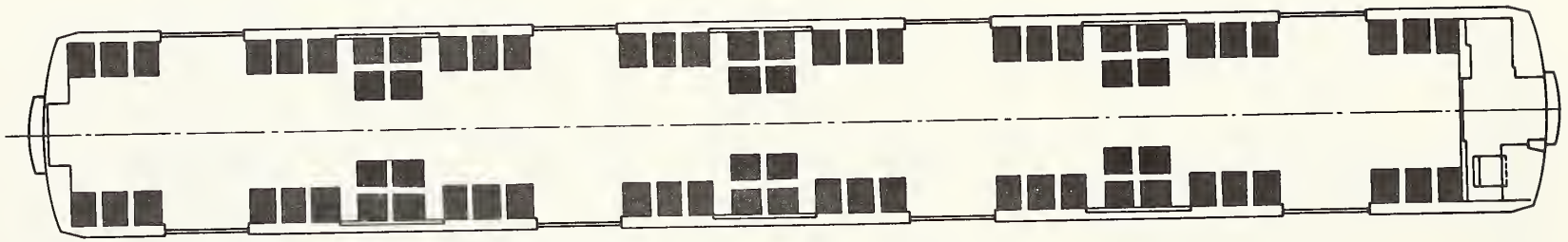

NOTES:

1. HARD INTERIOR: 50% OF PASSENGERS DEFLECT SURFACE 1/4 INCH
   50% OF PASSENGERS DEFLECT SURFACE 1/2 INCH
2. SOFT INTERIOR: 50% OF PASSENGERS DEFLECT SURFACE 1 INCH
   50% OF PASSENGERS DEFLECT SURFACE 2 INCHES
3. TOTAL OF 72 SEATED PASSENGERS:
   - 24 SEATS FACING FORE AND AFT WITH FREE SPACE OF 2 FEET (ASSUMED)
   - 48 SIDE-FACING SEATS WITH FREE SPACE OF 4 FEET (ASSUMED)
   - 228 STANDEES WITH FREE SPACE OF 12 FEET (ASSUMED)

Figure 7–1. Standard High-Density SOAC Car

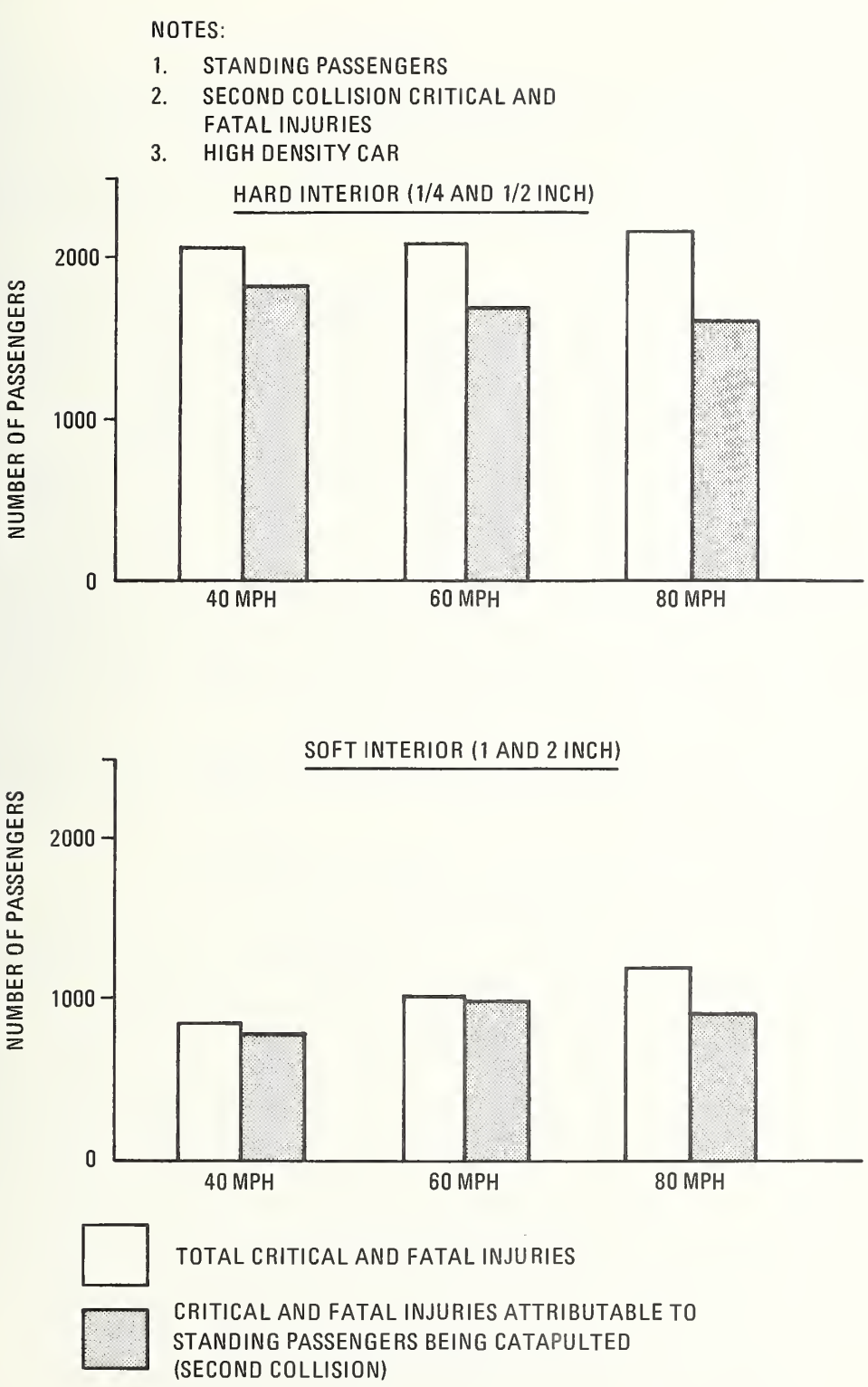

Figure 7–2. Second Collision Casualties for Hard and Soft Car Interiors

1) Impacted Object Crush Distance: At a maximum passenger load urban transit cars have a passenger density of one passenger for every two square feet. In this situation most of the passengers would not impact the relatively hard car interior but other passengers, and as shown in Figure 6-9, the SI is very sensitive to increases in (D).

2) Passenger Impact Velocity: The standing passenger's impact velocity will be affected by three factors: The distance of the standee from the impact point, the number of standees in the car and the degree of passenger restraint prior to impact. The impact point can be the car interior or other passengers. Standees in the rear of the car will travel the greatest distance to the impact point. This distance however, is varied depending upon the number of standees. The more standees in the car, the shorter the distance one will travel. Cushion is greater for those in the rear because of compression of passengers between them and the car interior. Impact velocity is also affected by restraint during vehicle deceleration. Most standing passengers will be holding onto posts or straps and this restraint will tend to reduce their impact velocity.

Since data concerning the interaction between the impacted object and the standing passenger are not fully understood, it was decided to limit the scope of the following sections to seated passengers.

COLLISION SPEED SENSITIVITY - SEATED PASSENGERS

Figure 7-3 shows the passenger injuries as a function of collision speed for the hard and soft high density SOAC. The six injury categories of the AMA abbreviated injury index Table 5-1 used in reference 2 were grouped into three classes: (1) No injury and minor injury (N&M) (SI<500); (2) moderate to serious injury (M to S) (500<SI<2000); and (3) critical and fatal injury (C&F) (SI>2000). As would be expected, as the collision speed increases from 20 mph, the number of N&M injuries falls off as these are translated into M&S injury. At the same time, some N&M injuries become C&F level injuries. It should be noted that while the number of injuries are shown as continuous curves, the number of injuries is in reality a discreet function, since a person is either in or out of a given class and secondly, people are transferred from injury levels to groups (i.e., all passengers in Car A having X feet of (D) and Y feet of X_p are fatally injured at speed V_p). For the purpose of establishing general trends, however, it is felt the use of curves will not seriously affect the conclusions.

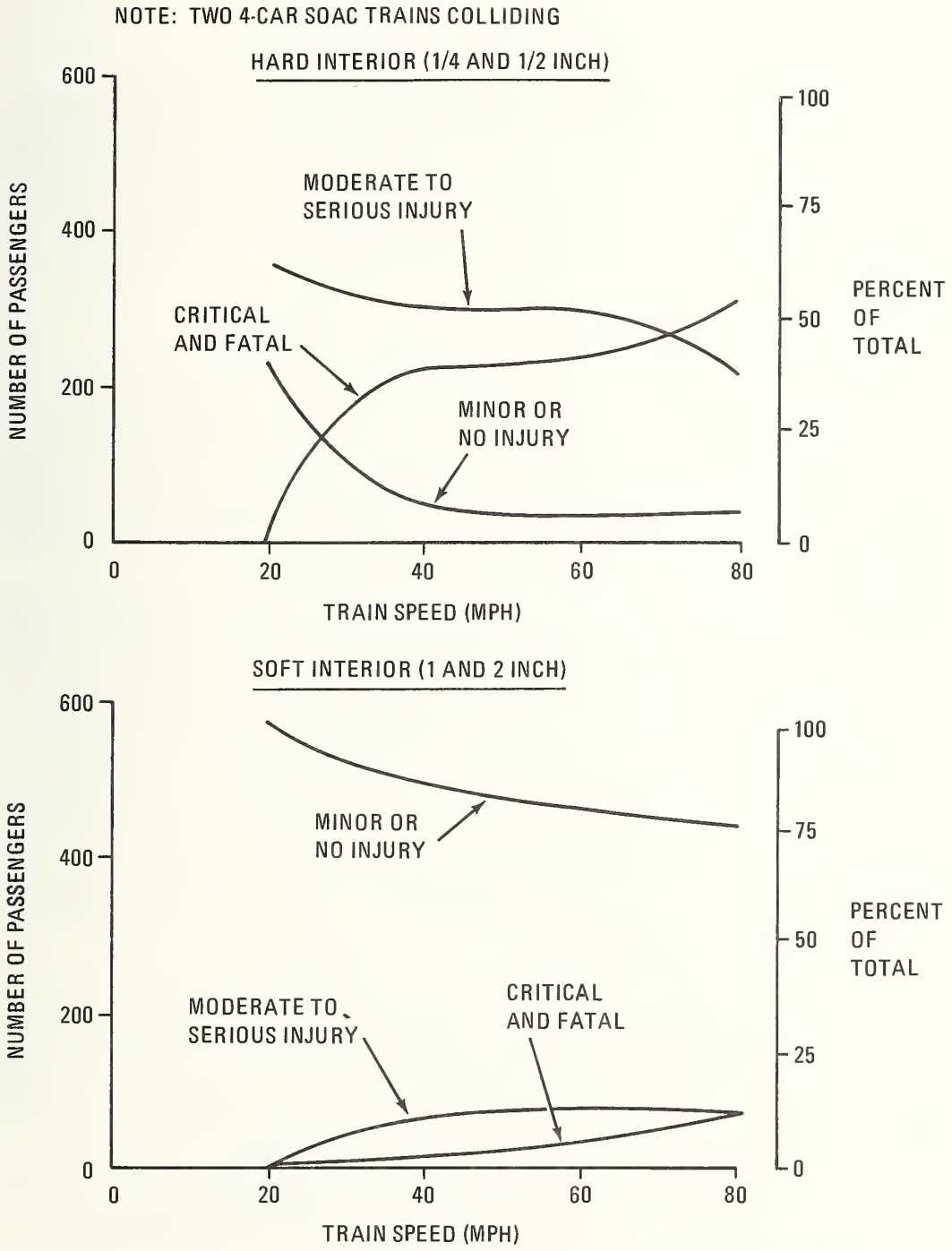

Figure 7–3. Casualties for Hard and Soft Car Interiors as a Function of Closing Velocity

As Figure 7-3 shows, the impacted-object crush distance has a very large influence on the overall injury level. For example, at 40 mph in the soft interior car, 86% (494) of the passengers receive only N&M injuries while in the hard interior car only 8% receive N&M injuries, 53% S to M injuries and 39% C&F injuries. In general, Figure 7-3 shows that one of the most important criteria in determining the "crashworthiness" of a railcar will be whether it has a hard or soft interior.

EFFECT OF STRUCTURAL STIFFNESS ON TOTAL CASUALTIES

In order to limit the number of combinations for the variables being evaluated, it was decided to analyze the effect of structural stiffness at a constant collision speed. As was seen in Figure 7-3, a large increase in casualty levels occurs as collision speed increases from 20 to 40 mph. This and the feeling that 40 mph seems like a "reasonable" collision speed for urban rail accidents was the basis for selecting 40 mph as the speed at which to evaluate structural stiffness.

Figure 7-4 displays the sensitivity of the overall injury levels for stiffness factors from 0.5 to 4.0 times that of the present SOAC. Since any increase or reduction in the stiffness of the SOAC will affect car crush and passenger impact speed, the basic tradeoff is between injuries due to car crush and passengers being catapulted (first- and second-collision injuries). For example, if the criteria for crashworthiness is to minimize the number of C&F injuries, Figure 7-4 indicates the structure of the hard interior car should be made weaker. Any increased stiffening to reduce first-collision C&F injuries would be more than offset by increased second-collision C&F injuries. In the soft interior car, as shown in Figure 7-4, the minimum number of C&F injuries is reached at a stiffness factor of about 1.0.

Figure 7-5 illustrates C&F injuries and identifies them as to cause. Figure 7-5 also shows the first-collision C&F injuries to standing passengers. These were calculated by finding the floor space per passenger (1.735 sq. ft.) at maximum load (228 standees) and dividing this into the total available floor space which was destroyed by the car crush. The dotted line indicates the total C&F injuries. The inclusion of standing C&F injuries due to car crush does not affect the conclusion arrived at concerning the soft interior car. The hard interior car now shows that an increase in total C&F casualties will occur if the structure is weakened below 75% of the present SOAC stiffness.

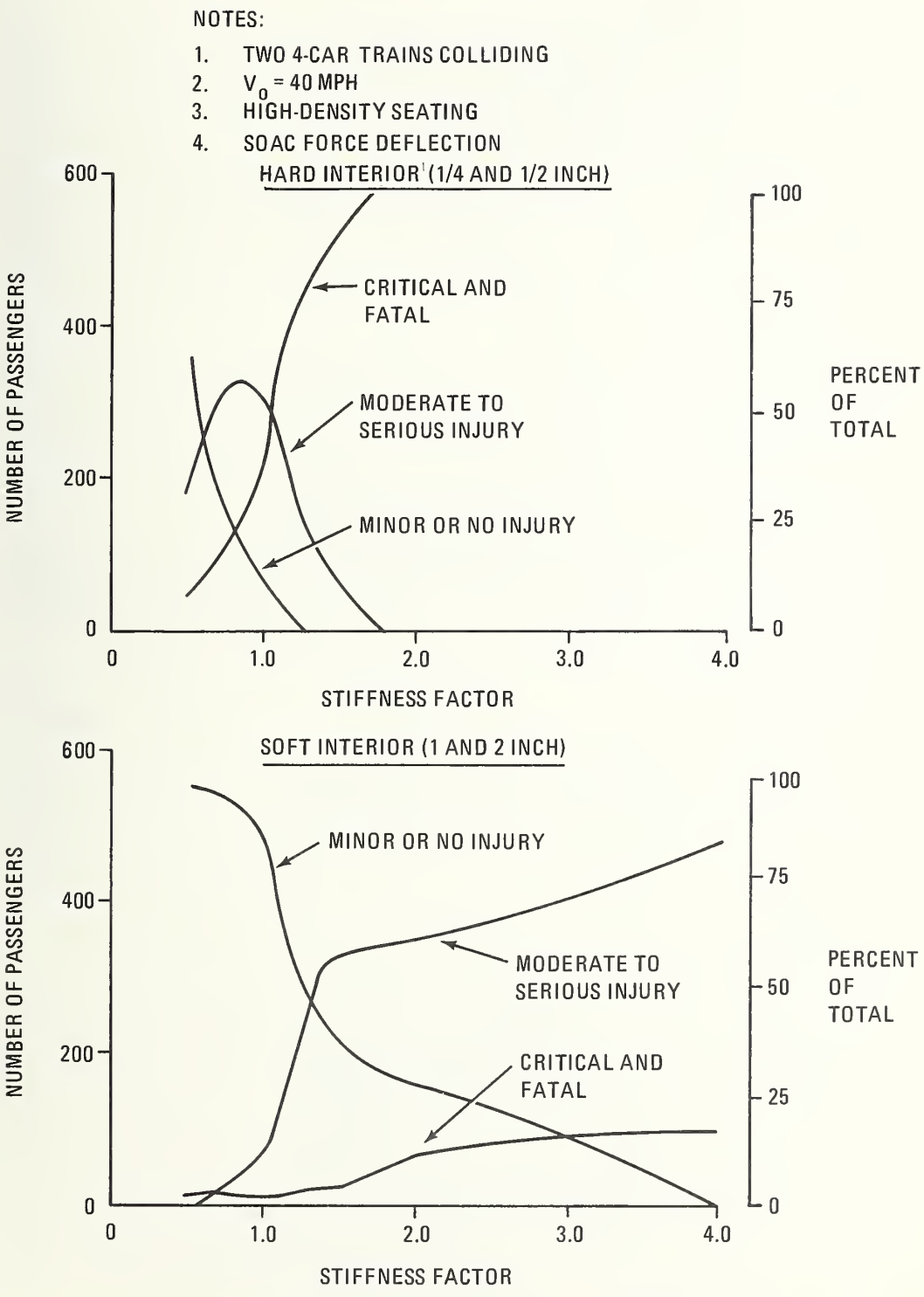

Figure 7–4. Casualties Versus Stiffness Factor for Hard and Soft Car Interiors

NOTES:

1. TWO 4-CAR TRAINS COLLIDING
2. V_0 = 40 MPH
3. HIGH-DESNTIY SEATING
4. SOAC FORCE DEFLECTION CURVE

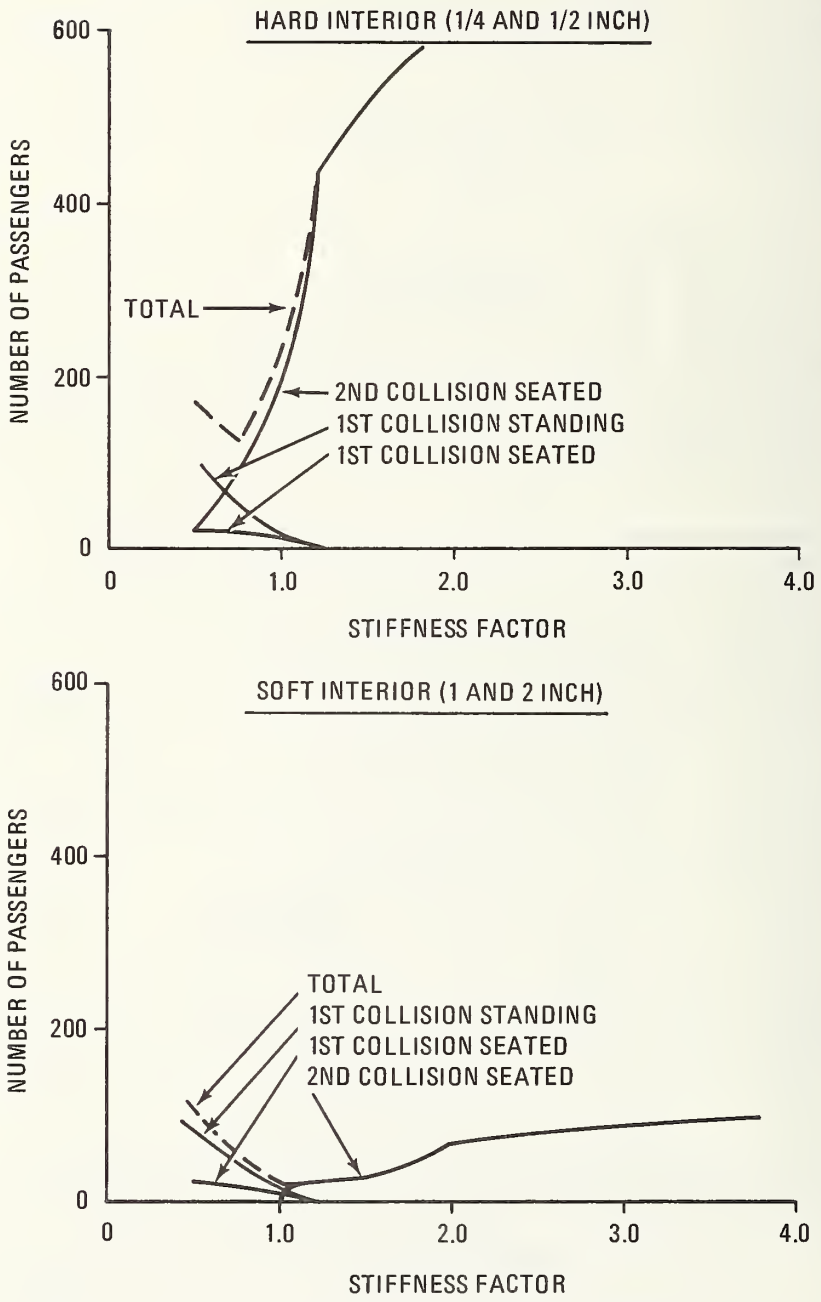

Figure 7–5. Passenger Fatality Cause for Hard and Soft Car Interiors

It is interesting to note that the crashworthiness problem for rail vehicles has two principal elements. First is the prevention of crush fatalities due to the first collision by adequate energy absorption to prevent penetration. Second, is providing a proper "soft" interior to eliminate fatalities and to reduce the severity of injury due to the second impact. Referring to Figure 7-5, the benefit of providing adequate stiffness for the crash conditions is readily seen. In this case the first collision fatalities could be eliminated by a modest increase in stiffness. For a higher energy level crash involving more cars, or increased velocity, or both, it is expected that the null point would move to a higher stiffness factor.

Second collision fatalities are reduced dramatically through the provision of additional softness over that of the "hard" car. The gradual rise in the second collision fatalities shows the sensitivity of SI to VP changes arising from the change in the car velocity at time of passenger impact. The benefit could be increased by providing additional cushioning.

Therefore, to provide crashworthiness to a given energy level, sufficient stiffness should be provided to minimize the first collision casualties. When this is done, the car interior should be provided with sufficient softness to minimize the second collision casualties.

PASSENGER SPACING

To evaluate the effect of reduced free space, the high density SOAC seating was reconfigured into an all forward-facing arrangement as shown in Figure 7-6. This eliminates the four feet of free space associated with the center facing seats. Figure 7-7 displays the variation in injury levels as a function of car stiffness.

In terms of C&F injuries, the revised seating is much the same as in the standard seating arrangement for hard interior car. In the soft interior car the C&F injuries go to zero at a stiffness factor of 1.0. The reason for this is that the region between the forward or aft bulkhead and the door can accommodate only one forward facing seat. The greater the distance between the bulkhead and the seat, the greater the car crush required to generate a first collision casualty and the reduced passenger free space prevents second collision C&F casualties for a stiffness factor up to 1.75. It should be noted, however, that if passengers are allowed to stand in the area between the seat edge and the bulkhead they would become first-collision C&F casualties for stiffness factors less than the 1.25 as shown in Figure 7-4.

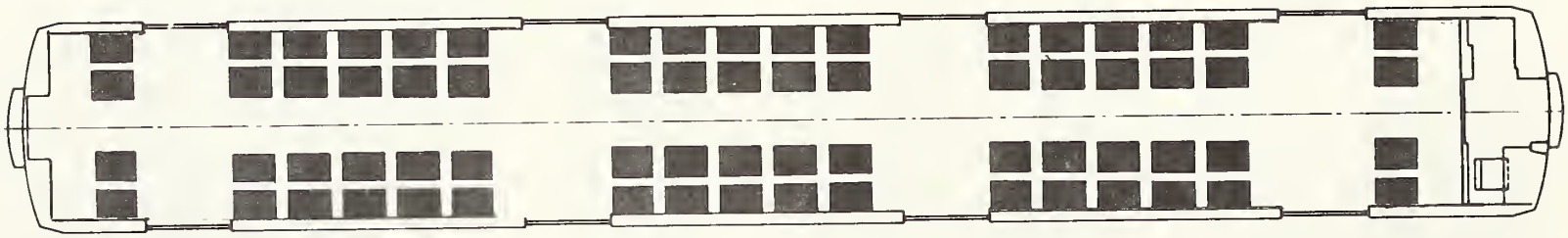

NOTES:

1. HARD INTERIOR: 50% OF PASSENGERS DEFLECT SURFACE 1/4 INCH
   50% OF PASSENGERS DEFLECT SURFACE 1/2 INCH
2. SOFT INTERIOR: 50% OF PASSENGERS DEFLECT SURFACE 1 INCH
   50% OF PASSENGERS DEFLECT SURFACE 2 INCHES
3. TOTAL OF 68 SEATED PASSENGERS (ALL FORWARD FACING WITH 2 FEET OF FREE SPACE)

Figure 7–6. Modified SOAC Seating (68 Forward-Facing Seats)

NOTES:

1. TWO 4-CAR TRAINS COLLIDING
2. V_0 = 40 MPH
3. ALL FORWARD FACING SEATS
4. SOAC FORCE DEFLECTION CURVE

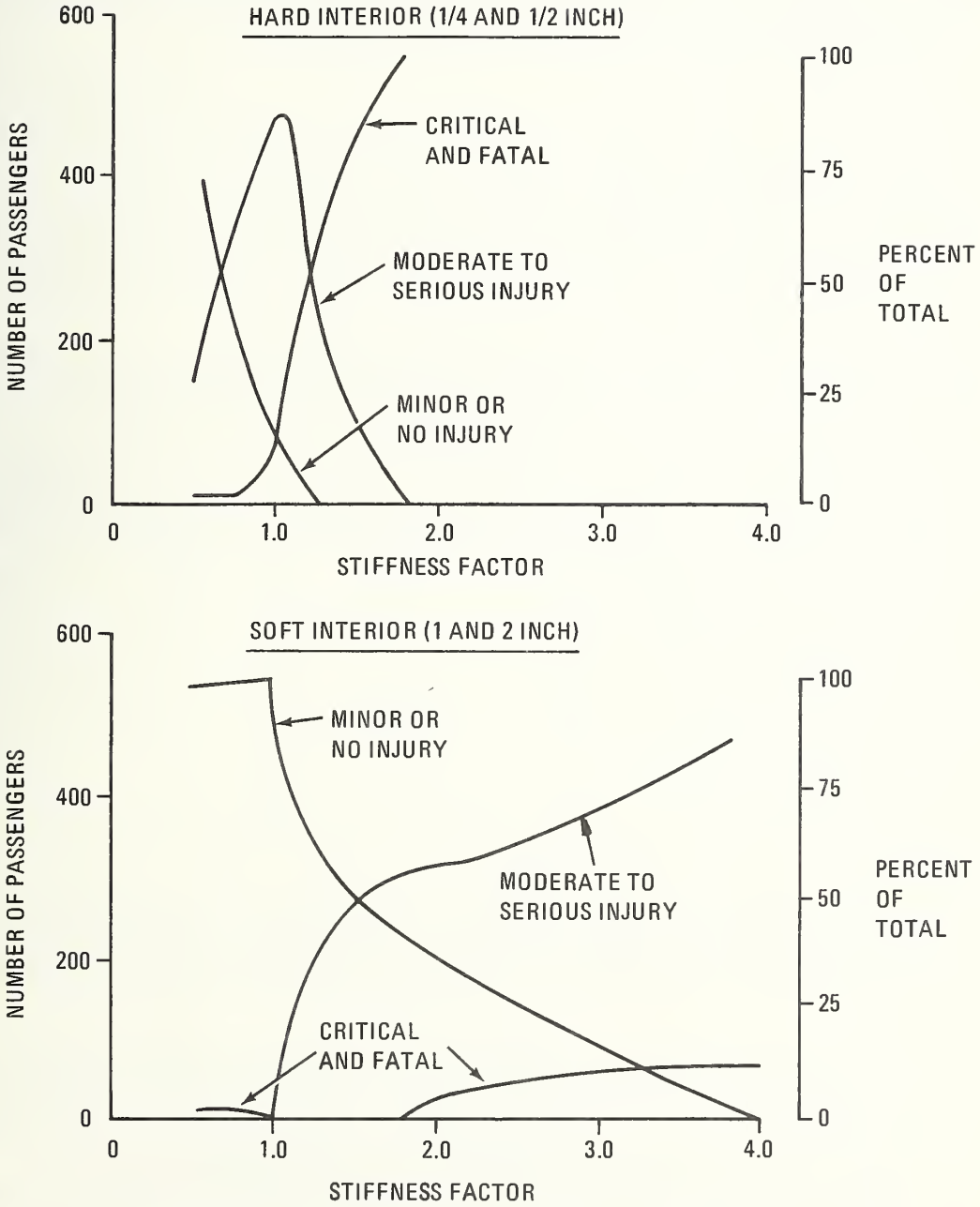

Figure 7–7. Casualties Versus Stiffness for Hard and Soft Car Interiors

When using forward-facing seats a reduction in moderate to serious injuries results as car stiffness is increased. For example, the soft interior car at a stiffness factor of 1.25 (the point where there is no penetration of passenger space due to crush) the moderate to serious injuries are approximately 35% of the total passengers while in the standard seating car approximately 45% of the passengers received moderate to serious injuries.

OVERRIDE

As was discussed in Section 6 the truck retention system in the SOAC reduces the car crush in an override accident. Data indicates that except for cars 4 and 5, the first-collision injury levels in the override crush are similar to those shown for the no-override case. Table 7-1 shows the overall injuries for the soft interior car at 20 and 40 mph collision speeds.

TABLE 7-1. INJURY DISTRIBUTION

(Two 4-Car SOAC trains, seated passengers, high density car.)

INJURY LEVEL	20 MPH		40 MPH	
	OVERRIDE	NO OVERRIDE	OVERRIDE	NO OVERRIDE
Minor or None	99%	100%	85%	86%
Moderate to Serious	0	0	12%	12%
Critical and Fatal	1%	0	3%	2%
First Collision	1%	0	3%	2%
Second Collision	0	0	0	0

As seen in Table 7-1 the override condition causes some first collision C&F injuries to seated passengers. In addition to this there is an increase in floor crush which will result in increased first-collision C&F casualties to standing passengers.

Table 7-2 summarizes the first collision C&F casualties for both seated and standing passengers. The benefit of eliminating penetration due to override is seen by comparing the override cases to the no override cases. For example, if the basic car end strength were developed by the superstructure, all override C&F casualties for first collision would be eliminated at 20 mph and the 40 mph total would be equal to the no override case.

TABLE 7-2. FIRST-COLLISION CRITICAL AND FATAL INJURIES
(Two 4-car SOAC trains)

	20 MPH		40 MPH	
	OVERRIDE	NO OVERRIDE	OVERRIDE	NO OVERRIDE
Seated Passengers	4	0	20	12
Standing Passengers	3	0	34	11
Total	7	0	54	23

8. ASSESSMENT OF SOAC CRASHWORTHINESS

In Sections 6 and 7 the sensitivity of SOAC crashworthiness to variations in selected design parameters was evaluated. More detailed data as to the crashworthiness of the SOAC is presented in this section. It was assumed the present SOAC has a "hard" interior and the data presented reflects impacted-object crush distance of 1/4- and 1/2-inch. The distribution of passenger spacing, impacted-object crush distance, and passenger seats are those shown in Figure 4-1.

Tables 8-1, 8-2 and 8-3 display, by car, the number of and degree of injury for collision speeds of 40, 60 and 80 mph. These tables also show the crush for each car and the total floor space destroyed. The first collision critical and fatal casualties to standees will depend on the number and distribution of standing passengers at the time of collision. Based on a maximum number of standees (228) and on equal distribution over the available floor space (one passenger for each 1.735 square feet), there would be 11 critical and fatal injuries at 40 mph, 102 at 60 mph, and 204 at 80 mph. Tables 8-1, 8-2 and 8-3 illustrate that if the SOAC is actually a "hard" interior vehicle, the highest priority for improving crashworthiness should be assigned to the "softening" of the SOAC's interior.

The lack of symmetry in the distribution of injury in Tables 8-1, 8-2 and 8-3 requires some comment. Collision dynamics yields a slight "skewness" between the impacting train and the impacted train in the passenger relative velocities for secondary impacts. This skewness is due to the use of brakes and amounts to the VP being up to 2 ft/sec higher in the impacting train than in the impacted train. The sensitivity of SI to VP, as shown in Section 6, results in the injury bias seen in the tables.

Table 8-4 shows the average value of the SI for each car at collision speeds of 40, 60 and 80 mph. The SI shown includes the SI for those passengers who suffer critical and fatal injuries in the first collision. The table shows that the highest SI occurs in the first and last car of each train (Cars 1, 4, 5 and 8) and the

TABLE 8-1. INJURY DATA BY CAR (40 MPH)

INJURY LEVEL	CAR 1	CAR 2	CAR 3	CAR 4	CAR 5	CAR 6	CAR 7	CAR 8	TOTAL
NONE	0	0	0	0	0	0	0	0	0
MINOR	0	12	35	0	0	0	0	0	47
MODERATE	12	36	35	12	12	35	12	0	154
SEVERE	0	0	0	22	0	0	24	12	58
SERIOUS	36	0	0	12	22	12	12	0	94
CRITICAL OR FATAL									
1ST COLLISION	0	0	2	4	4	2	0	0	12
2ND COLLISION	24	24	0	22	34	23	24	60	211
CAR NO	1	2	3	4	5	6	7	8	
CAR CRUSH FEET/CAR	0.8	0.9	2.2	6.2	2.2	0.9	0.8		
TOTAL STANDING FLOOR SPACE CRUSHED = 17.8 Sq. Ft.									

NOTES:

1. Present SOAC design
2. Collision of two 4-car SOAC trains
3. 72 seated passengers per car

TABLE 8-2. INJURY DATA BY CAR (60 MPH)

INJURY LEVEL	CAR 1	CAR 2	CAR 3	CAR 4	CAR 5	CAR 6	CAR 7	CAR 8	TOTAL
NONE	0	0	0	0	0	0	0	0	0
MINOR	0	12	35	0	0	0	0	0	47
MODERATE	12	36	35	12	0	35	12	0	142
SEVERE	0	0	0	18	12	0	24	12	66
SERIOUS	36	0	0	12	18	12	12	0	90
CRITICAL OR FATAL									
1st COLLISION	0	0	2	12	12	2	0	0	28
2nd COLLISION	24	24	0	18	30	23	24	60	203
CAR NO	1	2	3	4	5	6	7	8	
CAR CRUSH (FEET/CAR)	0.8	0.9	3.0	16.03	3.1	0.9	0.8		
TOTAL STANDING FLOOR SPACE CRUSHED - 176 SQ. FT.									

NOTES:

1. Present SOAC design
2. Collision of two 4-car SOAC trains
3. 72 seated passengers per car

TABLE 8-3. INJURY DATA BY CAR (80 MPH)

INJURY LEVEL	CAR 1	CAR 2	CAR 3	CAR 4	CAR 5	CAR 6	CAR 7	CAR 8	TOTAL
NONE	0	0	0	0	0	0	0	0	0
MINOR	0	12	34	0	0	0	0	0	46
MODERATE	12	36	34	8	8	34	12	0	144
SEVERE	0	0	0	13	0	0	24	12	49
SERIOUS	0	0	0	0	0	12	12	0	24
CRITICAL & FATAL									
1ST COLLISION	0	0	4	30	30	4	0	0	67
2nd COLLISION	60	24	0	21	34	22	24	60	245
TOTAL	60	24	4	51	64	26	24	60	313
CAR NO.	1	2	3	4	5	6	7	8	
CAR CRUSH (FEET/CAR)	0.80	0.90	3.54	30.8	3.6	0.9	0.8		

TOTAL STANDING FLOOR SPACE CRUSHED - 353 SQ. FT.

NOTES:

1. Present SOAC design
2. Collision of two 4-car SOAC trains
3. 72 seated passengers per car

TABLE 8-4. AVERAGE SEVERITY INDEX BY CAR

VELOCITY	CAR 1	CAR 2	CAR 3	CAR 4	CAR 5	CAR 6	CAR 7	CAR 8	OVERALL AVERAGE
40 MPH	2875	1329	643	1833	2737	1320	2070	3830	2080
60 MPH	3061	1352	648	1954	2764	1327	2100	4017	2153
80 MPH	3370	1403	670	2530	3263	1320	1910	3838	2280

NOTES:

1. High-density SOAC
2. 72 seated passengers
3. Two 4-car SOAC trains
4. Hard interior (1/4 and 1/2 inch)

lowest values occur in the cars behind the two cars involved in the initial impact (Cars 3 and 6). It should be noted that while the SI values shown in Table 8-5 are useful in illustrating accident severity among the various cars, they should not be used to determine overall injuries levels in a particular car. For example, Table 8-5 shows that at 40 mph Car 1 has an average SI of 2875 which is critical or fatal injury; however, Table 8-1 shows that in fact only 24 of the 72 passengers actually received critical or fatal injuries. Table 8-5 shows a comparison of the average SI values for the reference 2 evaluation of the R-44 car (Reference 1-2) and Boeing Vertol analysis of the SOAC. The table shows that the results obtained are generally in agreement. The higher values in the cars furthest from the impact point (Cars 1 and 7) are due to the inclusion of train action in the Boeing Vertol mode.

TABLE 8-5. AVERAGE PASSENGER SEVERITY INDEX (80 MPH)

CAR NUMBER	1	2	3	4	5	6	7	8
R-44	132	115	107	430	430	107	115	132
SOAC	338	152	97	278	380	143	231	415

Average based on:

19 passengers having 2-foot spacing and 1-inch deflection
19 passengers having 2-foot spacing and 2-inch deflection
18 passengers having 4-foot spacing and 1-inch deflection
18 passengers having 4-foot spacing and 2-inch deflection

In the event that overriding occurs, the truck retention system in the SOAC results in a significant reduction in the volume of passenger space destroyed in comparison to transit vehicles having no truck retention system. Table 8-6 shows the effect of override at speeds of 20 and 40 mph. The overrude results in a relatively large increase in crush to Cars 4 and 5 and a corresponding increase in the number of first collision injuries as shown in Table 8-7. The table shows that at 20 mph the override causes seven critical and fatal injuries and at 40 mph there are 51 additional critical and fatal injuries. From the above, it can be concluded the prevention of override will result in an appreciable increase in the SOAC's crashworthiness.

TABLE 8-6. COMPARISON OF CAR CRUSH WITH AND WITHOUT OVERRIDE

CAR NUMBER	1	2	3	4	5	6	7	8
20 MPH COLLISION WITH OVERRIDE	0.60	0.64	0.77	5.25	0.76	0.63	0.61	
NO OVERRIDE	0.72	0.78	0.80	1.20	0.80	0.80	0.72	
40 MPH COLLISION WITH OVERRIDE	0.78	0.88	2.13	9.64	2.13	0.90	0.76	
NO OVERRIDE	0.82	0.88	2.15	2.19	0.19	0.90	0.80	

NOTES:

1. Two 4-car SOAC trains
2. All distances are in feet

TABLE 8-7. NUMBER OF CRITICAL AND FATAL INJURIES WITH AND WITHOUT OVERRIDE

(Hard Interior: 1/4 and 1/2 inch)

EVENT	20 MPH		40 MPH	
	OVERRIDE	NO OVERRIDE	OVERRIDE	NO OVERRIDE
2ND COLLISION SEATED	0	0	231	211
1ST COLLISION				
SEATED	4	0	20	12
STANDING*	3	0	34	11
TOTAL	7	0	285	234

*BASED ON MAX DENSITY - 1.735 SQ. FT./PASSENGER

One aspect of assessing the crashworthiness involves consideration of the operating environment. Some insight into the crashworthiness of SOAC may be obtained from Figure 8-1, which shows first collision casualties as a function of closing speed for impacting an equivalent train. Data from Tables 8-1 through 8-3 for a 4-car SOAC train impacting a 4-car SOAC train have been used as a base. Data for the 2-car train and the 8-car train are projected from the 4-car train for the energy absorption (crush) that is proportional to the kinetic energy.

The problem of determining a "socially acceptable risk" is beyond the scope of this study. Such factors as accident probability, (as influenced by head ways, signal systems, visibilities, and track conditions), the system costs in terms of initial and fleet life cycle costs, and the societal costs of life and fast service should be considered in arriving at a "socially acceptable risk". Given a "socially acceptable" level of fatalities, the adequacy may be assessed.

For purposes of illustration, assume the socially acceptable level of casualties from any one accident is 12. Then, at the design speed of 80 mph, the fully loaded SOAC would experience excessive fatalities for all consists shown. The 2-car train could operate with other 2-car trains at 60 mph, the 4-car train at 40 mph, and the 8-car train would be reduced to 28 mph conditions. Doubling the stiffness of SOAC would have the effect of allowing the operation of the 8-car train at 40 mph, the 4-car train at 60 mph and the 2-car train at 80 mph. The restriction to 12 fatalities may be overly severe but it does illustrate the problem.

As regards the current industry practices for crashworthiness for urban rail vehicles, SOAC meets the requirements. The requirements should be improved as regards the provision for override protection. Also, the basic strength level (as a measure of crash energy absorption for this class of vehicle) has evolved from years of experience. Establishment of car strength levels has mainly resulted from specifications by operating properties and varies from property to property. The effects on the urban rail industry of changing these levels to provide additional passenger protection, and of establishing industry standards, requires further analysis.

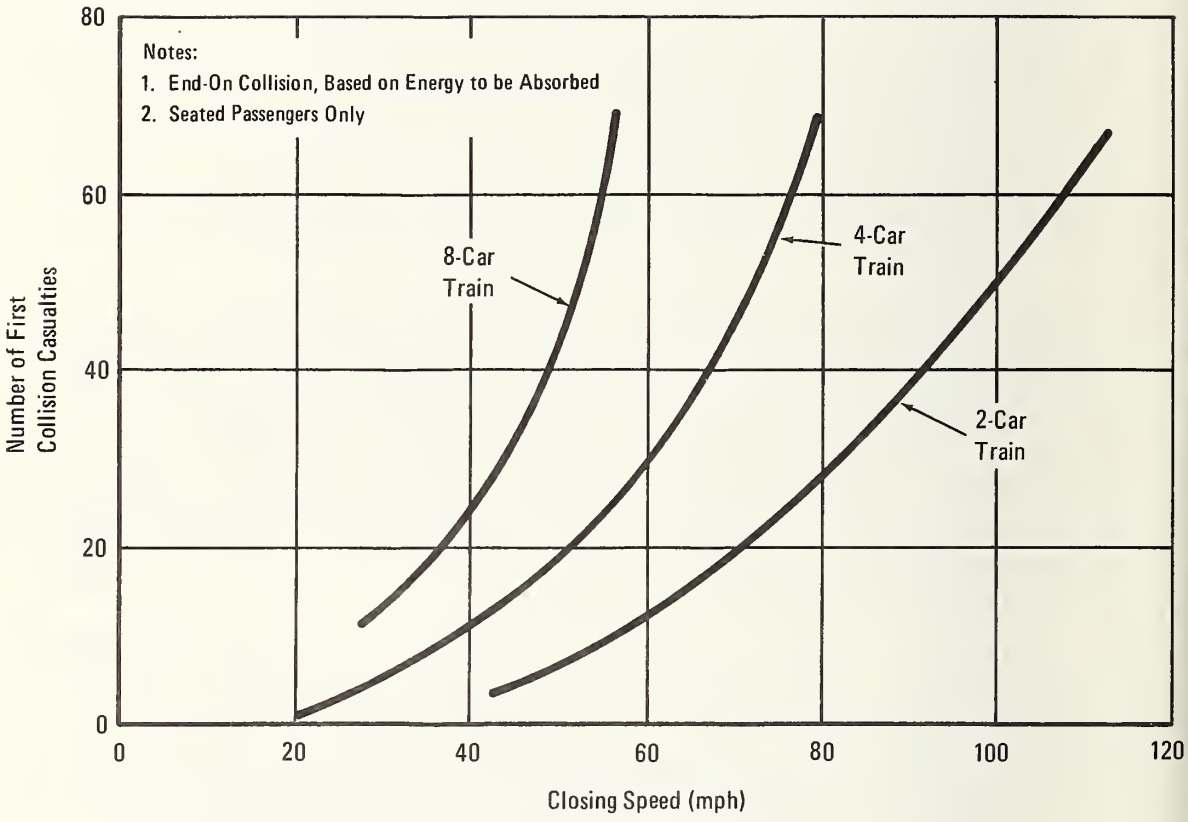

Figure 8–1. SOAC Train Hitting Equivalent SOAC Train

9. STUDIES TO IMPROVE SOAC CRASHWORTHINESS

As the result of the studies previously described, three areas of potential crashworthiness improvements have been identified. Of primary importance for improved crashworthiness is the prevention of penetration from overclimbing. Next, design improvements are needed to reduce the end-on crush. When the structural capability is improved, studies of interior arrangements are required to minimize injuries.

These studies are presented in this Section. In the structural studies, the engineering feasibility of the changes is shown through "preliminary design" sizing of major elements. The studies deal with the potential benefits and with the costs associated with recommended improvements. The costs are given in terms of weight increments and passenger capacity.

The force deflection relationships for the "improved" SOAC are also reviewed in this Section, and the predicted improvement in crashworthiness is assessed. Since the modifications discussed in this Section represent the results of analytical studies, they illustrate potential benefits. A test and evaluation cycle is needed to form a basis for a better understanding of crash energy management and for substantiating these analytical results.

THE OVERRIDE PROBLEM

As previously noted, the occurrence of override causes a marked increase in first collision critical and fatal injuries as compared with the no-override crash. Referring to Table 5-2 it may be seen that if override is eliminated, a casualty reduction of 7 people occurs at 20 mph. and a reduction of 31 casualties occurs at 40 mph. These casualties are directly related to the penetration (loss of survivable volume) of the overridden car.

Overriding might be eliminated by the development of effective anticlimbers which remain stable throughout the crash. However, since the mechanisms of overclimbing are not yet well

understood, even the presence of anticlimbers does not guarantee the complete elimination of climbing. In addition, climbing may occur when incompatible equipment is operated on the same track. A case in point is the accident reported in reference 8, where the overclimbing train did not have an anticlimber. In the SOAC accident, the gondola car body overrode the SOAC underframe after the gondola anticlimber deformed under the gondola.

Protection against penetration by overclimbing is required to achieve a fully crashworthy vehicle. The resistance to penetration must be provided by the car structure. In particular, the car structure above the underframe, including the car end with strong collision and corner posts, the car sides and coves, and the roof, must provide this resistance.

How much crash energy should be absorbed by the car superstructure? Figure 9-1 shows the force-deflection curve for the overriding case; the dashed curve is the force required to equal the resistance provided by the underframe. Thus, to provide the same level of protection to penetration in the overriding case as in the end-on crash, the ability to absorb the additional crash energy represented by the cross-hatched area should be provided by the superstructure. For the SOAC this amounts to approximately 33 million lb-in; and implies a resistance level of approximately 550,000 lb/in. over the 0-to-60-inch region.

STRUCTURAL CONSIDERATIONS

The problem of generating the desired override resistance involves providing resistance in the individual elements and transferring these resistive loads from the impact point to supporting and backup structure.

Impacting the "as-built" car end above the underframe loads the corner posts in bending and shear, and loads the car sides and roof in edge compression. In this mode these elements absorb very little crash energy (as indicated by the 100,000 lb/in. force deflection curve in Figure 9-1).

The capability may be increased further in the following three ways. First, the corner post may be constructed to provide assistance to the collision posts. Secondly, the car sides, the coves, and the roof may be strengthened. Thirdly, the collision post section modulus may follow the suggestions of federal regulations.

---

8. National Transportation Safety Board, Washington DC, Collision of Illinois Central Gulf Railroad Commuter Trains, Chicago IL, NTSB-RAR-73-5. October 1973.

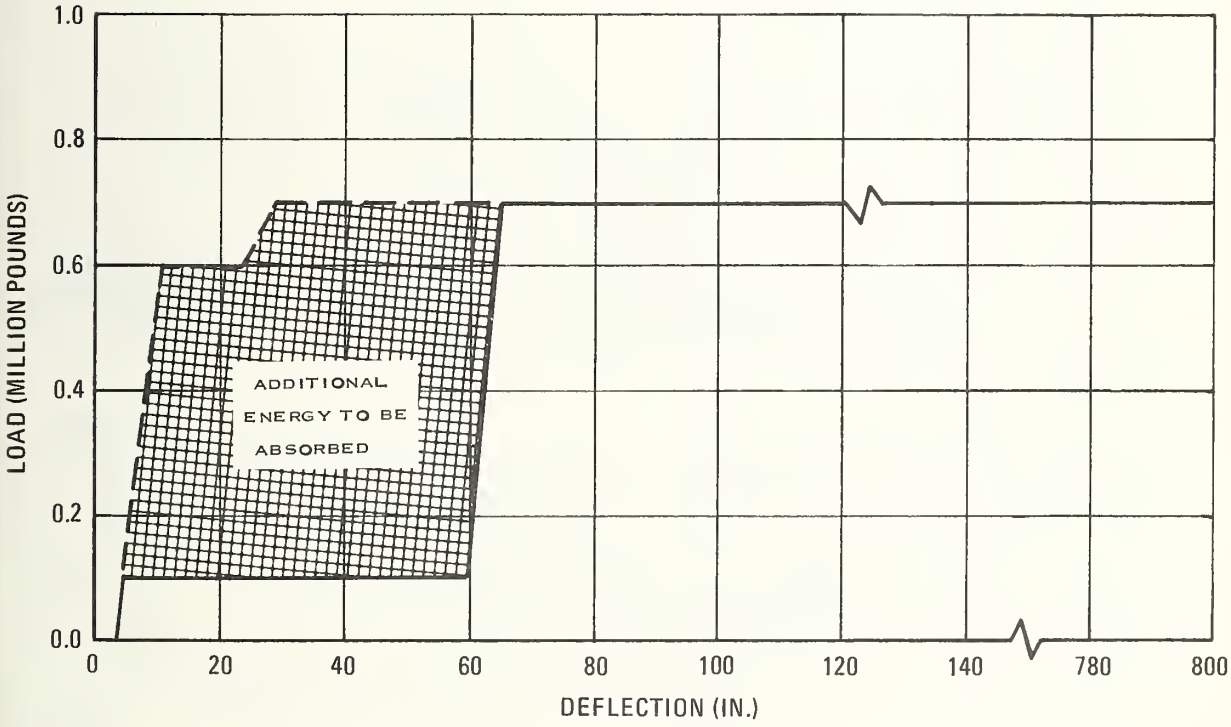

Figure 9–1. Crush Force Versus Deflection to Provide Buff Required Strength

The use of floor-to-ceiling vertical posts in the end shell to resist penetration in overclimbing has been specified in Reference 9 and recommended in Reference 10. Figure 9-2 shows idealized deformations involving a collision post, a sill, and the roof. In sketch (a)the collision post connections to both the sill and the roof are simulated as pinned joints and the major failure mechanism is a plastic hinge under the impact load. In (b) the roof support is weak in the direction of impact, the sill-post connection provides restraint against rotation, and single hinge forms close to the floor. Sketch (c) shows the formation of two plastic hinges. In (d), (e) and (f), the post-sill connection and the post roof connection both provide restraint against rotation, and three plastic hinges are formed.

The plastic hinge is a convenient idealization of the large deformation behavior of a beam. In the rectangular cross section shown in Figure 9-3, as the yield stress is obtained in the extreme fiber, the stress distribution is linear as shown in sketch (b). As the moment is increased past the onset of yield, the yielding progresses inward. In the plastic hinge idealization, the stress distribution is assumed to have developed as in (c). The moment that this section can resist is given by $Mp = \sigma \times I/C \times$ (shape factor). The shape factor relates the fully developed plastic moment to the yield moment. The plastic hinge absorbs energy simply as $M \times \Theta$, where Θ is the angle through which the moment has rotated.

Properties for floor-to-ceiling collision posts have been defined using the requirements outlined in References 9 and 10 as a guide. Based on the 200,000-lb transverse shear value at the floor due to a transverse load applied 30 inches above the floor, a section modulus (I/C) of 11 $IN.^3$ for each post has been selected as a first trial (see Figure 9-4). Using 50,000 psi yield stress for corten steel and a plasticity shape factor of 1.2, each collision post has the capacity to absorb 720,000 lb-in./radian for a single plastic hinge (type a) where the angle involved is the rotation at the plastic hinge.

As can be seen, the 720,000 lb-in./radian type (a) plastic deformation capacity in each post is inadequate to provide the absorption proposed by the cross-hatched region in Figure 9-1. Even for a 1.0 radian moment rotation, corresponding to a

---

9. Code of Federal Regulations, Title 49 Transportation, Subpart D-Multiple Operated Electric Units, Para 230.457 Body Structure, October 1974.

10. AAR Recommended Standards and Practices, Specifications for New Passenger Equipment Cars, Section 18, issue of 1972.

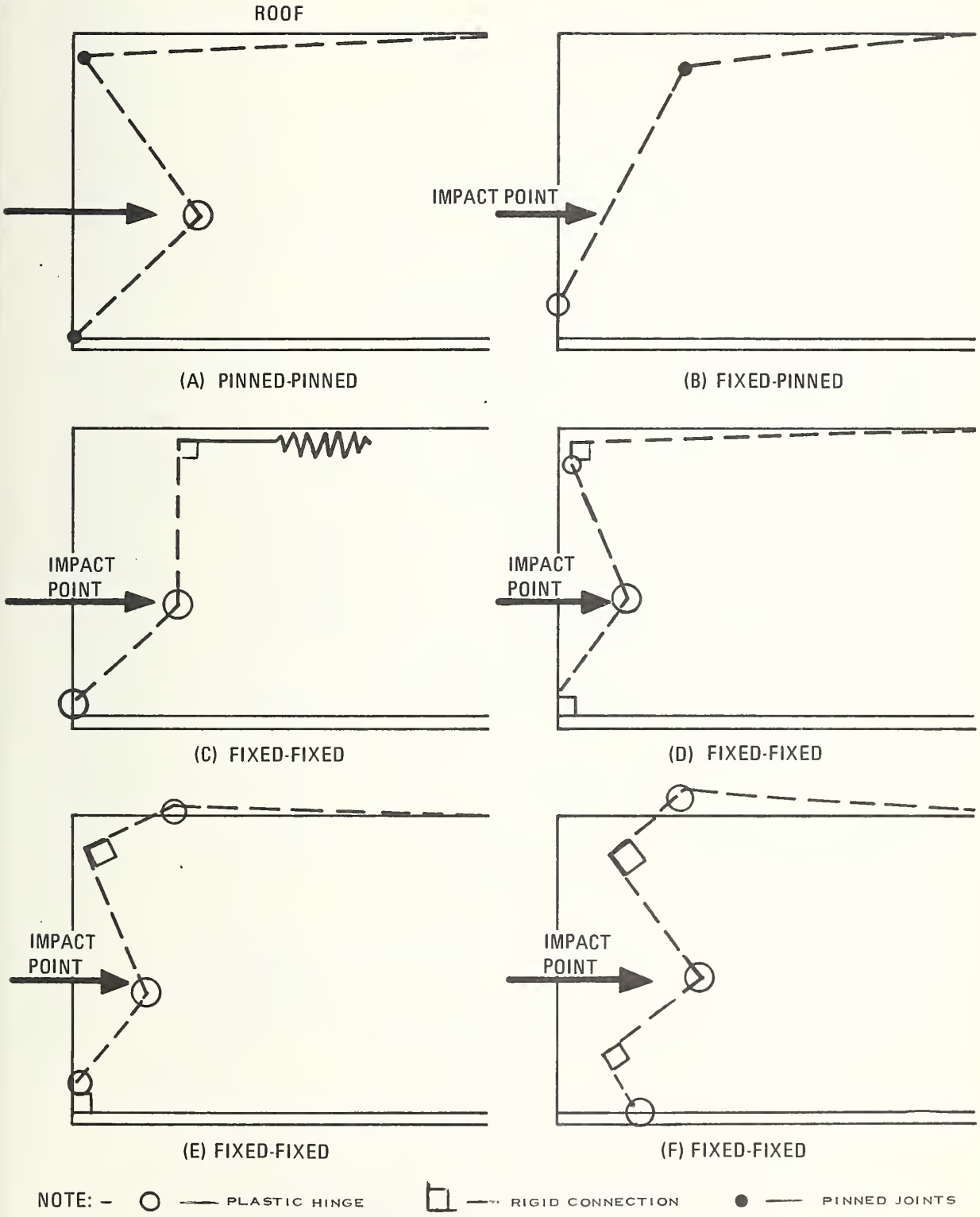

Figure 9-2. Collision Post Energy Absorbing Modes

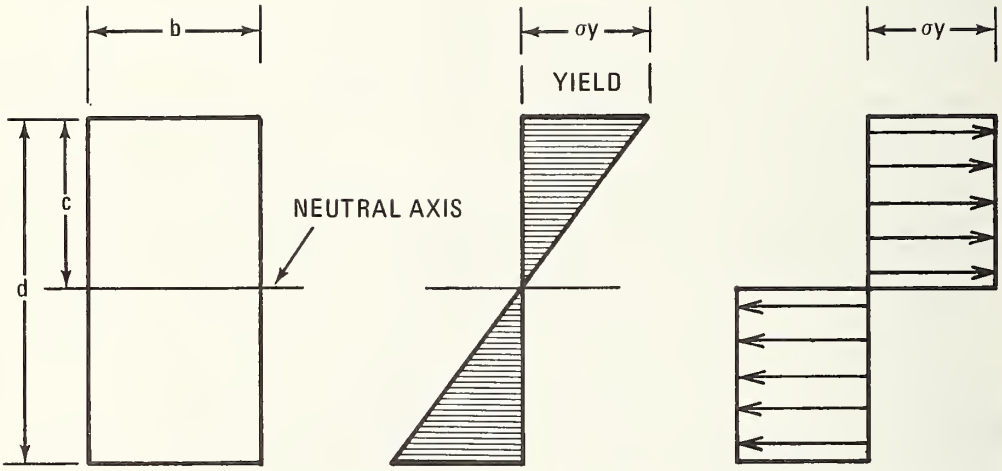

Figure 9–3. Definition of Plastic Hinges

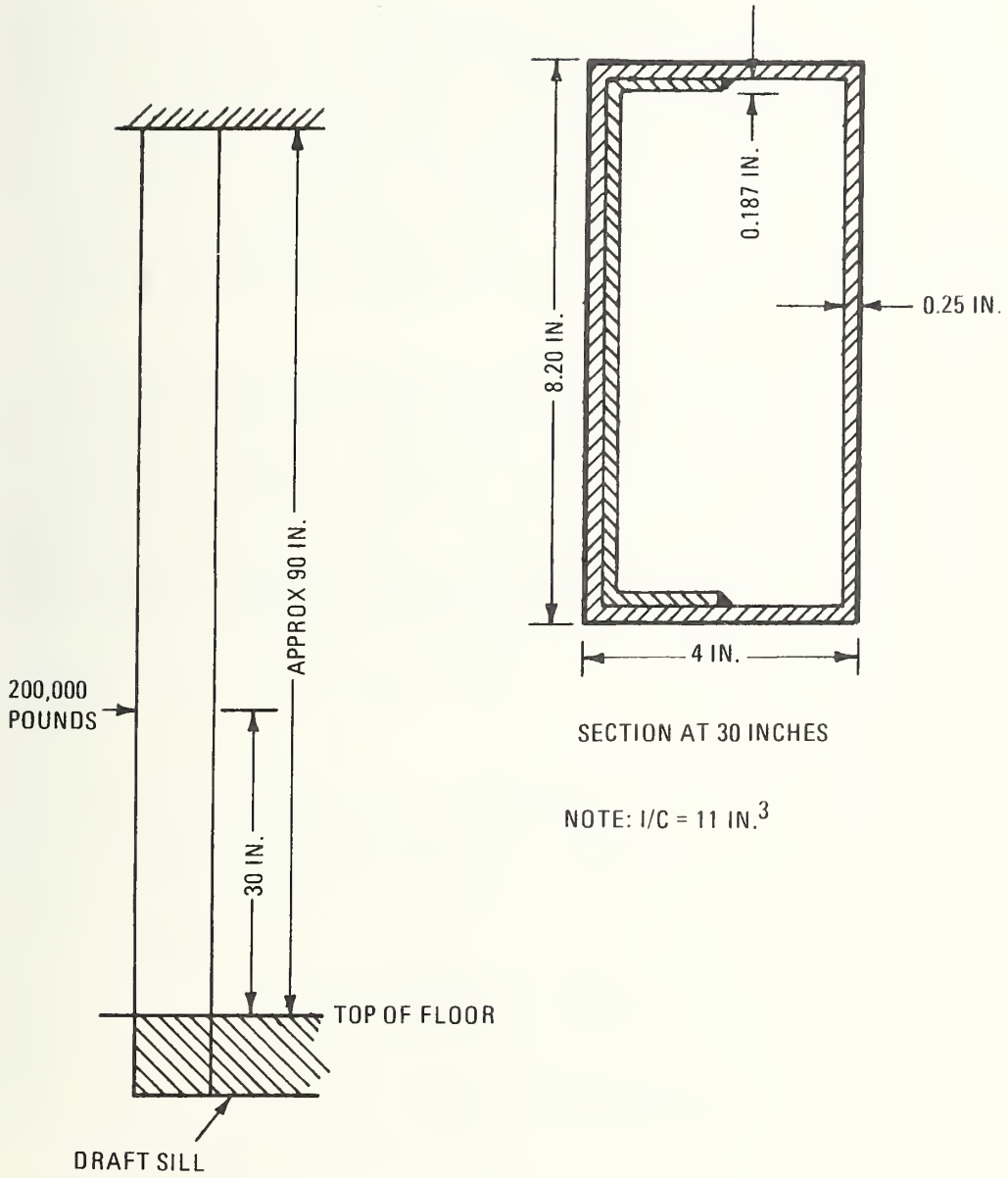

Figure 9–4. General Collison Post Arrangement

penetration of approximately 15 inches, the two collision posts provide only an additional equivalent 100,000 lb/in. to the force deflection curve in the 0-to-60 inch region.

The capability of the collision post may be increased by designing the post, the sill, and the backup roof structure to force the post to yield with three plastic hinges as in Figure 9-2 (D,E, or F). For a uniform post yielding as in (D), the energy absorption would be 2,160,000 lb-in. per radian for equal hinge angles and for each post. On an equivalent energy basis this level would approximate the resistance of 350,000 lb/in. in the force deflection curve for each post. For two posts, this energy absorption will provide a resistance similar to but slightly in excess of that for an end-on crash.

Consider the structural performance necessary to force the formations of three plastic hinges in the collision posts. Even a simple static idealization of the draft sill, collision post and roof results in a redundant frame analysis. The dynamic behavior is complicated further by the treatment of inertia loadings.

For the purposes of this study, the collision posts are treated as a built-in beam with a transverse load 30 inches above the floor, as in Figure 9-4. The reactions are:

$$R_1 = \frac{Pa^2}{L^3} \quad (a + 3b) \quad \text{Roof}$$

$$R_2 = \frac{Pb^2}{L^3} \quad (3a + b) \quad \text{Floor}$$

and a = the distance from roof to load $\frac{(2L)}{3}$

b = the distance from load to floor $\frac{(1L)}{3}$

$$R_1 = \frac{7}{27} P \text{ and } R_2 = \frac{20}{27} P$$

and the bending moments are:

$$M_1 = \frac{Pa\,b^2}{L^2} = \frac{2\,PL}{27} \quad \text{Roof}$$

$$M_2 = \frac{Pa^2b}{L^2} = \frac{4\,PL}{27} \quad \text{Floor}$$

and $$M_P = \frac{2Pa^2b^2}{L^3} = \frac{8\,PL}{81} \quad \text{Under load}$$

The collision post will yield in bending, first at the floor, then under the load, and finally at the roof.

The distribution of moment suggests that the section properties might be varied over the length of the collision post (beam) to reduce the margin between yield stress and actual stress at the critical sections. The variable section properties will permit the plastic hinges to be formed almost at the same time but with some increase in energy absorption over that for a uniform beam. Compared to the energy absorbed by the plastic hinge under the impact, the hinge at the floor absorbs 1.667 times as much energy and the hinge at the roof absorbs 0.833 times as much. Thus, even from static considerations, each properly designed collision post might absorb 3.5 times the energy absorbed by a single hinge and 1.167 times the energy absorbed by the uniform post with 3 hinges.

The structural weight of each such collision post is approximately 80 pounds: 60 pounds for the post and 20 pounds for joint details. The draft sill "as built" is adequate for the overclimb case. The roof will require an increase in strength to react the impact loads with the inertia loads of the roof (and the equipment mounts). An effective area of approximately 4 sq. in. of Corten steel extending from the collision posts to the bolster (120 in.) would require approximately 140 pounds for each car end. Thus, it would appear that the override casualties could be reduced to those for the end-on crash by the addition of 320 pounds of collision posts and 280 pounds of steel in the roof, or 600 pounds per car.

Further improvements could be effected by the improvement of the corner posts in the same manner as the collision posts. Also, further benefits might be obtained by strengthening the car sides back to bolster and distributing the added material in the roof.

The installation of collision posts on the SOAC design places constraints on styling. The improved collision posts would interfere with the large front window, and possibly with the external lines of the vehicle. The improved joints between the collision posts and the draft sill may intrude into the existing floor space by approximately 6 inches. The strengthened roof might also reduce the available head room at each car end.

THE END-ON COLLISION

The SOAC crashworthiness for end-on collisions, as measured by the car crush distance, might be improved. Simply on the basis of crash energy absorption, fatal crush could be eliminated by increasing the total resistance level. Such an

increase would correspond to a general increase in buff load capability (as discussed in Chapter 7).

The object of the present discussion is to investigate what might be obtained through better use of material in the "as-built" design requirements. Associated with this objective is the problem of developing the potential energy absorption assumed to be present through design. These studies represent a "first attempt" at treating railcar structure in detail and are limited to showing representative gains which might be achieved. As future studies are completed, some additional increases are anticipated.

Some caution should be exercised in approaching this problem. In the attempt to increase the energy absorption in a desired location, the changes incorporated may induce a mode of failure at an undersirable location. An example of this is increasing the car end strength until the failure mode changes from plastic hinges in the draft sill to column collapse at the car center.

The distribution of structural steel in the underframe of passenger vehicles is based on a static and load requirement.[9] The magnitude of this load is based on the light weight of the consist and contains a safety factor of approximately 2. In some instances, the operating properties have included a progressively stronger car from the anticlimber to car center. The barrier KRASH model has been used here to study the energy absorption properties of the car end.

When the load distribution observed in crashes (such as that shown in Figure 5-7)is considered, it appears to be desirable to increase the energy absorbing material forward of the bolster. It was therefore decided to improve the end weldment to transfer load to the side sills. This modification effectively increases the car end axial resistance to approximately 1.2×10^6 pounds while the car center remains at approximately 0.7×10^6 pounds. The following studies treat the effect of modifying the strength distribution between the draft sill and the side sills; the effect of removing the eccentricity from the draft sill is also treated.

Five cases have been examined using a 300 in./sec impact velocity. The results are summarized in Table 9-1. The first

TABLE 9-1. RELATIVE CAR DEFORMATIONS

Nodes	Undeformed Length (In.)	CRUSH (IN.)					Component
		Case 1	Case 2	Case 3	Case 4	Case 5	
4-8	106.50	10.25	3.48	3.30	3.33	4.07	Draft sill
4-11	447.5	11.03	8.35	8.14	7.57	7.60	Car
5-6	23.0	9.66	2.69	2.75	2.84	3.54	End sill to draft anchor
9-10	76.0	.07	0.90	0.90	1.40	2.35	Side sill fwd of bolster
10-11	341.0	.28	5.18	5.90	4.17	3.3	Car Center

NOTES

1. Crush taken at minimum kinetic energy conditions
2. Vo = 300 in./sec
3. Barrier impact

case establishes the baseline for the study with the model representing the "as-built" car, featuring the draft sill eccentricities shown in figure 9-5 and weld joints defined in Table 2-2.

The significant deformations of the underframe are schematically shown in Figure 9-6 (a) where the characteristic downward buckling of the draft sill is seen. The bolster did not undergo any appreciable deformation. The car deflection (total shortening) was 11.03 inches. At this instant (T = 0.07 seconds), approximately 90% of the kinetic energy had been consumed. The draft sill between the end sill and the draft anchor (element 5-6) experienced 9.66 inches of axial compression. The remaining car shortening is in small plastic deformation of the draft sill and in the elastic compression of the side sills. The damage is confined to the region forward of the bolster.

The second case introduces an improved end weldment. Here, it is assumed that the welds are sufficiently strong that the energy absorption of the member is developed prior to rupture of the joint. Further, the rigidity of the end closing sill and the end weldment were increased. The beam properties in the plane of the underframe were doubled and the torsional rigidity was arbitrarily taken as 10^8 lb-in/ radian for each half(elements 4-9 and 5-9 taken in concert).

From preliminary runs (not reported here)it was seen that, for the stiff end weldment to be effective in transferring loads to the side sills, some reduction in draft sill stiffness must be made. On this basis the draft sill stiffness was reduced to 80% of that for the first case.

The results for the second case indicated that the crash energy was being absorbed by more structural members than in the first case. The schematic deformation of the car end is shown in Figure 9-6(b) wherein the draft sill tends to follow the shape for the "as-built" model. However, the draft sill buckle is more pronounced and additional plastic hinges are indicated.

The total car shortening for the second case is 8.35 inches as compared to 11.03 inches for the first case. The draft sill axial shortening (element 5-6) is reduced from 9.66 inches in the first case to 2.69 inches in the second case. The side sill forward of the bolster (element 9-10) now experiences 0.90 inches of deflection. Between the bolsters, the side sill shortens 5.18 inches. The forward bolster also "takes a set" in vertical bending.

To show the effects of removing the draft sill eccentricity, a third case was run with a straight draft sill neutral axis.

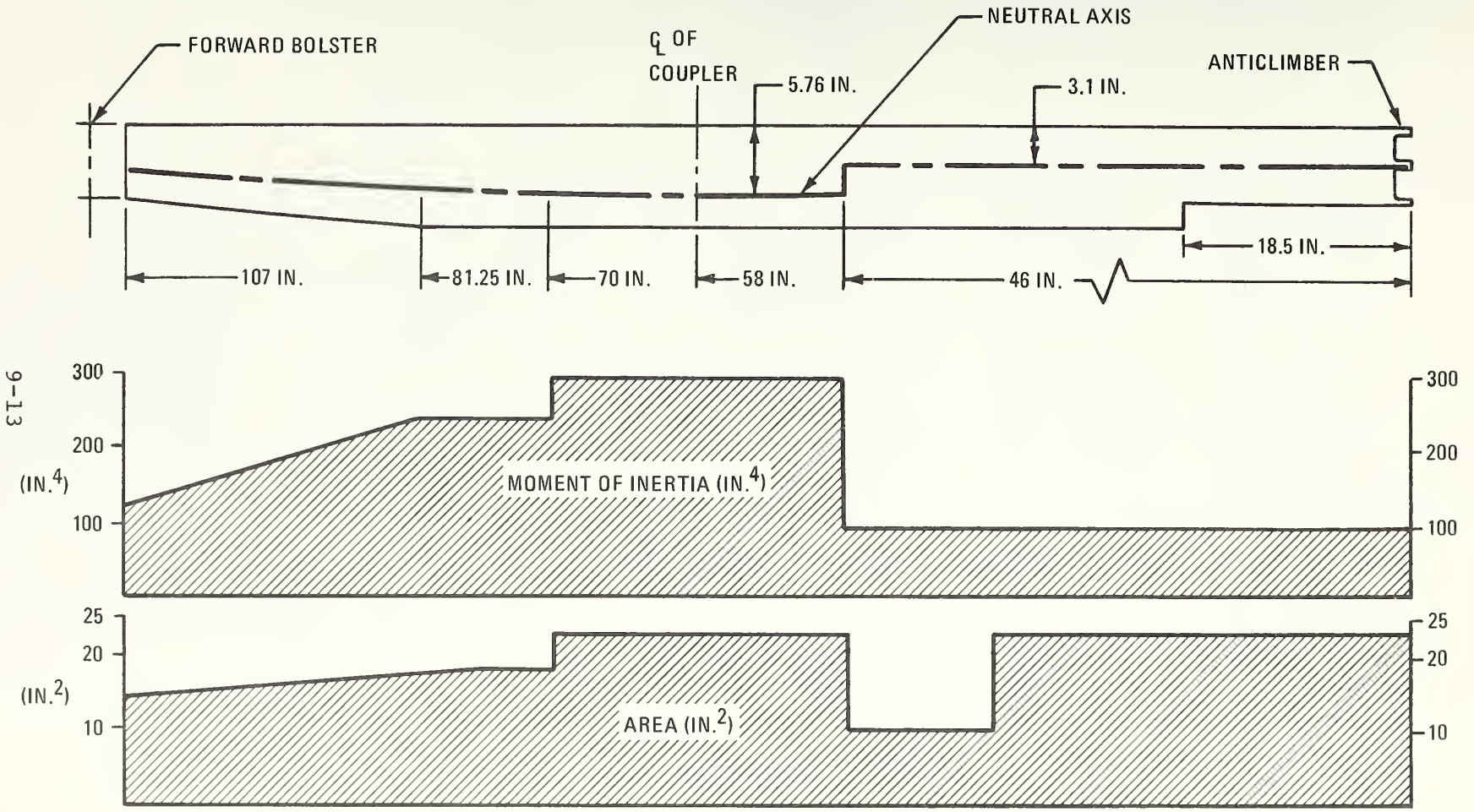

Figure 9–5. Draft Sill Section Variation

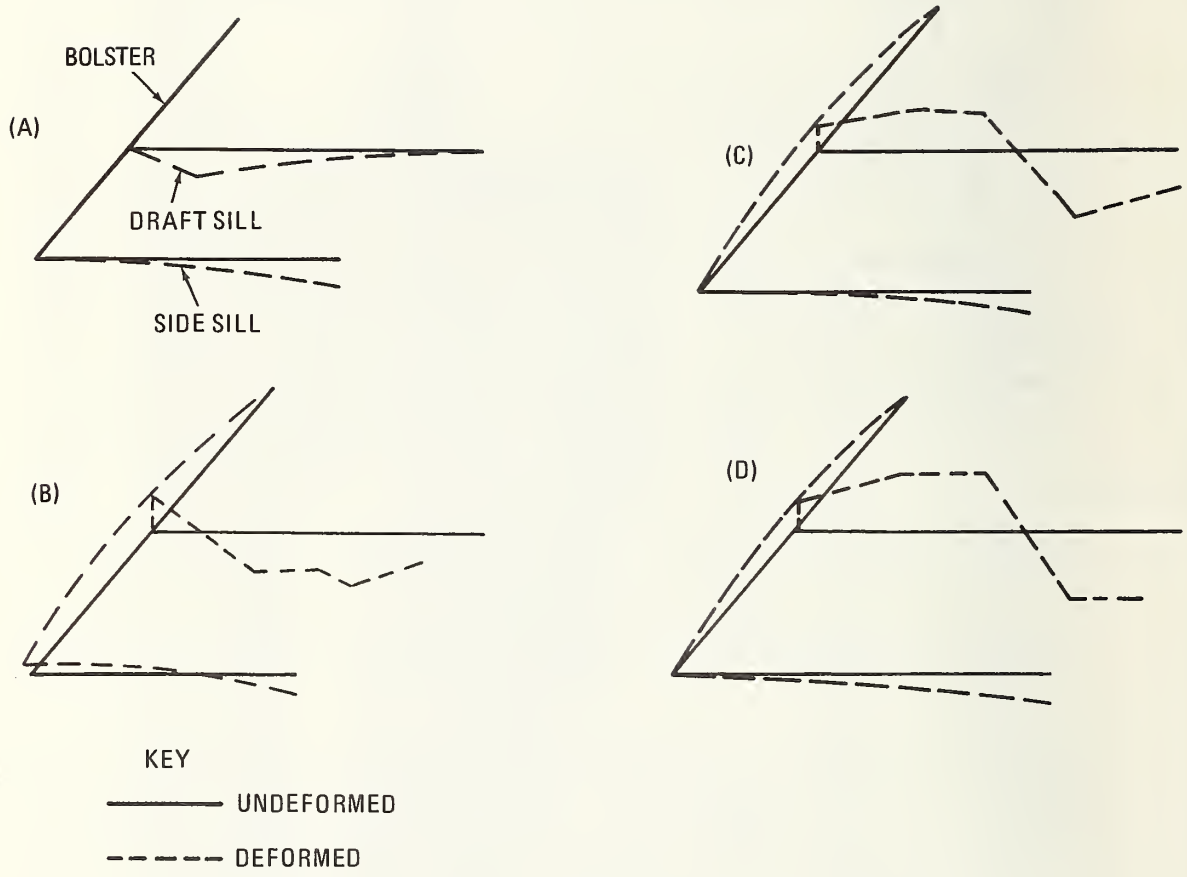

Figure 9–6. Characteristic Car End Deformations

Figure 9-6 (c) shows the characteristic deformation shape. Comparison of shape (c) with (a) and (b) shows that a major change has occurred. The bolster heaves upwards as before, but the draft sill now buckles up as well as down. Element 5-6 shortens 2.75 inches. As in Case 2, the forward side sill shortens 0.90 inches and the side sill between the bolsters shortens 5.90 inches. The total car shortening for this case was 8.14 inches.

A fourth case with the straight draft sill was run to reduce the side sill deformation between the bolsters. From the third case it appears that reducing the loads in the side sill forward of the bolster would lead to the desired result. The side sill (element 10-11) deformation was reduced from 5.90 inches to 4.17 inches by this change. Draft sill participation remained essentially the same. The total car shortening for the fourth case was 7.57.

In the fifth and last case, the side sills forward of the bolster were reduced to approximately 60% of the original strength. This case has an effective car end resistance of 800,000 pounds. A total car shortening of 7.60 inches was shown, compared with the fourth case this does not represent any gain. However, the draft sill and the side sill both stroked more than in the fourth case, while the structure between bolsters deformed 3.38 inches as compared to 4.17 inches.

Further modifications were not attempted but it appears possible to achieve a balanced design that would provide better energy absorption than the "as-built" SOAC.

In assessing the capability of the above models to absorb crash energy, consideration must be given to the failure modes which are developing. Referring again to Figure 9-6, the basic case (a) only has the two plastic hinges in the draft sill working, the end weldment having ruptured and the side sills element (9-10) being disconnected. The presence of the superior end weldment with the draft sill eccentricities showed a 25% improvement in energy absorption compared to the basic case. It should be noted that the large compressive deflection of the base case draft sill may not be achievable. However, the reserve potential of the side sills element (9-10) and of the end weldment to absorb additional energy is more important.

The removal of the eccentricities from the draft sill with the reduction in draft sill strength allowed a similar increase in strength but transferred the energy absorption to the side sills. The large "set" between the bolsters is undesirable but, in general, this configuration has more reserve energy absorption than the second case. The three

plastic hinges in the draft sill promise to provide more total absorption than in the second case.

The fourth case is a transition from the third to the fifth case, the rationale being the same. The fifth case has the best potential for energy absorption. Based on car shortening, the fifth case car end is 30% better than the basic case. Further, less deflection has been experienced in the car center section.

It should again be pointed out that these results are of an exploratory nature. The modeling technique could be further refined to include more nodes (masses) in the side sills and in the car center section to better distribute the inertial loading. Other energy level crashes, with additional car effects, should also be examined.

The importance of a test and evaluation program must be borne in mind. Controlled test conditions will provide further insight into the energy absorption process as well as data for the improvement of the simulation process.

CAR INTERIOR CRASHWORTHINESS

Two requirements for improving interior crashworthiness have resulted from the studies in Sections 7 and 8. The first requirement is to arrange the passenger placement to keep passengers out of areas which may be crushed in collisions. The second requirement is to provide adequate "cushion" or a soft car interior. Further consideration is given here to applying the severity index to injuries to standing passengers.

Examination of the casualty results in Tables 8-1 through 8-4 indicates an abnormally high count of critical and fatal second collision injuries. For example, in a commuter train accident (Reference 9-1) where the closing velocity is estimated to be between 50 and 70 mph, only 45 fatalities and 332 injuries (of which 28 were classified serious), were obtained from both primary and secondary collisions. Since they were confined to the impacted car where severe crushing occurred, all fatalities might be categorized as "first collision". These 45 fatalities compare to 28 first collision casualties for the 60 mph case shown in Table 8-2.

The second collision critical and fatal casualties for 60 mph are 203, with 90 serious injuries, compared to 28 serious

injuries in the accident. This comparison implies that severity index as applied in collision dynamics methods, overpredicts the serious casualties by a factor of 10; lesser casualties appear to be of the correct order.

The above results follow the passenger distribution and the space-to-obstacles criteria outlined by reference 2. Since these applications represent a first attempt to quantify a difficult problem, the results are open to question. The cases that show the abnormal casualties are those for the maximum passenger loads in all cars. In the severity index application, the passenger relative velocity to the obstacle is determined. Relative velocity is a function of the initial distance between the passenger and the obstacle. The severity index is a function of acceleration and of duration and is based on experience for specific impacted surfaces, as in the case of the automobile.

For the fully loaded railcar, the passenger exposure to a hard obstacle is limited to those passengers adjacent to the obstacle. The interior passengers impact other passengers who are, for the most part, "soft". Therefore, it may be argued that only those passengers adjacent to car ends and/or bulkheads would experience the high-acceleration, short-duration conditions applicable to the severity index. These passengers would also be subjected to longer duration inertial loads due to the pile up of people against the obstacles. In such a pile up, injuries to the thorax (chest) are more significant than injuries to the head and to the limbs.

Several different mechanisms for thoracic injuries may be considered.[11] The first case involves the rapid acceleration of the chest in which the internal organs experience loads that impair their function and/or result in local damage to the tissues. In this type of mechanism the rib cage may be fractured due to the impact loads, but the reduction of the chest dimensions does not play a primary role. This mode of injury corresponds to that defined in References 12 and 7. The chest index is based on resultant acceleration and follows the form of the severity index.

---

11. Patrick, L.M., Kroell, C.K. and Mertz, H.J. Jr., Forces on the Human Body in Simulated Crashes, 95th Stapp Car Crash Conference, 1966.

12. Motor Vehicle Safety Standard No. 208, Occupant Crash Protection, other topics, 49 Transportation, Para 571.208, revised 1973.

A second mechanism for serious chest injury involves the rib cage supporting a long duration compression load. Injury occurs when the rib cage fractures, resulting in punctures of the lung and/or the inability to breath. If assistance is immediately available, neither of these occurrences need be fatal. However, death is a distinct possibility.

If the chest is loaded past the rib cage fracture point, fatality becomes most probable as the volume of the chest cavity is decreased until insufficient space is available for the heart to function. According to Patrick (Reference 9-4) the chest may support approximately 600 pounds prior to rib cage fracture in this mode. To distinguish this mode from other chest and severity index modes, it is referred to as "SQUASH".

The foregoing discussion suggests that further research may be required to determine the standing passenger environment in collisions. The distribution and magnitude of loads on the body and the duration of the loads during collisions should be determined. Using these data, the injury mechanisms applicable to the standing passengers should be identified and injury indices quantified. This research is beyond the scope of the present study; however, to illustrate the effect or indicate injuries that might be obtained, it was assumed that SQUASH did not inflict critical or fatal casualties on standing passengers in the maximum load condition. These results are noted in the following paragraphs.

The critical and fatal (C&F) injuries to standing passengers can be assigned to two injury mechanisms. Passengers standing in the floor area destroyed by the vehicle crash will receive 1st collision C&F injuries, while those standing adjacent to the bulkhead and not crushed are assumed to suffer second collision injuries based on 2 feet of free space and 1/4 inch of impacted object crush distance (D). For the standard high-density seating it was assumed that five passengers per car would be adjacent to the bulkhead. Table 9-2 shows the number of C&F injuries to standing passengers under the above conditions. The table also shows C&F injuries to standing passengers under the original assumptions (i.e., 12 feet of free space and D = 1/4 and 1/2 inch) set forth in reference 2.

As may be noted in Tables 9-2 and 9-3, the second collision C&F injuries are substantially reduced by the modified assumptions and are more representative of experience. This is not to say that the modified assumptions are correct, but that such an approach tends toward the proper mark. Further

TABLE 9-2. C&F INJURIES TO STANDING PASSENGERS (Collision of Two 4-Car SOAC Trains at 40 MPH)

	Modified Assumptions	Original Assumptions
Total Standing Passengers	1,824	1,824
1st Collision C&F Injuries	11	11
2nd Collision C&F Injuries	10	1,813
Total C&F Injuries	21	1,824

In the all forward facing seating configurations (see Figure 7-6) it was assumed that passengers would not stand between the bulkhead and the first seats and that there would be standing passengers adjacent to the bulkhead. The C&F injuries to standing passengers are shown in Table 9-3.

TABLE 9-3. C&F INJURIES TO STANDING PASSENGERS (Collision of Two 4-Car SOAC Trains at 40 MPH; all forward facing seats; 191 standees)

	Modified Assumptions	Original Assumptions
Total Standing Passengers	1,528	1,528
1st Collision C&F Injuries	6	6
2nd Collision C&F Injuries	6	1,522
Total C&F Injuries	12	1,528

research is required to more accurately define the actual injury mechanisms and to put the quantification on a rational basis.

COMPARTMENTALIZED FLOOR AREA

One suggested technique to reduce injury levels to standing passengers is to insert a series of barriers in the car which will reduce the free space to a level comparable to that of seated passengers. In the Calspan study the free space for standing passengers was estimated to be 12 feet in a SOAC type vehicle. Table 9-4 shows the effect compartmentilization has if the free space for standing passengers was reduced to 2 or 4 feet. The tables are based on the collision of two 4-car SOAC trains at 40 mph. From the tables it can be seen that the reduced free space will result in a significant reduction in casualty levels. However, it should be noted that unless the barriers provide at least 1 to 2 inches of impacted object crush distance, unacceptably high injury levels may still be incurred.

TABLE 9-4. NUMBER OF SECONDARY INJURIES IN COLLISION OF TWO 4-CAR SOAC TRAINS AT 40 MPH

A. COMPARTMENTALIZED SPACING

	SOFT INTERIOR				HARD INTERIOR			
PASSENGER SPACING	2 ft	2 ft	4 ft	4 ft	2 ft	2 ft	4 ft	4 ft
CRUSH DISTANCE	1 in.	2 in.	1 in.	2 in.	¼ in.	½ in.	¼ in.	½ in.
Injury Level								
None or Minor	1,824	1,824	1,140	1,824	0	456	0	0
Moderate to Serious	0	0	624	0	1,140	1,368	228	1,596
Critical/Fatal	0	0	0		684	0	1,596	228

B. CALSPAN SPACING

PASSENGER SPACING	12 ft	12 ft	12 ft	12 ft
CRUSH DISTANCE	1 in.	2 in.	1/4 in.	1/2 in.
Injury Level				
None or Minor	0	228	0	0
Moderate to Serious	1,596	1,596	0	0
Critical/Fatal	228	0	1,824	1,824

10. CONCLUSIONS AND RECOMMENDATIONS

CONCLUSIONS

An engineering assessment of the crashworthiness of the SOAC has been made. The general conclusions to be drawn from the study are:

- The SOAC "as built" meets the crashworthiness standards implied in the current practice of specifying buff strength.
- The penetration of occupant areas by overriding must be reduced to the buff specified equivalent.
- The provision of adequate vertical posts in the car-end and truck retention would be an effective remedy to override penetration.
- The reduction of first collision casualties may be achieved by increasing the buff strength requirement and by provision of adequate resistance in the superstructure.
- The reduction of second collision casualties may be most effectively achieved by providing a "soft" car interior and may be treated independently of the first collision (to the first order).

In addition to the above general conclusions the following specific observations have been made:

SOAC Crashworthiness

SOAC crashworthiness, as measured by the injury to occupants, might be improved. The absence of effective collision posts extending from floor to roof allows the car to be susceptible to penetration due to override. Overriding should be prevented since it will result in significant increases in critical and fatal injuries, especially in situations where large numbers of standing passengers are involved.

The addition at the car ends of vertical collision posts designed to provide resistance to override penetration has been shown to be one method of improving crashworthiness. The weight penalty for posts compatible with SOAC strength is 600 pounds per car.

The provision of a "soft" car interior provides improved protection from second collision injuries. "Cushion" in the amounts of 1 to 2 inches would dramatically reduce both critical and fatal injuries as well as moderate to serious injuries.

The control of passenger spacing can be used to improve SOAC crashworthiness. An all-forward-facing seating arrangement (see Figure 5-6) would eliminate the 4-foot spacing for center-facing seats and all passengers would have 2 feet of free space. When used in conjunction with a "soft" interior, the all-forward-facing configuration resulted in the elimination of critical and fatal injuries in the two 4-car train collisions at 40 mph. It should be noted that the reconfiguration of the high-density car to an all-forward-facing arrangement costs 4 seats and results in a 16% reduction in useable floor space.

The results of these studies indicate that the dynamic loads in the vicinity of the point of impact exceed the static design loads by factors of approximately 2.5. These results imply that design for crashworthiness must account for these factors in the design of joints and in the distribution of structural material. Further, the side sills between the bolster and the car end contribute little to the end-on crash. The transfer of crash loads from the draft sill to the side sills could reduce the penetration by providing additional energy absorption.

Technologies

The crashworthiness methodology developed by TSC has proven to be a useful tool for comparative studies between classes of vehicles and for identifying the effects of basic vehicle parameters on crashworthiness. The approach reduces the collision dynamics and the injury mechanisms to simple representations. This reduction does limit the "resolving power" of the results.

Sensitivity studies were conducted for the parameters entering the calculation of the severity index. For the primary impact the car crush as related to loss of survivable volume was important. The car crush is controlled by the area under the force deflection curve. For the secondary impact the important parameters were occupant relative velocity to the vehicle and the cushioning of the surface impacted by the occupant. The passenger relative velocity is relatively independent of

the car initial velocity and strongly dependent on the distance travelled by the occupant to reach the secondary impact. The cushion displacement governs the occupant acceleration which controls the injury mechanism (severity index).

The effect of train action (longitudinal vibrations) on the severity index was found to be most pronounced at low speeds. At the lower speeds, the longitudinal wave may result in reinforcing the relative velocity by having the surface possess a component of velocity that adds to the passenger velocity. This condition occurs when the time for the occupant to travel to the target is greater than the quarter period and the three quarters period of the oscillation.

Validation of the collision dynamics analysis was achieved by a comparison of the analytical crush distances simulating the accident case with the deformations of the SOAC draft sill and the gondola observed in the accident. The force deflection curve was supported by comparison with the KRASH model and by static test data for the R-44 car. Also used was the energy balance from momentum theory in which the strain energy of deformation was closely accounted for by both the SOAC model and the elemental free body analysis. This indicates that as a first approximation the TSC methodology gives reasonable results and that engineering estimates of energy absorption provide a usable approach to the development of force-deflection curves.

The KRASH finite element studies of the structural behavior of the car in barrier impacts and of the accident have demonstrated that this approach provides a good tool for the detailed analysis of car bodies. The identification of the characteristic failure modes of major elements is readily made. The dynamic load distribution and the propagation of the loads through the structure are obtained from this type of analysis.

Significant car crush distance has been shown to be confined primarily to the car(s) immediately adjacent to the plane of impact. Crush distance, while a function of the number of cars in the consist and of the closing velocity, is strongly dependent on the level of resistance provided by the force-deflection curve. This level is closely related to the ultimate buff strength requirements of the car; hence, the buff strength specification provides the inherent crashworthiness of the car.

The crash resistance of car ends to the end-on collision may be increased by designing energy absorbing elements to dynamic crash load conditions. The design process must treat the structural system to ensure that improvements do not introduce undesirable failure modes at other locations in the car. Early indications point to a potential local increase in energy absorption on the order of 25%.

An area that requires further consideration is the treatment of standees. The assignment of free space distribution under rush hour "crush" car loading condition should be established on the basis of actual conditions. The injury mechanisms for the severity index are based on automotive accident experience. The extension of the severity index to the standing passenger requires validation with respect to injury mechansims. In particular the cases of passengers impacting passengers, the "squash" compression of the thorax by passenger pile up, and spinal injuries resulting from longer trajectories should be established.

Crashworthiness Specification

The results of the engineering studies raise questions on the specification of crush resistance only through buff conditions. Crashworthiness specifications should treat the prevention of catastrophic collapse of car center sections. Stability criteria relating the design crash loads to the structural beam column properties should be provided. Vertical end collision posts providing overclimbing resistance equal to the end-on crash are necessary. Standard anticlimber geometry and backup structure designed for crash loads should be included. Truck retention loads adequate for a second line of defense should be defined.

It appears that the goal should be the establishment of crashworthiness performance specifications or standards. These performance standards for each class of car would account for such factors as number of cars in the consist, different types of consists operating on the system, maximum operating speeds, and accident probability.

RECOMMENDATIONS

Based on the results of this engineering analysis the following recommendation is made:

- Vertical "collision" car end posts should be required for urban rail vehicles. Acting with the underframe, these posts must develop crash energy absorption equal to that of the underframe.

- Truck retention requirements sufficient to develop the full car center resistance should be established to provide protection against high-energy override crashes.

- Specification methods should be developed for urban vehicles to achieve acceptable crashworthiness standards reflecting the operating environment.

In support of the above, studies are recommended in the following areas:

- Studies to define standards for car interiors leading to a soft interior and the reduction of second collision casualties.

- A study to identify the cost effect on urban rail systems of specifying crashworthiness in terms of vehicle usage. Trade studies showing the cost effect of varying acceptable first crash fatality level, buff strength size, operating speed, equipment initial costs, and fleet life costs.

- Finite element structural dynamic studies of car-end characteristics be extended to further develop principles of crashworthiness design and crash design loads methods.

- Further research into the applicability of the severity index to the mechanisms of injury in the rail vehicle collision environment.

- Test and evaluation of crash design requirements, energy absorbing principles, and crashworthiness concepts.

11. REFERENCES

1. National Transportation Safety Board, Washington DC, Collision of State-of-the-Art Transit Cars with a Standing Car, High Speed Ground Test Center, Pueblo CO, NTSB-RAR-74-2, August 1973, PB233254.

2. Department of Transportation, Urban Mass Transportation Administration, Washington DC, Cassidy, R.J. and Romeo, D.J., Assessment of Crashworthiness of Existing Urban Rail Vehicles, Report in preparation.

3. Department of Transportation, Urban Mass Transportation Administration, Washington DC, Detail Specification for State-of-the-Art Car. IT-06-0026-73-2, May 1973, Revision A, October 1973.

4. U.S. Army Air Mobility Research and Development Laboratory, Wittlin, G. and Gamon, M.A., Experimental Program for the Development of Improved Helicopter Structural Crashworthiness 72-72A, 72-72B, May 1973, AD764985.

5. Blodgett, Omer W., Design of Welded Structures, The James F. Lincoln Arc Welding Foundation, Cleveland, Ohio, 1966.

6. U.S. Army Air Mobility Research and Development Laboratory, Crash Survival Guide. 71-22. Revised October 1971.

7. Society of Automotive Engineers, Human Tolerance as Related to Motor Vehicle Design, Information Report, SAEJ885A. 1964; revised 1966.

8. National Transportation Safety Board, Washington DC, Collision of Illinois Central Gulf Railroad Commuter Trains, Chicago IL, NTSB-RAR-73-5. October 1973.

9. Code of Federal Regulations, Title 49 Transportation, Subpart D-Multiple Operated Electric Units, Para 230.457 Body Structure, October 1974.

10. AAR Recommended Standards and Practices, Specifications for New Passenger Equipment Cars, Section 18, issue of 1972.

11. Patrick, L.M., Kroell, C.K. and Mertz, H.J. Jr., Forces on the Human Body in Simulated Crashes, 95th Stapp Car Crash Conference, 1966.

12. Motor Vehicle Safety Standard No. 208, Occupant Crash Protection, other topics, 49 Transportation, Para 571.208, revised 1973.

APPENDIX A

CAR COLLISION SEQUENCE FROM BOEING STUDY
(Figures are presented at end of section in order of callout)

2.3 CAR COLLISION SEQUENCE REV LTR A

Based on inspections and measurements made at the crash site and on study of the photographs of the crash, a "most likely" sequence has been postulated for the structural contribution during the crash. This sequence for the basic structural involvement of the crash is described by Figures 2.3-1.

It is expected that while the SOAC is braking, initial contact is made by the coupler of the SOAC impacting and engaging the coupler of the gondola. (New marks inside the pockets of the SOAC coupler and the transition car coupler indicate the hooks went home and may have engaged.) It is expected the SOAC traveled about 5.2" (1-3/4" clearance on each coupler and 1.7" anticlimber channel depth) as the couplers are loaded. The SOAC coupler pins sheared. The pins between SOAC #2 (the lead car) and SOAC #1 (trailing) are all sheared subsequently and the anticlimbers engage and the faces are partly buckled.

At the collision end the emergency release and SOAC draft gear at 120,000 lb. provide 3.0" and 1.75" of travel and the estimated travel of the transition car draft gear at 225,000 lb. buff load is 2.75", giving a total possible travel of 7.5" which is sufficient to permit the anticlimber engagement.

Figure 2.3-2 shows that at some time the SOAC anticlimber has been engaged and flanges bent upward. It is suggested as in sketch (3) of Figure 2.3-1 that the anticlimber of the transition car begins to yield in such a manner that the anticlimber face rotates downward and begins to peel the upper deck downward away from the gussets. The final result of this will be to leave the gussets exposed as in Figure 1.9-13.

The structural failure of the gondola anticlimber assembly is a critical event, in that the failure permitted the overriding

of the SOAC draft sill and subsequent penetration of the SOAC car by the gondola body, the fatal injury of the motorman, and affected the order in which damage was incurred. The lower pan of the transition car anticlimber support begins to pull loose from the channel sections. Upon yielding of the anticlimber support the couplers are then subjected to heavy loads (see Section 2.4 for testimonies) and the coupler drawbars both begin to rotate downward. The SOAC coupler head pivots sharply downward, causing damage to the vertical alignment fitting and the transition car coupler head pivots upward, causing heavy impact damage between the coupler head and the carrier hook. It is expected the SOAC coupler anchor is broken (inspection indicates failure in shear) and the end is jammed backwards and upwards into the right-hand side of the center sill. The load and moment which caused the SOAC coupler anchor failure may have imparted a preferred direction for a later column failure of the SOAC center sill. The SOAC coupler face lower right-hand side contacts the rail and the coupler passes under the car, damaging the bottom of the chopper box and damaging about 11 ties over a distance of 18 feet on the roadbed.

After the failure of the SOAC coupler anchor, the SOAC anticlimber probably pulls the transition car anticlimber face downward away from the gussets, with the upper deck still attached to the face, and drives this face toward the transition car bolster (see Figures 2.3-3 and 1.9-12). The lower pan of the transition car anticlimber support pulls off the channels downward as the transition coupler carrier is pulled downward and eventually the front edge of the lowest pan is pulled over the coupler carrier and also down toward the transition car bolster (see Figure 1.9-14).

The drawbar anchor is failed and the drawbar falls to the tracks. The gondola car body overrides the SOAC anticlimber. The exposed gussets have penetrated the front of the SOAC, permitting the SOAC corner angles to hit the end of the transition car (see Figures 2.3-4 and -5). The gussets shear the lower attachment of the right-hand corner angle of the SOAC, pushing it toward the bulkhead. As the gussets penetrate further into the SOAC the alignment goes off center and the left side sheets of the SOAC are collapsed. The lower step on the right-hand side at the end of the transition car (Figure 2.3-3) was turned outward and cut the right side sheets of the SOAC (Figure 2.3-6), indicating a maximum penetration of about six feet into the SOAC on the motorman's side, but carrying aft and left to a maximum of nine feet at the left door.

The SOAC anticlimber and underframe fold the gondola lower plate backwards and impact the gondola anchor post plate. The impact shears the anchor post plate from the body and causes the SOAC draft sill to buckle. As this buckling progresses, the SOAC end sill moves downwards, and the structural members connecting the draft sill and the side sill cause the side sills to twist inwards. The side sills were permanently twisted and the connecting members failed. At this point of maximum penetration it is expected the transition car and the locomotive have been accelerated to their greatest speed (12 to 20 mph) and the gondola will have been given a pitching motion which detaches it from the locomotive. The locomotive is then free to subsequently coast to a stop. At the point of maximum penetration the transition car has buckled the center sill of the SOAC and this sill has detrucked the impact end of the transition car.

It appears the lead truck of the SOAC caught the drawbar assembly from the transition car and pushed it along the right-hand rail, damaging ties with the coupler end of the drawbar. The coupler end appears to have lifted the SOAC wheel off the track and permitted the left-hand wheels to ride lightly on the left-hand tie stubs. The anchor end of the drawbar spread the rails and finally contacted a rail splice and brought the SOAC to a very abrupt stop, pitching the truck forward violently and bending both anchor rods, slewing the end of the SOAC to the left around the drawbar length as a radius and dropping the lead truck into the ballast halfway off the track (see Figure 2.3-7). This abrupt stop permitted the transition car to slip out of the penetrated area of the SOAC and brought forward the impacted debris and the motorman, who then slipped out of the front of the SOAC onto the tracks.

The gondola came to rest slightly yawed lying atop its trucks with the trailing truck crosswise on the tracks, and having damaged about nine ties. The locomotive coasted to a stop about 575 feet from its original location.

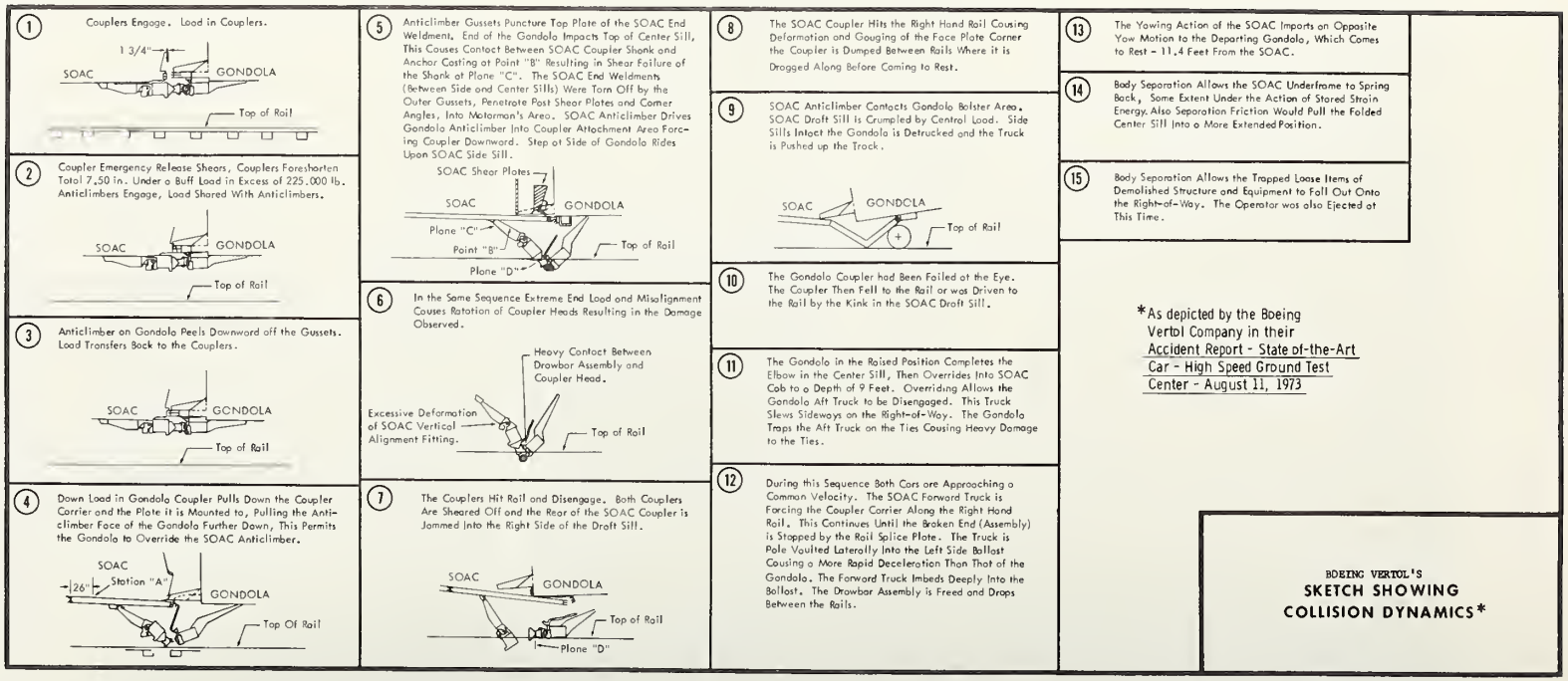
1 Couplers Engage. Load in Couplers.
1 3/4"
SOAC
GONDOLA
Top of Rail
2 Coupler Emergency Release Shears, Couplers Foreshorten Total 7.50 in. Under a Buff Load in Excess of 225,000 lb. Anticlimbers Engage, Load Shared With Anticlimbers.
SOAC
GONDOLA
Top of Rail
3 Anticlimber on Gondola Peels Downward off the Gussets. Load Transfers Back to the Couplers.
SOAC
GONDOLA
Top of Rail
4 Down Load in Gondola Coupler Pulls Down the Coupler Carrier and the Plate it is Mounted to, Pulling the Anticlimber Face of the Gondola Further Down, This Permits the Gondola to Override the SOAC Anticlimber.
SOAC
26"
Station "A"
GONDOLA
Top Of Rail
5 Anticlimber Gussets Puncture Top Plate of the SOAC End Weldment, End of the Gondola Impacts Top of Center Sill, This Causes Contact Between SOAC Coupler Shank and Anchor Casting at Point "B" Resulting in Shear Failure of the Shank at Plane "C". The SOAC End Weldments (Between Side and Center Sills) Were Torn Off by the Outer Gussets, Penetrate Post Shear Plates and Corner Angles, Into Motorman's Area. SOAC Anticlimber Drives Gondola Anticlimber Into Coupler Attachment Area Forcing Coupler Downward. Step at Side of Gondola Rides Upon SOAC Side Sill.
SOAC Shear Plates
SOAC
GONDOLA
Plane "C"
Point "B"
Plane "D"
Top of Rail
6 In the Same Sequence Extreme End Load and Misalignment Causes Rotation of Coupler Heads Resulting in the Damage Observed.
Heavy Contact Between Drawbar Assembly and Coupler Head.
Excessive Deformation of SOAC Vertical Alignment Fitting.
Top of Rail
7 The Couplers Hit Rail and Disengage. Both Couplers Are Sheared Off and the Rear of the SOAC Coupler is Jammed Into the Right Side of the Draft Sill.
SOAC
GONDOLA
Top of Rail
Plane "D"
8 The SOAC Coupler Hits the Right Hand Rail Causing Deformation and Gouging of the Face Plate Corner the Coupler is Dumped Between Rails Where it is Dragged Along Before Coming to Rest.
9 SOAC Anticlimber Contacts Gondola Bolster Area. SOAC Draft Sill is Crumpled by Central Load. Side Sills Intact the Gondola is Detrucked and the Truck is Pushed up the Track.
SOAC
GONDOLA
Top of Rail
10 The Gondola Coupler had Been Failed at the Eye. The Coupler Then Fell to the Rail or was Driven to the Rail by the Kink in the SOAC Draft Sill.
11 The Gondola in the Raised Position Completes the Elbow in the Center Sill, Then Overrides Into SOAC Cab to a Depth of 9 Feet. Overriding Allows the Gondola Aft Truck to be Disengaged. This Truck Slews Sideways on the Right-of-Way. The Gondola Traps the Aft Truck on the Ties Causing Heavy Damage to the Ties.
12 During this Sequence Both Cars are Approaching a Common Velocity. The SOAC Forward Truck is Forcing the Coupler Carrier Along the Right Hand Rail. This Continues Until the Broken End (Assembly) is Stopped by the Rail Splice Plate. The Truck is Pole Vaulted Laterally Into the Left Side Ballast Causing a More Rapid Deceleration Than That of the Gondola. The Forward Truck Imbeds Deeply Into the Ballast. The Drawbar Assembly is Freed and Drops Between the Rails.
13 The Yawing Action of the SOAC Imparts an Opposite Yaw Motion to the Departing Gondola, Which Comes to Rest - 11.4 Feet From the SOAC.
14 Body Separation Allows the SOAC Underframe to Spring Back, Some Extent Under the Action of Stored Strain Energy. Also Separation Friction Would Pull the Folded Center Sill Into a More Extended Position.
15 Body Separation Allows the Trapped Loose Items of Demolished Structure and Equipment to Fall Out Onto the Right-of-Way. The Operator was also Ejected at This Time.
*As depicted by the Boeing Vertol Company in their Accident Report - State-of-the-Art Car - High Speed Ground Test Center - August 11, 1973
BOEING VERTOL'S
SKETCH SHOWING
COLLISION DYNAMICS*

FIGURE 2.3-1

FIGURE 2.3-2

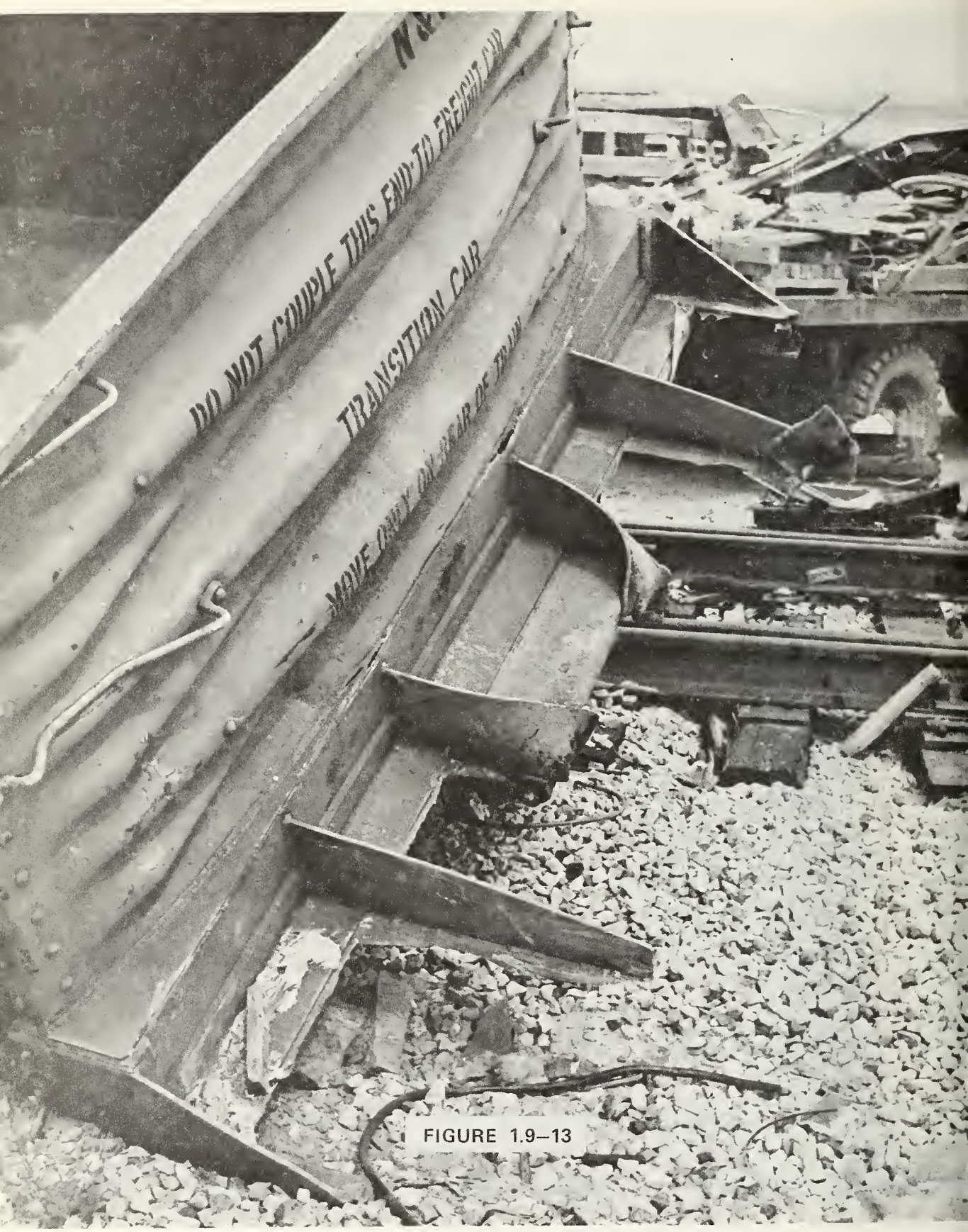

FIGURE 1.9–13

FIGURE 2.3–3

FIGURE 1.9–12

FIGURE 1.9–14

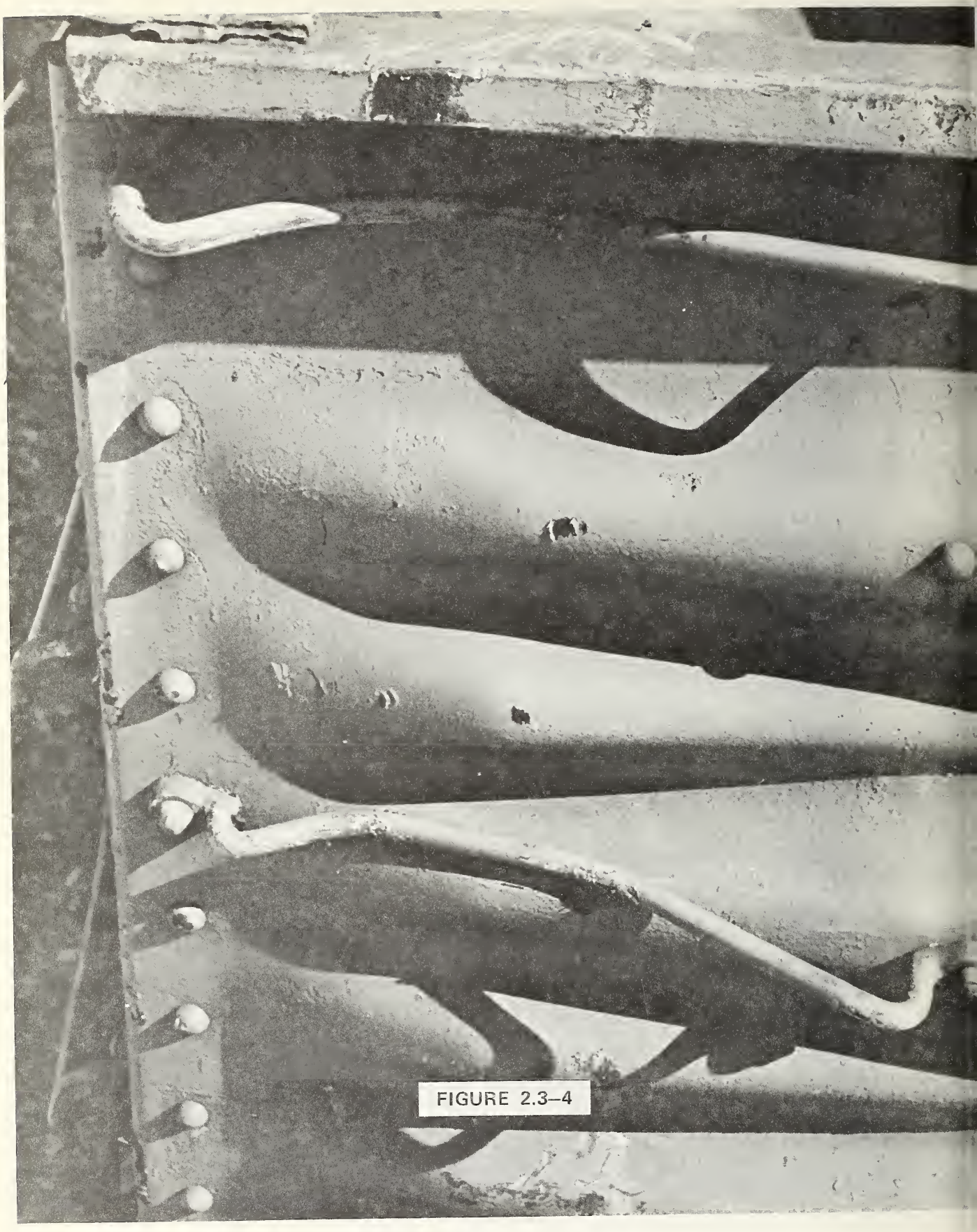

FIGURE 2.3–4

FIGURE 2.3–5

FIGURE 2.3–6

FIGURE 2.3-7

APPENDIX B

SOAC MASS PROPERTIES

1. Weights:

Empty Weight		90,000 lb
Car Body Equipped	60,000	
Trucks (2)	30,000	
Maximum Permitted Load		40,000 lb
266 People at 150 lb each		
Maximum Permitted Weight		130,000 lb

2. Mass Moments of Inertia: (About C.G. Location)

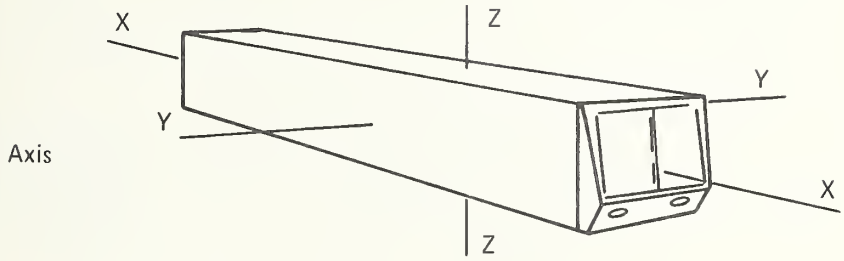

Case 1. Empty Car Less Trucks:

Weight:	60,000 lb
Long. CG:	Sta 448.56 in.
Lat. CG:	Assumed to be Car $\mathbb{C}$ (BL Zero)
Vert CG:	59.5 in. above top of rail
I_{xx} (roll):	1,150,390 lb ft^2
I_{yy} (pitch):	29,520,218 lb ft^2
I_{zz} (yaw):	29,435,825 lb ft^2

Case 2. Case 1 Plus Maximum Permitted Load

Weight:	100,000 lb
Long CG:	Sta 449.14 in.
Lat. CG:	Assumed to be car $\mathbb{C}$
Vert CG:	68.3 in above top of rail
I_{xx} (roll):	850,495 lb ft^2
I_{yy} (pitch):	45,060,436 lb ft^2
I_{zz} (yaw):	45,336,404 lb ft^2

3. SOAC Car Concentrated Masses

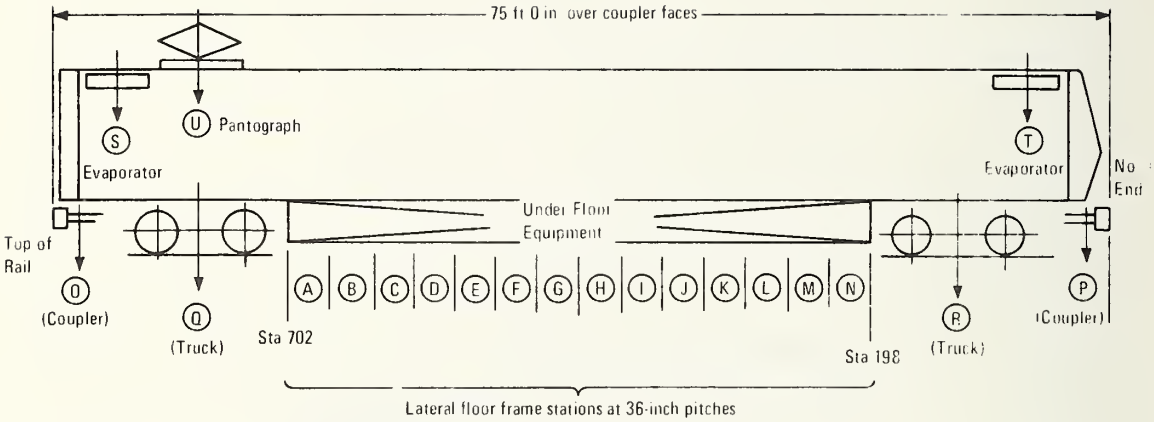

Item	Weight (lb)	Sta (in.)	WL (in.) Above top of rail
A	300	684	24
B	867	648	24
C	685	612	24
D	568	576	24
E	455	540	24
F	1,575	504	24
G	2,150	468	24
H	953	432	24
I	1,613	396	24
J	909	360	24
K	895	324	24
L	670	288	24
M	1,060	252	24
N	455	216	24
O	1,400	884	26
P	1,400	16	26
Q	15,000	774	?
R	15,000	126	?
S	350	800	133
T	350	118	133
U	775	774	150

TOTAL 47,410

Note. The 42,590 lb of remaining car weight undefined and therefore assumed distributed in similar proportions as CTA 3700 car.

APPENDIX C

BEAM STIFFNESS MATRIX

The beam stiffness matrix (6x6) for use in the KRASH program is obtained by modification of the general matrix* (12x12) for a finite beam element according to the equilibrium equations:

$$\{F\} = [K]\{u\} \tag{1}$$

where $\{F\}$ is a vector of the forces and moments at the two ends of the element, and $\{u\}$ is the corresponding displacement and rotation vector.

To adapt this to the KRASH program it is necessary to identify the ends of the element by indices "i" and "j" with the axial direction from i to j oriented in the positive x direction*
Thus equation (1) becomes

$$\begin{Bmatrix} F_i \\ M_i \\ F_j \\ M_j \end{Bmatrix} = \left[\begin{array}{c|c|c|c} K_{11} & K_{21}^T & K_{31}^T & K_{41}^T \\ \hline K_{21} & K_{22} & K_{32} & K_{42} \\ \hline K_{31} & K_{32} & K_{33} & K_{43} \\ \hline K_{41} & K_{42} & K_{43} & K_{44} \end{array}\right] \begin{Bmatrix} u_i \\ \phi_i \\ u_j \\ \phi_j \end{Bmatrix} \tag{2}$$

where Fe and Me represent end force and moment vectors and u and ∅ are the corresponding displacements and rotations. The original stiffness matrix is now partitioned into 3x3 submatrices as indicated. The following inherent characteristics of the sub-matrices are noted:

$$\begin{aligned} K_{31} &= K_{11} = -K_{33} \\ K_{32} &= -K_{21}^T \\ K_{41} &= K_{21} \\ K_{43} &= -K_{21} \\ K_{44} &= K_{22} \end{aligned} \tag{3}$$

*See for example Eqn. 5.116, Theory of Matrix Structural Analysis by J. S. Przemieniecki, McGraw Hill Book Co., 1968.

Isolating the forces and moments at the jth end and using the above relations

$$\begin{Bmatrix} F_{ej} \\ M_{ej} \end{Bmatrix} = \left[\begin{array}{c|c|c|c} -K_{11} & -K_{21}^T & -K_{11} & -K_{21}^T \\ \hline K_{21} & K_{42} & -K_{21} & K_{22} \end{array}\right] \begin{Bmatrix} u_i \\ \phi_i \\ u_j \\ \phi_j \end{Bmatrix} \qquad (4)$$

The KRASH program representation is given by

$$\begin{Bmatrix} F_{ej} \\ M_{ej} \end{Bmatrix} \quad \left[\begin{array}{c|c} \underline{K}_{11} & \underline{K}_{21}^T \\ \hline \underline{K}_{21} & \underline{K}_{22} \end{array}\right] \begin{Bmatrix} \Delta u \\ \Delta \phi \end{Bmatrix} \qquad (5)$$

where Δu is the displacement vector at the jth end relative to the i^{th} end in the i^{th} body axes (i.e., x axis remains tangent to i^{th} end during deformation) and $\Delta\phi$ is the relative rotation between i^{th} and j^{th} ends

It can be shown

$$\begin{Bmatrix} \Delta u \\ \Delta \phi \end{Bmatrix} \quad \left[\begin{array}{c|c|c|c} -I & LTr & I & 0 \\ \hline 0 & -I & 0 & I \end{array}\right] \begin{Bmatrix} u_i \\ \phi_i \\ u_j \\ \phi_j \end{Bmatrix} \qquad (6)$$

where

$$[Tr] = \begin{bmatrix} 0 & 0 & 0 \\ 0 & 0 & 1 \\ 0 & -1 & 0 \end{bmatrix}$$

Substituting (6) and (5)

L = ELEMENT LENGTH

$$\begin{Bmatrix} F_{ej} \\ M_{ej} \end{Bmatrix} = \begin{bmatrix} -\underline{K}_{11} \; ; & \underline{K}_{11} L T_r - \underline{K}_{21}^T \; ; & \underline{K}_{21}^T \\ -\underline{K}_{21} \; ; & \underline{K}_{21} L T_r - \underline{K}_{22} \; ; & \underline{K}_{22} \end{bmatrix} \begin{Bmatrix} u_i \\ \phi_i \\ u_j \\ \phi_j \end{Bmatrix} \tag{7}$$

Comparison with (4) yields

$$\begin{aligned} \underline{K}_{11} &= K_{11} \\ \underline{K}_{21} &= -K_{21} \\ \underline{K}_{22} &= K_{22} \end{aligned} \tag{8}$$

Hence the stiffness matrix $\underline{K}$ for the KRASH program approach is related to that of the general expression as follows:

$$\left[\underline{K}\right] = \begin{bmatrix} K_{11} & -K_{21}^T \\ -K_{21} & K_{22} \end{bmatrix} \tag{9}$$

This corresponds to the form given in Section 2.

APPENDIX D

TESTS CONDUCTED ON THE R-44 CARS

(Excerpted from the R-44 equipment contract specification)

"SPECIFICATIONS--3.2--Car Body Construction and Assembly

Each subsequent spray application shall be uninterrupted for not less than 10 minutes if the shutdown period has been in excess of 2 hours.

Water testing shall be of duration to demonstrate watertightness of the car body to the satisfaction of the superintendent.

(c) Electrical High Potential Tests. Before leaving the Contractor's plant, on each completed car, ready for shipment, all circuits and connected apparatus, except electronic solid state devices, shall be subjected to dielectric tests in accordance with the latest IEEE Standards. Circuits energized by the 32-volt storage battery shall withstand a potential of 1,000 volts ac, applied continuously for 5 seconds between ground and/or the current carrying parts. Circuits energized at 600 volts dc and ac powered circuits shall withstand a potential of 3,000 volts ac applied continuously for one minute between ground and the current carrying parts.

(d) Material Tests. Materials and devices received at the Contractor's plant which are subject to the Authority's inspection, or which are manufactured or finally treated at the Contractor's plant, shall be subject to physical and chemical tests in accordance with these specifications. Adequate facilities for conducting the tests shall be provided by the Contractor.

(e) Loading Tests. Accurate tests of the heavier of the completely equipped sample pair of cars shall be conducted by the Contractor in the presence of the superintendent, showing the static deflection at all important points of the car structure, due to the maximum passenger load, plus 26% for impact (a total distributed live load of 62,000 pounds), and showing the set when this load is removed. Stress readings shall be

"taken as directed by the Superintendent and complete data giving location of instruments, stresses and load conditions shall be furnished to the Superintendent.

In addition to the foregoing, there shall be furnished data giving the deflection of all truck springs on the car so tested due to the above load of 62,000 pounds.

(f) Squeeze Test. A squeeze test shall be performed on one car structure by the Contractor in the presence of the Superintendent. The car shall withstand a static end compression load of 250,000 pounds applied on centerline of anticlimber end sills, without exceeding 50% of the yield point of the structural material and shall not have a vertical deflection between body bolsters greater than 0.205 inch.

From a nominal approved zero loading, the car shall be loaded to 50,000, 100,000, 150,000, 200,000 and 250,000 pounds with the load reduced to the nominal approved zero loading after each load increment. At each load level, vertical deflections shall be read in at least 10 approved locations on each side sill by means of wires stretched between the corner posts. Strain gauge readings shall be recorded for at least 38 approved gauge locations on the car structure. The records of the complete test results shall be furnished to the Superintendent.

3.13 ADDITIONAL TESTS

225,000 pounds end load on centerline of coupler, light car plus 49,000 pounds for passengers; exploratory by agreement.

400,000 pounds end load on anticlimber, light car plus 49,000 pounds for passengers, 80 percent y.s. maximum; exploratory by agreement."

APPENDIX E

SOAC ACCIDENT ENERGY BALANCE

Two SOACs ballasted to 105,000 lbs. each impacted 46,000-lb. gondola and 88,000-lb. locomotive. Velocity at impact was approximately 35.3 mph (51.8 ft./sec.).

Assuming wheels locked at impact

$$KE_1 = 1/2\ M_1V_1^2 = 1/2\ \frac{(210,000)}{32.2} \times 51.8^2 = 8.75 \times 10^6 \text{ ft-lbs.}$$

From simple momention considerations and neglecting brake losses during crush, the velocity after impact is

$$V_2 = \left(\frac{M_1}{M_1+M_2}\right) \times V_1 = \frac{(210,000)}{(136,000 + 210,000)} \times 51.8$$

$$= 31.4 \text{ ft/sec.}$$

and

$$KE_2 = 1/2\ \frac{346,000}{32.2} \times 31.4^2 = 5.3 \times 10^6 \text{ ft-lbs.}$$

Strain energy is given by

$$SE = KE_1 - KE_2 = 3.45 \times 10^6 \text{ ft-lbs.}$$

This strain energy is distributed between the lead SOAC and the gondola for the most part.

From accident damage review (Reference 1-1)
the major energy-absorbing elements damaged were

Draft sill: 45-50° plastic hinge
Car side and roof damage
End weldment damage and secondary items

ENERGY CONSUMED (SOAC - See Table 3.1 of Reference 1)

Draft sill (Plastic hinge: 45°) 16 x 10^6in.-lbs.

Sidwall, cove and roof crushed: 10 ft. (120 in.)

$$\left(\frac{80{,}000 + 64{,}000 + 4{,}000}{4}\right) \times 120 = 4.5\ 10^6\text{in.-lbs.}$$

plus secondary sources.

GONDOLA

Lock and swivel plate:

214" of .090 sheet torn and rolled back
70" of .125 " " " " "
70" of .375 " " " " "

$$SE = N \times 0.22\ F_{sy} t^2 L + F_{ty}\ \frac{\text{Volume}}{6}$$

Where: N = No. tears
L = Length

$= 5.9 \times 10^6$in.-lbs.

anticlimber supports (area = 6.28 in.^{2})

axial load = 50,000 x 6.28 = 314,000 lbs.
stroke - 3 ft.
SE = 36 x 314,000 = 11.4 x 10^6in.-lbs.

SUMMARY

		10^6in.-lbs.
SOAC:	Draft Sill	16.0
	Sidewall, etc.	4.5
GONDOLA:	Anticlimber	11.4
	Plates	5.9
		37.8 x 10^6in.-lbs.

Thus from major sources approximately 90% of the strain energy is accounted for. The contribution of secondary members would easily fill the balance.

Significantly, the comparison of consumed energy to the theoretical loss indicates a good representation of the accident.

APPENDIX F

REPORT OF INVENTIONS

A diligent review of the work performed under this contract has revealed no innovation, discovery, improvement, or invention.